POLITECNICO

MILANO 1863

SCUOLA DI INGEGNERIA INDUSTRIALE
E DELL'INFORMAZIONE

Hardware-in-Loop Simulation and Testing of Series Hybrid Architectures

TESI DI LAUREA MAGISTRALE IN
ELECTRICAL ENGINEERING - INGEGNERIA ELETTRICA

Author: **Prateek Pati**

Student ID: 955035
Advisor: Prof. Giambattista Gruosso
Co-advisors: Prof. Giancarlo Storti Gajani, Marziyeh Hemmati
Academic Year: 2022-23

Abstract

With rising concerns over climate change, the automotive industry has undergone a gradual transition of integrating electrical components into its powertrains. The powertrain is the fundamental system in any vehicle that allows for movement and mobility. The same shift in powertrain trends has also been observed in the agriculture machinery sector, with tractor powertrains being "hybridized" by incorporating a Battery Pack and Electric Motors, along with a traditional Internal Combustion (I.C.) Engine. Hybrid tractor powertrains aim to offer an optimized balance between performance and emissions, thereby helping in bringing down carbon footprints of individual vehicles, while ensuring uncompromising performance benefits of a regular I.C. Engine powered tractor.

In this thesis, an attempt has been made to design and simulate a series-hybrid tractor powertrain, while employing an Energy Management System (EMS) to efficiently optimize and prioritize power output distribution between the Engine and the Battery Pack. The entire powertrain, including electrical loads, battery pack, converter, and the EMS, has been modeled and simulated using Typhoon-HIL Schematic Editor and Typhoon-HIL SCADA. These two workbenches are part of the Typhoon-HIL Software Package, which is aimed at conducting real-time electrical simulation, testing and validation. Representative modeling of four $3\sim$ AC loads, two DC loads, and one $1\sim$ AC load has been carried out, enabling simulation and data collection of various load cases.

Based on the simulations and results, it can be concluded that the EMS plays a vital role in optimizing powertrain performance by balancing energy flow between the Engine and the Battery Pack. The EMS, in conjunction with the Battery Pack, significantly impacts the power requirement from the Engine itself. This highlights the importance of hybridizing automotive powertrains, to reduce the reliance on high-displacement Internal Combustion Engines and decrease the vehicle's overall carbon footprint during operation. Therefore, employing an effective Energy Management System with a robust algorithm can not only enhance powertrain efficiency and improve overall performance, but also significantly cut down on emissions in the long run.

Keywords: HIL Simulation, Hybrid Powertrains, Energy Management

Abstract in lingua italiana

Questa tesi presenta la simulazione e l'ottimizzazione di un powertrain ibrido in serie per trattori, che incorpora un efficiente sistema di gestione dell'energia per regolare la distribuzione di potenza tra il motore a combustione interna e la batteria. L'intero powertrain, compresi i carichi elettrici, la batteria, il convertitore e il sistema di gestione dell'energia, è stato modellato e simulato utilizzando Typhoon-HIL Schematic Editor e Typhoon-HIL SCADA. È stata raggiunta una modellazione accurata di quattro carichi in corrente alternata a 3~ , due carichi in corrente continua e un carico in corrente alternata a 1~ , consentendo simulazioni realistiche.

Attraverso simulazioni di successo e osservazioni registrate, il funzionamento di tutti i carichi elettrici, del bus in corrente continua, della batteria e del sistema di gestione dell'energia è stato esaminato approfonditamente. I risultati dimostrano che il powertrain ibrido funziona in modo efficace all'interno delle condizioni operative definite, con una corretta scambio di potenza e dati tra i diversi componenti. La batteria riduce efficacemente la potenza generata dal generatore, soddisfacendo l'obiettivo principale della tesi. Inoltre, il sistema di gestione dell'energia gestisce con successo la ricarica della batteria durante i periodi di bassa richiesta di potenza, migliorando la durata del powertrain attraverso cicli continui di carica e scarica.

Sulla base delle simulazioni e dei risultati ottenuti, si può affermare con fiducia che il sistema di gestione dell'energia svolge un ruolo vitale nell'ottimizzazione delle prestazioni del powertrain bilanciando il flusso di energia tra il motore e la batteria. L'algoritmo di gestione dell'energia, in combinazione con la batteria, influisce in modo significativo sulle esigenze di potenza del motore. Ciò sottolinea l'importanza dell'ibridazione dei powertrain automobilistici per ridurre la dipendenza da motori a combustione interna potenti e diminuire l'impronta di carbonio del veicolo durante il funzionamento. L'impiego di un sistema di gestione dell'energia efficace può ulteriormente migliorare l'efficienza del powertrain.

Parole chiave: Simulazione HIL, propulsori ibridi, gestione energetica

Contents

1 | Introduction

1.1. Understanding the term "Powertrain"

In the automotive context, the term "powertrain" refers to the mechanism or system responsible for generating and transmitting power to propel a vehicle. It encompasses the components that work together to convert the energy from the engine into a usable form that can drive the wheels [21]. The powertrain typically includes the engine (internal combustion or electric), transmission, driveshaft, differential, and the final drive components. The engine generates power by burning fuel or converting electrical energy, while the transmission transfers and modulates this power to the wheels based on the driver's input and road conditions.

In this thesis, the term "Powertrain" has been used as a derivative of the traditional mechanical drivetrain. The powertrain used used in this thesis refers to the system which includes the I.C. Engine itself, which has been electrically modeled as a Generator, the Battery Pack, the electrical loads, and the Energy Management System, which controls the flow of energy in the system. The type of powertrain employed in the model can be classified as a Series Hybrid Powertrain [28], which is a very popular hybrid powertain architecture for automotive applications. The powertrain, therefore, will be referred to as the system responsible for supplying power, and ensuring that the supplied energy is delivered at the loads.

1.2. Evolution of Non-Road Mobile Machinery Powertrains

The evolution of tractor powertrains has been a fascinating journey from its early days to modern times. Tractors were first powered by steam engines [5], but in the early 20th century, gasoline engines replaced the primitive technology. In the 1930s, diesel engines became a more effective substitute, which led to their widespread use in tractors. Tractor power output has greatly risen throughout time as a result of advancements in engine

technology like turbocharging and electronic fuel injection. From the earliest manual gears to the contemporary hydrostatic and continuously variable transmissions, transmission technologies have also advanced. Electric and hybrid powertrains have become practical substitutes in recent years, giving better fuel economy and lower pollutants.

In the domain of agricultural technology, electric and hybrid powertrains are relatively recent innovations, but they are rapidly gaining acceptance owing to their ability to lower emissions [20] and boost efficiency. Batteries that power electric tractors may be charged either from the grid or using clean energy sources like solar or wind energy. On the other hand, hybrid tractors combine an electric motor with a conventional diesel engine, enabling the tractor to run on one or both of the power sources. Compared to conventional diesel-only tractors, this leads to increased fuel economy and fewer emissions. Despite the fact that electric and hybrid tractors are still more expensive than standard tractors, they are a desirable alternative because of the multiple advantages they provide in terms of lower running costs [17] and environmental effects.

1.3.   Hybrid Systems

The use of hybrid powertrains in tractors is becoming increasingly important in the agriculture industry due to its potential to reduce fuel consumption and emissions while maintaining high levels of productivity. The combination of a traditional diesel engine and an electric motor in a hybrid powertrain allows for the tractor to operate on electric power when possible, reducing the amount of fuel needed and minimizing emissions. This can result in significant cost savings for farmers in terms of fuel expenses and environmental benefits through the reduction of greenhouse gas emissions.

Furthermore, the use of hybrid powertrains in tractors can also help to improve the efficiency and reliability of farm operations. A hybrid tractor's electric motor can deliver instantaneous torque and power, resulting in faster performance and improved results. Regenerative braking technology may also be used to recover energy during acceleration and braking. This energy can then be stored in a battery and utilized later to power the electric motor on the tractor. In addition to lowering fuel consumption and pollutants, this also lessens the number of starts and stops required by the conventional diesel engine, extending its lifespan.

The next section will go into more detail about hybrid architectures used in contemporary tractor powertrains and highlight some of their benefits and drawbacks.

1.4. State-of-the-Art

This section aims to highlight the current technologies and hybrid powertrain architectures employed in agricultural machinery. Some electrical components, including storage technology and drive machines have also been discussed, including their governing mathematical principles.

1.4.1. Series Hybrid Architecture

With a series hybrid setup, the traction loads are supplied only by an electric motor that is coupled to a fuel cell or generator that is run by an internal combustion engine. In extension, a secondary motor may also be employed to power the PTO unit. The engine acts as a generator [18] to recharge the battery that drives the electric motors rather than directly driving the wheels. This allows for the engine to operate at a constant, optimal speed, improving efficiency and reducing emissions. The following schematic shows a generic layout of a typical series hybrid architecture used in powertrains of agricultural machinery.
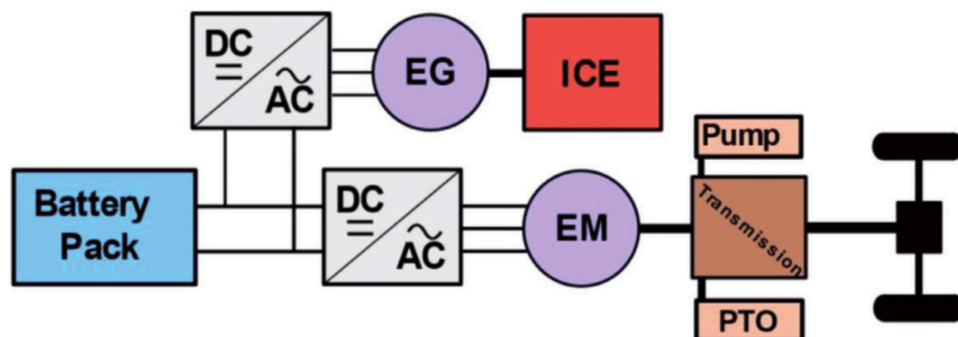

Figure 1.1: Series Hybrid Tractor Architecture [18].

A series hybrid design has the flexibility to run on a variety of fuels, including diesel, petrol, or biofuels, and the ability to decouple the engine speed from the vehicle speed for a more reliable and effective operation. However, from a practical standpoint, it must be noted that the initial cost of installing a series hybrid system is typically higher than that of a conventional diesel-only powertrain, and the increased complexity can further raise maintenance costs.

1.4.2. Parallel Hybrid Architecture

The parallel hybrid architecture [18] offers more flexibility than the series hybrid architecture in terms of driveline control. In this layout, traction can be provided by either the electric motor or by the internal combustion engine. The electric motor provides additional power and torque to the wheels when needed, improving efficiency and reducing emissions. The internal combustion engine can also operate on its own, especially during high power demands or when the battery charge is low, offering immense flexibility to the powertrain.
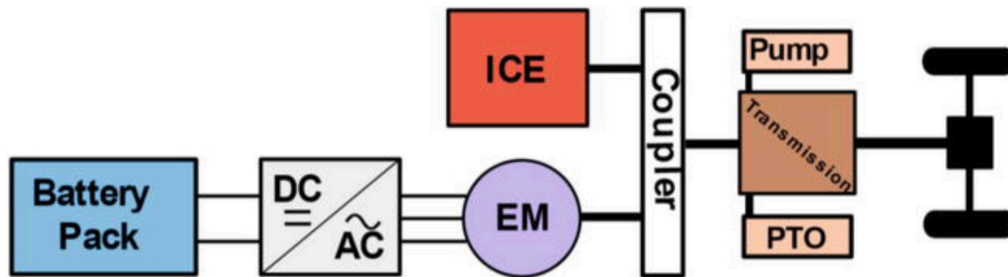

Figure 1.2: Parallel Hybrid Tractor Architecture [18].

The electric motor can provide additional power and torque during heavy workloads, reducing the strain on the diesel engine and improving overall fuel efficiency. Additionally, the electric motor can operate on its own during low-power demands, reducing emissions and noise levels. However, parallel hybrid systems can be more complex than series hybrid systems, leading to higher maintenance costs, and they may require larger batteries to accommodate the additional power demands.

1.4.3. Series-Parallel Hybrid Architecture

The series-parallel hybrid architecture [3] is a system of hybrid powertrain that incorporates the advantages of both series and parallel hybrid systems. The diesel engine can either directly drive the wheels in a series-parallel hybrid system or it can function as a generator to charge the battery that powers the electric motor. In addition, the electric motor may be used to give additional power and torque by itself or in combination with the diesel engine. This gives power management more flexibility and enables the tractor to work in various modes according to the task at hand.
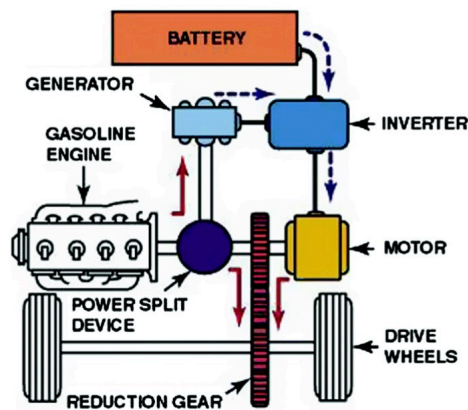
Figure 1.3: Series-Parallel Hybrid Tractor Architecture [3].

The system can operate in series mode during low-power demands, which allows for reduced emissions and improved fuel efficiency. In contrast, the system can operate in parallel mode during high-power demands, providing additional power and torque when needed. This flexibility in power management can improve overall performance and productivity while reducing environmental impact. However, as the system requires many more additional components, including far more sophisticated controllers, the deployment of such an architecture in tractor powertrains can be a far more expensive affair, compared to parallel hybrid systems.

1.4.4. Electrical Systems on Tractors

Ideally, removing the internal combustion engine, and replacing the entire mechanical powertrain with powerful electric motors, suitable converters, and a sizable battery pack would solve many challenges faced by hybrid tractor powertrain. A full electric architecture [18] brings down the system complexity drastically, and allows for easier control of the traction torque, as well as PTO power control. The system is also economical in the long run, as it offers relatively lower fixed costs, and operates at high efficiencies.
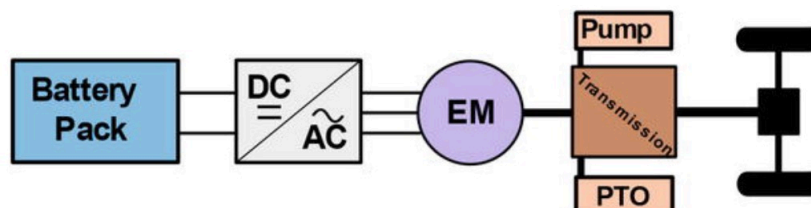

Figure 1.4: Full-Electric Tractor Architecture [18].

While full electric tractor powertrains offer numerous advantages, such as zero emissions and low noise levels, they also have some limitations that limit their use in agriculture. The restricted range and battery life of electric tractors are some of the most significant difficulties. Unlike diesel-powered tractors, which can run for extended periods of time on a single tank of gasoline, electric tractors have a limited range that is determined by the capacity of their batteries. This might limit the variety of tasks that electric tractors can accomplish and may demand regular recharging, which can be time-consuming and decrease output.

For these reasons, in this study, we will take a closer look at some of the electrical systems deployed in hybrid tractors, while only using a series hybrid architecture for the powertrain model. In the following sections, some basics of batteries, electric motors, and the concept of implement electrification have been covered.

1.4.5. Energy Storage

or automotive applications, the easiest and most economical way to store electrical energy is by using a battery pack. A properly designed battery pack can offer high energy density, as well as good power density. Lithium-ion cells are used in the vast majority of modern battery packs, as these cells offer excellent thermal characteristics, have high efficiency, and are easier to maintain. Battery packs are made of several modules, which, in turn, comprise several hundred individual cells. The following diagram illustrates the structure of a typical battery pack used in modern EVs. In this study, a Lithium-ion battery pack has been used, whose specifications have been illustrated in later sections.
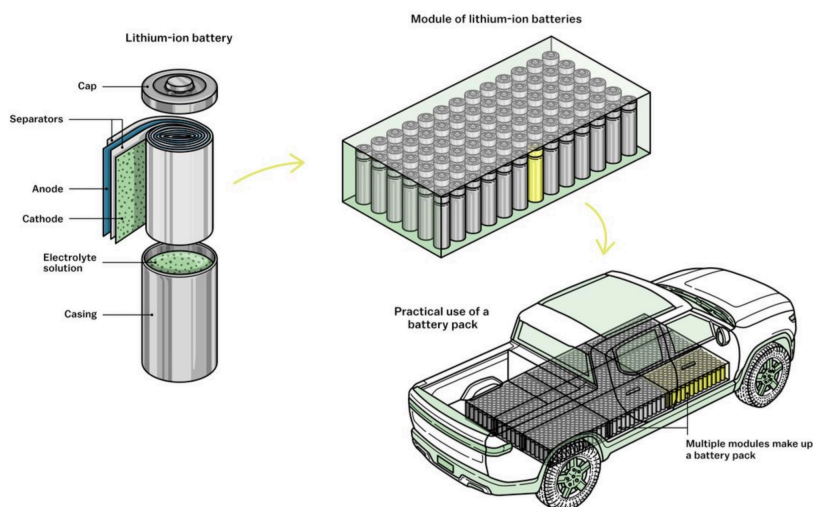

Figure 1.5: Lithium-ion battery pack construction and deployment [1].

The State of Charge, or SoC, is a very fundamental and important parameter of a battery pack. SoC is the measure of the amount of energy stored in a battery relative to its maximum capacity, expressed as a percentage. Knowing a battery pack's SoC can assist improve its longevity in addition to providing an indicator of available energy. Overcharging or deep discharging the battery can cause irreparable harm, lowering its capacity and overall performance. Users can prevent these detrimental situations and extend the life of the battery by monitoring the SoC of a battery pack.

Determining the SoC of a battery pack is also critical for guaranteeing the battery's and the surrounding environment's safety. Overcharging or deep discharge can result in the release of hazardous chemicals or gasses, which in certain situations can be deadly or even explosive. Users may avoid these dangerous scenarios and maintain safe and efficient operation by monitoring the SoC of the battery pack.

There are certain approaches to calculating the SoC of a battery pack:

- **Open Circuit Voltage (OCV) Measurement:** This is a simple approach for measuring battery SoC, [7] as it correlates the internal voltage of the battery with the SoC and a lookup table of specified values. Because it is so simple, it cannot be used in online applications as the internal voltage of the battery can only be retrieved by disconnecting it and waiting for it to stabilize. This is why Battery Management Systems (BMS) do not usually employ this approach for measuring SoC.
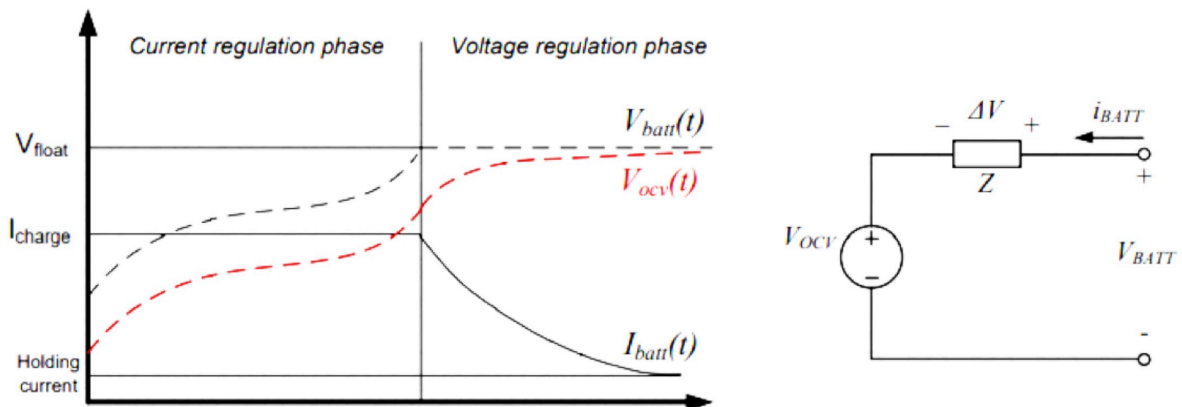

Figure 1.6: OCV evolution and equivalent circuit of a battery [7].

- **Coulomb Counting:** Because of its simplicity, this approach [7] is one of the most commonly used for calculating the SoC. It is based on measuring the input and output currents as well as estimating the initial state. It is critical in this

estimating approach to know the battery's initial state of charge and to precisely measure the current. After the battery is fully charged, its initial value is generally updated.

$$SoC(t) = SoC_0 - \frac{1}{C_{nom}} \times \int_{t_0}^{t} i_{batt}(t)\,dt \times 100 \quad [7] \tag{1.1}$$

This study has been carried out using Typhoon-HIL, which uses Coulomb Counting for estimating the SoC of a given battery pack. The software also offers the feature of adjusting coulombic efficiency coefficients. The following equation highlights the equation used by the software to accurately map the SoC of a battery pack:

$$SOC_{(t)} = \int \frac{i_t \times \eta_{(SoC,T)}}{Q_{(SoC,T)}} dt \quad [7] \tag{1.2}$$

One of the key advancements in tractor hybridization is the electrification of agricultural implements. Traditionally, farming implements have been powered by the PTO, which is an auxiliary shaft powered by the internal combustion engine of the tractor, and driven through a dedicated gearbox. However, with the advent of hybrid technologies, the need for electrification of agricultural implements plays a key role in decreasing emissions and improving powertrain efficiency without compromising agricultural productivity. Additionally, electrified implements bring down system complexity, which can aid in the long-term reduction of maintenance costs. Shown below are some commonly used agricultural implements that have a scope for electrification.

1.4.6.   Traction Drives

In automotive applications, some of the most common types of traction drives are primarily based on Induction motors and Permanent Magnet Synchronous motors. In this study, we will be using a PM Synchronous motor for traction loads. For our application, we will take into account a PM Synchronous motor that runs on 3-phase power, and gives out torque and speed as output. The output speed and torque can be used as basic parameters to further control the motor, depending on reference speed inputs given by the user. It is vital to understand the real-time operating points of the motor, as the power drawn by the electrical machine varies with speed and load.
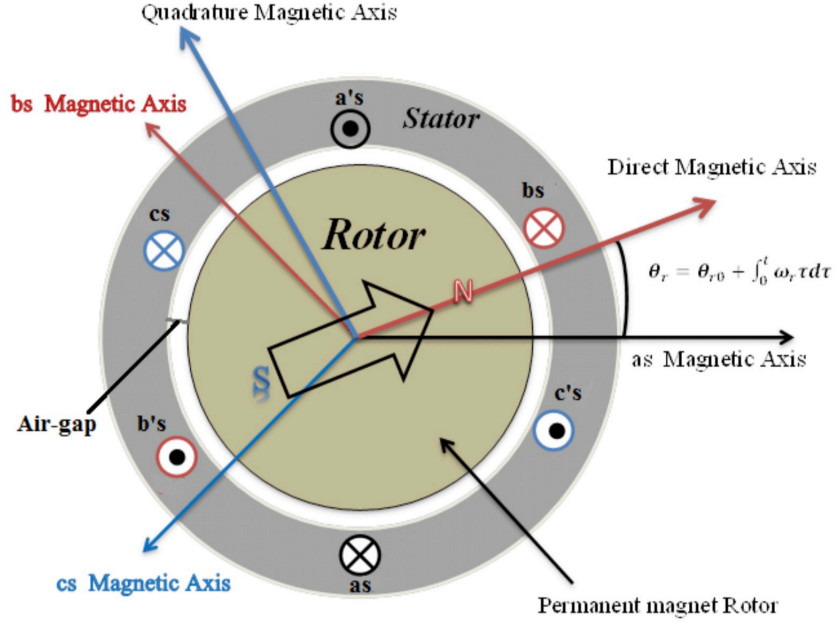
Figure 1.7: d-Axis and q-Axis modeling of PM Synchronous Motor [2].

In order to understand and control the machine precisely, a robust control algorithm must be deployed. As the intention of the study is to precisely control energy flow between the different subsystems of the powertrain, the control, and measurement of motor power plays a critical role. The most fundamental way to approach designing the control system for a Permanent Magnet Synchronous motor is by understanding the stator equations, which are given by:

$$V_{sd} = R_s isd + L_d p(i_{sd}) - \dot{\theta}_m L_q i_{sq} \quad [27] \tag{1.3}$$

$$V_{sq} = R_s i_{sq} + L_q p(i_{sq}) + \dot{\theta}_m L_d i_{sd} + \dot{\theta}_m \Psi_{PM} \quad [27] \tag{1.4}$$

Where V_{sd} and V_{sq} are d-Axis and q-Axis stator voltages of the PM Synchronous machine respectively; R_s is the stator resistance, L_d and L_q are d-Axis and q-Axis inductances respectively; i_{sd} and i_{sq} are the d-Axis and q-Axis stator currents; θ_m is the electrical angle between the α-Axis reference and the instantaneous d-Axis of the rotor; and Ψ_{PM} is the magnitude of the flux produced by the permanent magnet.

Additionally, the output torque of the Permanent Magnet Synchronous motor is given by the following equation, as is further used to model the control system and understand traction torque:

$$\tau_e = n_p \left[(L_d - L_q) i_{sd} i_{sq} + \Psi_{PM} \right] \quad [27] \tag{1.5}$$

In this equation, n_p is the number of poles used in the synchronous machine. The first term inside the square bracket represents the torque term due to magnetic reluctance, while the second term is the result of magnetic excitation between the rotor and the stator. The following curve highlights the typical relationship between the torque output and speed [16] of an Interior Permanent Magnet (IPM) Synchronous motor:
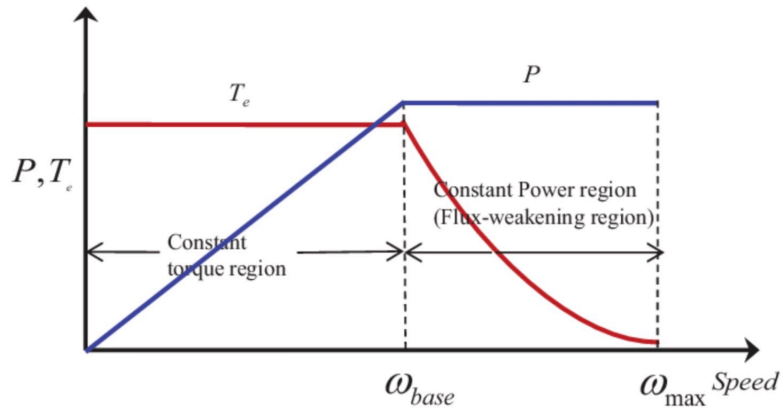

Figure 1.8: Torque and Power vs Speed characteristics of Interior Permanent Magnet Motor [16].

1.4.7. Implement Electrification

One of the key advancements in tractor hybridization is the electrification of agricultural implements. Traditionally, farming implements have been powered by the Power Take-Off Unit (PTO), which is an auxiliary shaft powered by the internal combustion engine of the tractor, and driven through a dedicated gearbox. However, with the advent of hybrid technologies, the need for electrification of agricultural implements plays a key role in decreasing emissions and improving powertrain efficiency without compromising agricultural productivity. Additionally, electrified implements bring down system complexity, which can aid in the long-term reduction of maintenance costs. Shown below are some commonly used agricultural implements that have a scope for electrification.

(a) Mechanical Seeder

(b) Fertilizer Spreader

(c) Rotary Harrow

(d) Snowblower

Figure 1.9: Commonly used Agricultural Implements.

One of the most efficient ways to achieve implement electrification is by replacing the entire PTO unit with a powerful electric motor that can deliver power and torque in the right quantities for achieving various agricultural tasks. The idea is to minimize the dependency on internal combustion engines for powering implements. By using an electric motor in tandem with a battery pack, power, and energy flow can be optimized to enhance efficiency, while managing all load demands in real time.

1.4.8. Powertrain Architecture Chosen for this Thesis

For the purpose of this thesis, the Series-Hybrid Powertrain Architecture has been adopted and employed for modeling and simulation. This powertrain layout offers simplicity, while allowing the installation of different types of electrical loads in order to achieve holistic modeling. All the necessary simulation and testing conditions can be conveniently carried out using this architecture, and it aims to simplify and streamline potential development processes.
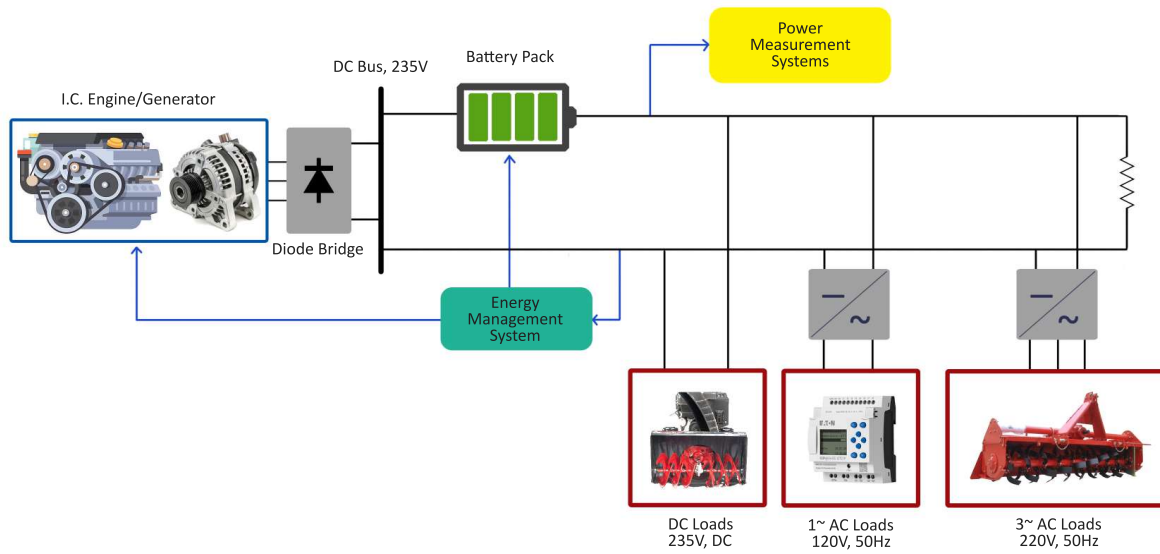
Figure 1.10: Overview of the Powertrain Architecture.

The schematic shown above illustrates the Series-Hybrid architecture adopted for this thesis. The architecture contains an I.C. Engine, which is coupled with a Battery Pack to support power requirements at the load. The implements have been modeled as electrical loads, and have been installed to emulate the mechanical machinery they represent. Although this thesis does not highlight traction loads, the focus remains primarily on the simulation of the PTO-based implements.

1.5.　Motivation for Thesis

With hybrid and electric powertrains gaining traction in the automotive industry, the need for improved efficiency and reduced emissions is becoming increasingly important in the non-road mobile machinery sector. Not only does hybridization help positively impact the environment, but it also helps consumers from a long-term economic point of view.

In countries such as India, where government incentives [14] have been largely directed towards the electrification of passenger and commercial vehicles, the need for the development of energy-efficient, electrified NRMMs is important. This is especially valid for countries having a large portion of their GDPs dependent on the agricultural sector, as large-scale farming with hybridized machinery can cause a significant impact on long-term economics on a grass root level, while also bringing down emissions on a potentially large scale.

This clearly highlights the need for a robust energy management system that can accurately gauge the power needs of electrified implements in real-time, while actively balancing energy output from the engine and the battery pack, whenever required. A good energy management algorithm, therefore, has the potential to dramatically improve energy consumption at the vehicle level, and in the process, drastically bring down the dependency on inefficient internal combustion engines.

2 | Technical Tools Used

For the purpose of this, two technical tools have been majorly utilized. MATLAB-Simulink has been used extensively for the purpose of preliminary model building, and understanding of the functioning of basic electrical and mechanical models. For the deployment of the actual schematic and carrying out all electrical simulations, Typhoon-HIL has been used. Further, two workbenches of Typhoon-HIL have been used: Schematic Editor and HIL SCADA, both of which have been introduced in this section.

2.1. MATLAB - Simulink

As mentioned, MATLAB-Simulink has been used to carry out preliminary model tests, and to understand if general systems are functioning. Blocks from the Simulink and Simscape libraries have been utilized for this purpose, and relevant outputs have been used to conduct a preliminary understanding of how systems behave.
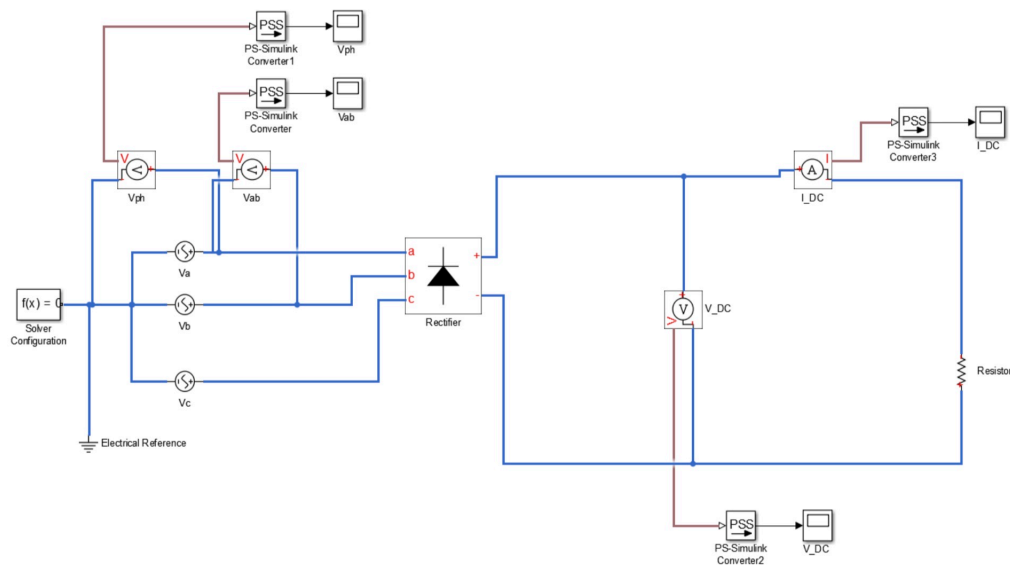
Figure 2.1: Preliminary Test Model of the DC Bus in Simulink.
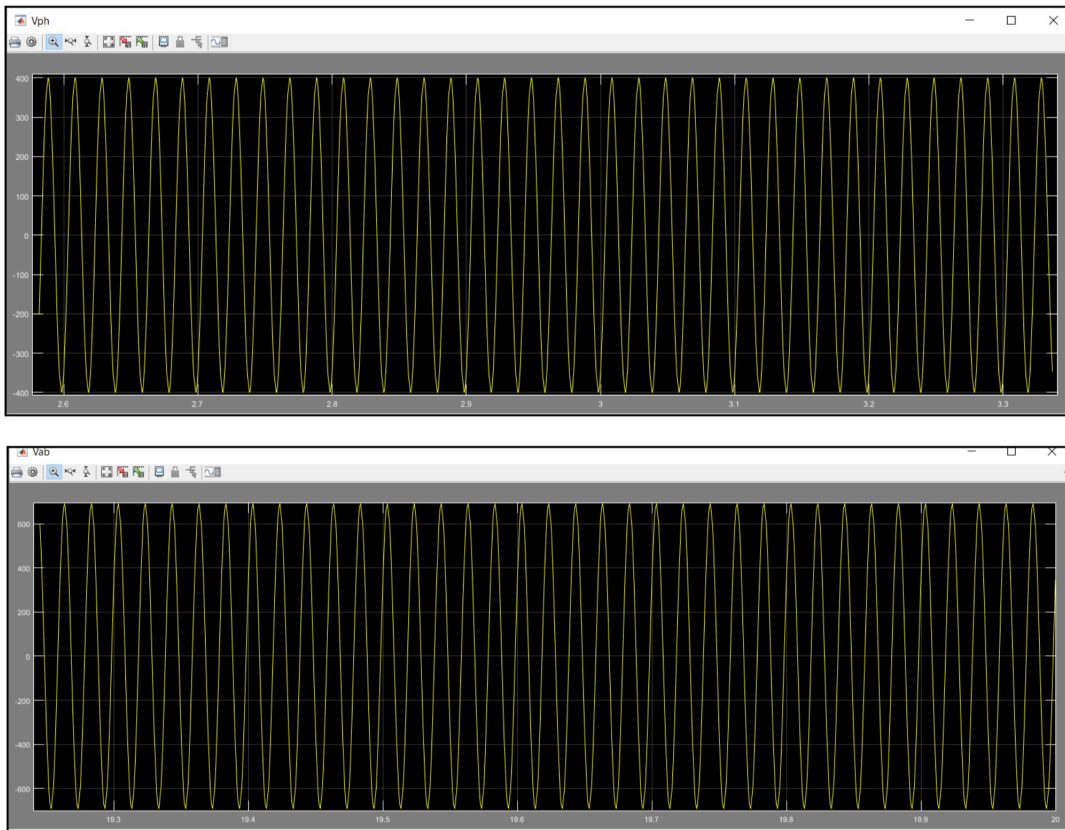
Figure 2.2: Test Voltage Waveforms captured using Scope

Shown above is an example of a test AC-DC conversion circuit created at the start of the thesis, to understand how the DC bus can be electrically modeled and how loads could potentially be modeled in the future. Scopes were used to identify and understand the AC and DC waveforms, and to potentially find any errors in the system prior to modeling in Typhoon-HIL.

2.2.   Typhoon - HIL

Typhoon-HIL is a software platform aimed at real-time simulation and testing of complicated power systems, and can be used for the simulation and validation of electric drives, as well as power electronics. Typhoon-HIL Schematic Editor and HIL SCADA provide a virtual environment that allows users to model and test designs before deploying them in the real world. The software allows simulating a wide range of scenarios, from basic control systems to advanced fault scenarios, and evaluate the performance of their designs under various conditions.

2.2.1. HIL 404

Typhoon-HIL is based on hardware implementation prescribed on the company's recommended devices, which offer a wide range of power, control and flexibility options. The HIL 404 is one such device [26], which allows for high-performance real-time simulation, ideally for testing and validating power electronics and electrical drives.

Figure 2.3: HIL 404 Board.

It features a potent FPGA and analog Input/Output channels that enable high-fidelity simulation of complex systems [25]. The HIL 404 device is commonly used in research and development, academia, and industrial applications, providing a reliable and cost-effective solution for testing and validation of power system designs. For this thesis, HIL 404 has been used as reference while creating all the models in Typhoon-HIL, and while deciding model partitioning, along with signal processing limits.

	HIL402	HIL404	HIL602+	HIL604
Generation	3rd	4th	3rd	3rd
Simulation capacity				
Detailed (switching) DER models (1ph / 3ph)	8 / 4	8 / 4	12/6	16/8
Average DER models with detailed control loops (3ph)	20	30	30	40
Distribution network simulation	✓	✓	✓	✓
Time resolution				
Minimal simulation step	500 ns	**200 ns**	500 ns	500 ns
DI sampling resolution	6.2 ns	**3.5 ns**	6.2 ns	6.2 ns
IO				
Analog I/O	16/16, +/- 10V, 16bit	16/16, +/- 10V, 16bit	16/32, +/- 10V, 16bit	32/64, +/- 10V, 16bit
Digital I/O	32/32	32/32	32/32	64/64
Connectivity				
USB	✓	✓	✓	✓
Ethernet	✓	✓	✓	✓
CAN		✓	✓	✓
RS232		✓	✓	✓
Time synchronization (PPS and IRIG-B)				✓
Paralleling		up to 4 units	up to 4 units	up to 16 units

Figure 2.4: Technical Comparison of HIL 404 with other Devices.

2.2.2.   Schematic Editor and HIL SCADA

Typhoon-HIL Schematic Editor is a competent graphical tool that can be used to create, modify, and simulate electrical network schematics in a virtual environment. It is designed to work seamlessly with the Typhoon-HIL real-time simulator, allowing users to create and edit schematics in real-time and see the impact of their changes immediately. The software includes a library of pre-built components, such as power supplies, filters, and amplifiers, which can be easily integrated into the schematics.
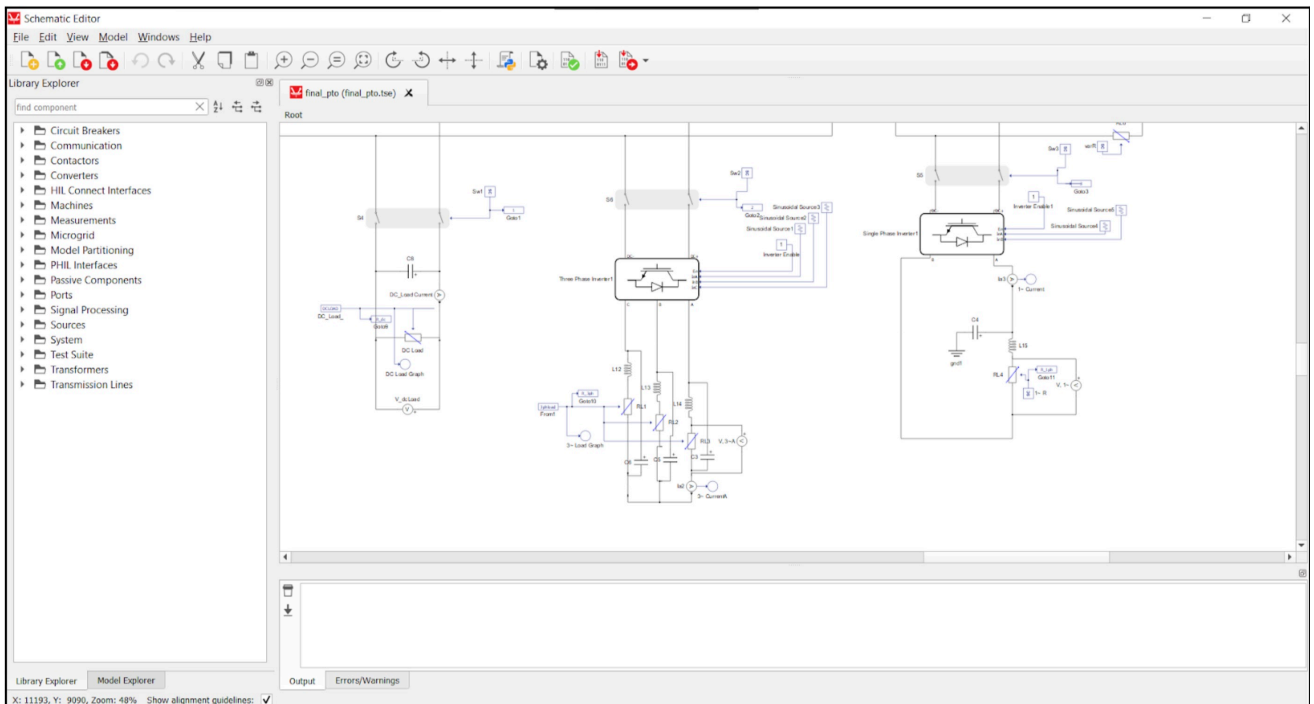
Figure 2.5: Typhoon-HIL Schematic Editor Interface.

The following image illustrates the Model Configurations available for the HIL 404 device. Typhoon-HIL offers a wide range of configuration settings, depending on the complexity and requirements of the model. For this thesis, the configuration adopted for modeling the powertrain architecture in Typhoon-HIL is Configuration 1. This configuration was chosen because it offers a good optimization for the model's requirements. With 3 available cores, the option of employing one machine per core, up to 6 Ideal Switches and a Maximum Converter Weight of 3 per core, Configuration 1 met all of the model's requirements, and was therefore the best way forward for designing the architecture.

	Configuration 1	Configuration 2	Configuration 3	Configuration 4	Configuration 5	Configuration 300
Number of SPCs	3	4	2	3	3	3
Machine solvers	1	0	1	2	0	1
DC-DC converter solvers	0	0	0	0	1	0
Signal generators	12	12	12	12	12	12
Look Up Tables	8	8	8	8	8	8
PWM modulators	12	12	12	12	12	12
PWM analyzers	4	0	0	0	0	4
SPC peak processing power [GMACS]	1.12	1.12	1.12	1.12	1.12	1.12
SPC matrix memory [KWords]	16.0	16.0	16.0	16.0	16.0	16.0
SPC output memory size [variables]	512	512	512	512	512	512
Max converter weight (ideal switches) / SPC	3	3	4	3	4	3
Contactors (ideal switches) / SPC	6	6	6	6	6	6
Non-ideal switches / SPC	0	0	32	0	32	0
Time varying elements / SPC	16	16	16	0	16	16
Nonlinear machine support	yes	no	yes	no	no	yes
Nonlinear machine LUT size [KWords]	32	0	32	0	0	32
Converter power loss calculation	yes	yes	yes	no	yes	yes
Converter forward voltage drop	yes	yes	yes	yes	yes	yes
Switch-level GDS oversampling	no	no	yes	no	yes	no

Figure 2.6: Model Configuration Settings for the HIL 404 Device.
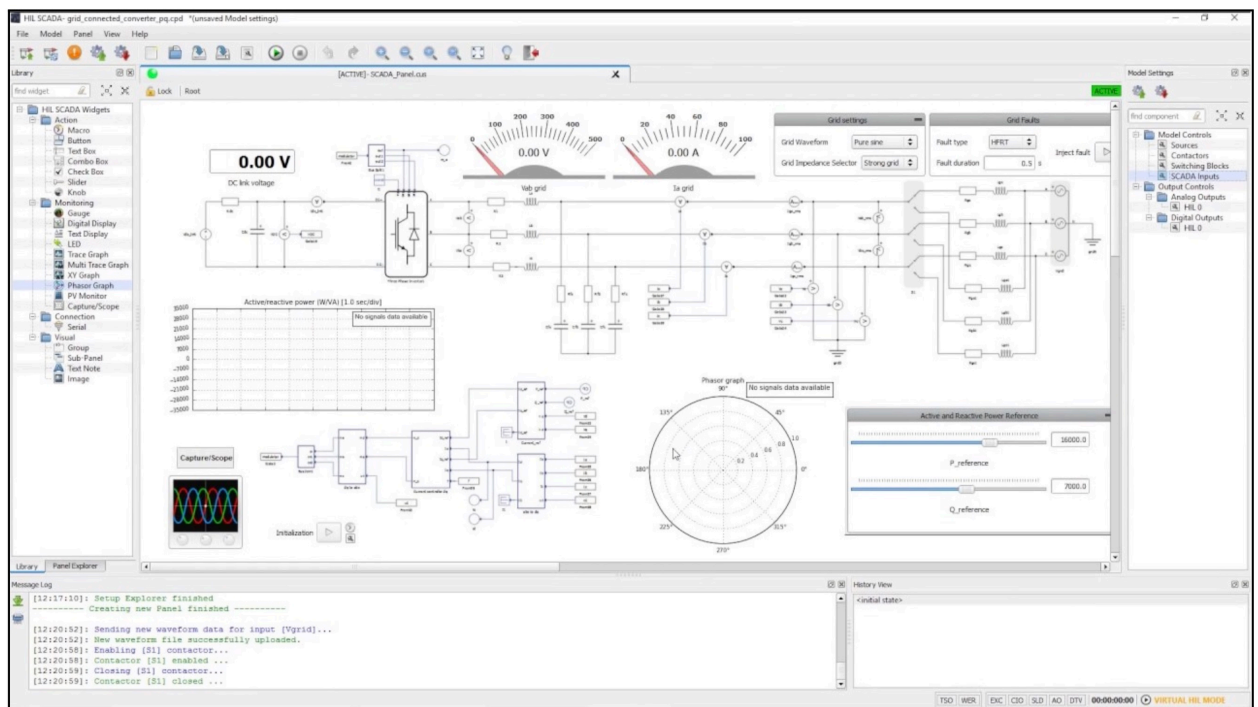
Figure 2.7: Typhoon-HIL SCADA user Interface.

HIL SCADA is a workbench that works synchronously with Schematic Editor, and lets you add control or monitoring widgets based on the user's schematic model. Widgets can be added to introduce a user-input into the model, or a probe can be utilized to view changes in signals in real-time. More complex actions using Macros allows users to trigger certain events, for example faults, and then capture critical phases such as transients.

3 | Overview of the Approach

The thesis aims at developing an energy management solution for hybrid tractor drives, in such a way that efficiency of the overall powertrain is increased, while ensuring that carbon emissions are reduced. One way to ensure this is by replacing the mechanical PTO with electric motors for individual loads, and minimizing the power contribution of the internal combustion engine. In fact, a battery pack must be incorporated to compensate for the power requirements of the loads, such that the engine must only provide sufficient power whenever it is absolutely needed.

Keeping this approach in mind, one of the first steps towards achieving high efficiency and powertrain hybridization was to model mechanical PTO power demands as electrical loads. In this study, several tractor implements have been considered, and all of them have been modeled into electrical systems with time-varying power consumption based on real-world duty cycles.

In practical cases, electrical and mechanical devices draw power from the source in different ways, and follow highly contrasting trends in power consumption, primarily based on what purpose they serve. This trend in power consumption as a function of time is termed as "duty-cycle" in the context of power. Therefore, the objective was to understand the fashion in which these devices draw power in practical cases, and therefore gain a better understanding of how this trend can be mathematically modeled.

In addition, a battery pack has been suitably modeled, which is explained in later chapters, to compensate for the power demand in the absence of the I.C. engine. Finally, a Power Management algorithm has been designed, developed, tested, and deployed which accurately maps the power requested from various load combinations, and then adjusts the percentage of power contributions from the I.C. engine and the battery pack in order to optimize performance and reduce the involvement of the engine. The following sections highlight the overall approach that has been adopted in achieving this target.

3.1. Introduction

The problem statement is to develop an energy management system that can accurately map the power requested from the electro-mechanical loads, and make adjustments to the power output of the engine and the battery pack in order to reduce the involvement of the IC engine, while ensuring that the battery pack remains optimally charged. In order to achieve this objective, this thesis adopts the following stages of progression:

1. Development of the basic Architectural Layout of the Electric Powertrain.

2. Selection and Modeling of PTO loads, and understanding Duty Cycles.

3. Testing and Validation of modeled loads, and ensuring all Power Quality criteria are met.

4. Designing a suitable Power Measurement system, and running simulations on all load combinations to understand long-term loading scenarios.

5. Developing and deploying an Energy Management System that can successfully gauge power requirements, and govern the output of the Engine as well as the Battery Pack.

Keeping this approach in mind, the next sections dive into the details of how these stages have been implemented, and the mathematics behind the modeling of these steps.

3.2. Model Layout

In order to model the desired electrical network and employ the intended Energy Management algorithm, the following schematic model has been implemented for the purpose of this thesis. This model has been designed from ground-up, containing all necessary electrical loads, power electronics, and requisite filters, along with both the power sources and signal processing blocks.
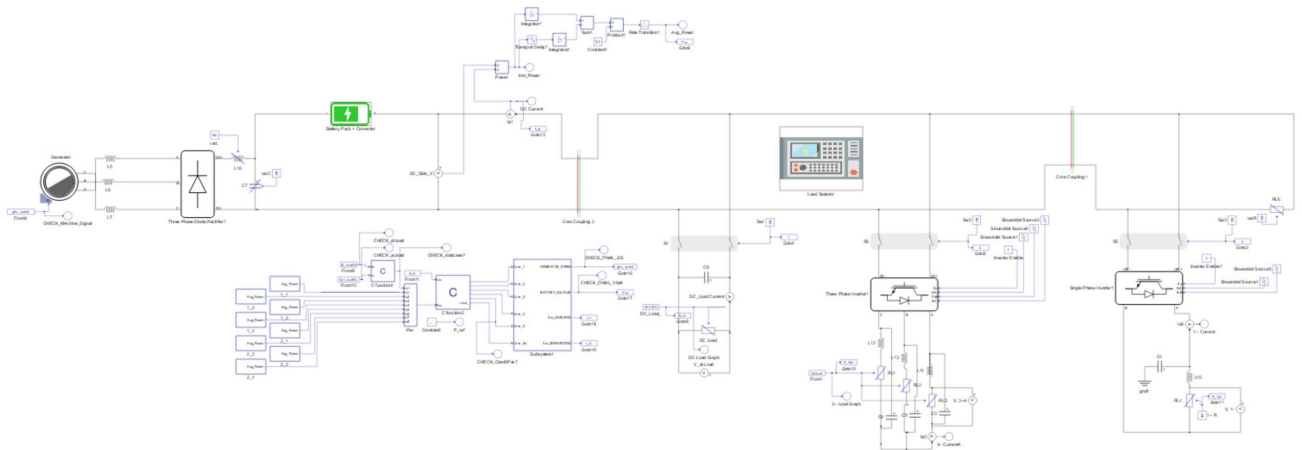
Figure 3.1: Full Model Overview.

The model contains a generator, which essentially behaves as an internal combustion engine alternator. The AC power produced is sent to the diode bridge, which rectifies the AC regardless of frequency, into DC voltage and the subsequent filter [19] removes unwanted harmonics from the microgrid.

In series with the DC bus is the battery pack + converter unit, which supplies appropriate DC voltage whenever necessary to complement the power produced by the engine, and reduce the system's dependency on the engine as much as possible.

On the load side of the network are three types of loads: one variable DC load, a fixed single-phase AC load, and one variable three-phase AC load, all of which mimic the electric behavior of various implements modeled for this thesis.

On the signal processing side, a Load Selector algorithm has been deployed, which changes the load characteristics of the DC and 3∼ loads based on the user's selection. Additionally, the final unit worth mentioning is the Power Management Unit itself, which has the responsibility of controlling generator speed and inverter control signals for regulating the battery output voltage. All of these mentioned sub-systems have been explained in detail in subsequent sections.

3.3.   Generator and DC Bus

The generator is the primary source of power in this model. Its speed, and therefore, output voltage is controlled by the Power Management Unit, which sends a signal to the generator input to control its speed. Three inductors are installed in each of the three phases, and act as snubbers to stabilize any fluctuations in line currents, and therefore

play a key role in maintaining the stability of the overall operation of the network. The 3~ voltage is fed to a simple 3-leg diode bridge, which rectifies the sinusoidal voltage into a rippled DC output.
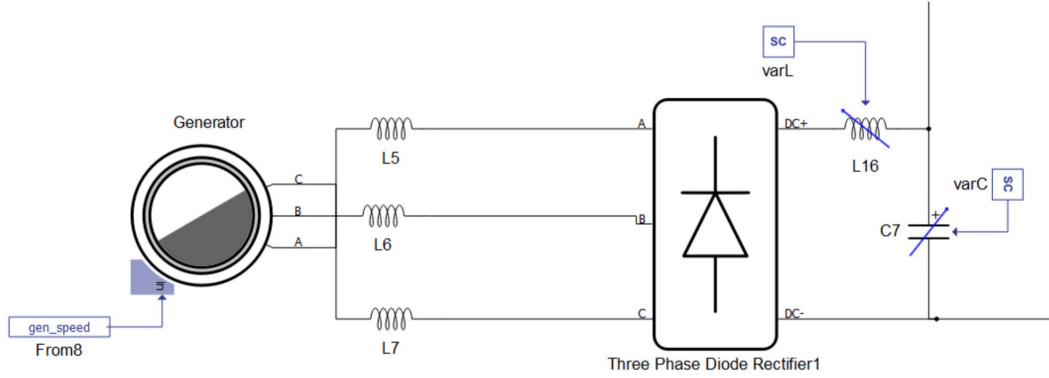
Figure 3.2: Generator and DC Bus.

The generator has been modeled with the following parameters:

- Stator Resistance, $R_{ms} = 1\Omega$

- Stator Equivalent Inductance, $L_{ms} = 100\mu H$

- PM Flux at rated load, $\Psi_{PM} = 0.5$ Wb

- Number of Poles, p $= 4$

- Moment of Inertia of rotor, $J_m = 0.01$kg-m^2

The inductor and the capacitor installed after the diode bridge effectively serve the purpose of a low-pass filter, and efficiently manage to filter out higher order harmonics. The resulting voltage waveform is almost entirely a consistent DC output of 235V, which is the desired bus voltage.
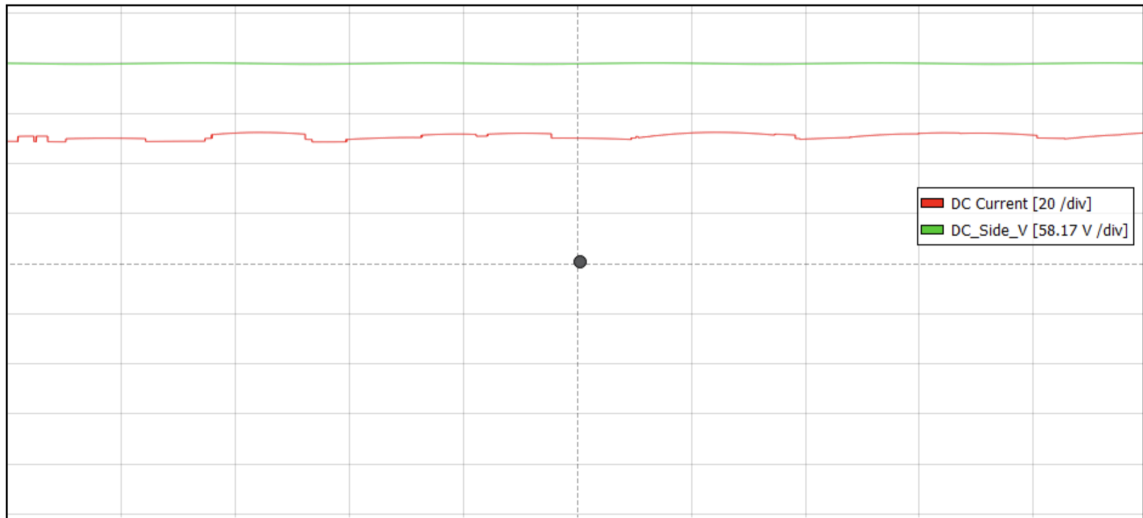
Figure 3.3: Voltage and Current at DC Bus.

From the probe observation shown in the image above, the output voltage is nearly ideal, while the current has minor distortions due to the harmonics injected by the inverters at the loads. While the current is not completely free of harmonics, its impact is relatively insignificant. Figure 3.4 closely highlights the ripples in voltage, along with the distortions in the current waveform before the low-pass filter was installed.
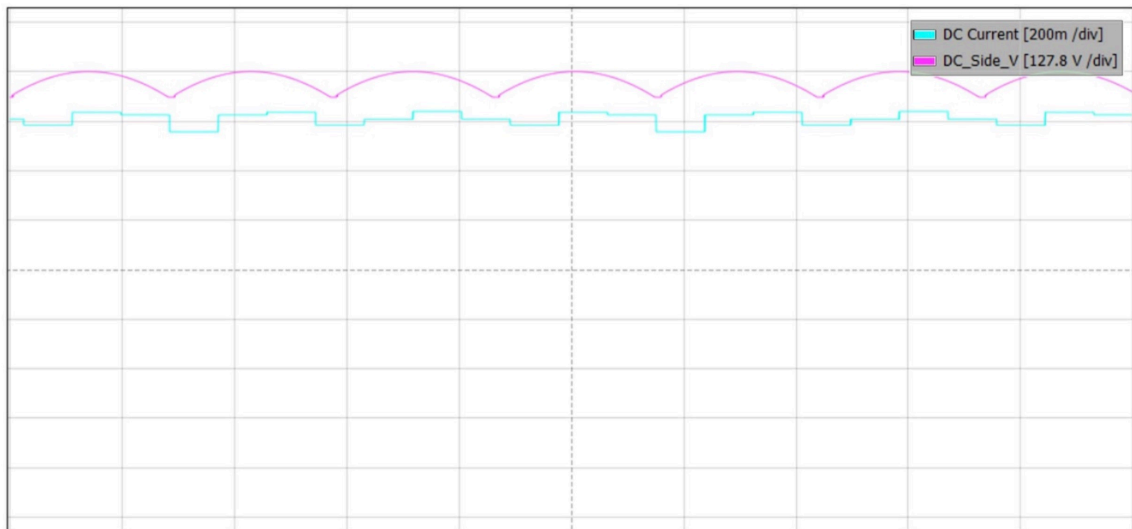
Figure 3.4: Ripples at the DC Bus without Filter.

To put things into perspective, the voltage sees a peak-to-peak ripple of around 0.64%, while the peak-to-peak current ripple is slightly higher, at 3.21%. However, this does not play a major impact in the functioning of the overall electrical network. This has been

the result of a basic low pass filter, which has been tuned at a Capacitance of 45μF and an Inductance of 105μH.

3.4. DC Loads

As it is commonly known, an agricultural tractor can employ a wide range of implements in order to make farming easier. Many of such implements can either be as simple as a hoe with only passive mechanical characteristics or can be as complex as large harrows, featuring multi-system mechanics with large-scale electrical and electronic integration.

(a) Flood Lights
(b) Hydraulic Pump

Figure 3.5: Common Tractor Implements modeled as DC Loads.

In this study, two relatively simple tractor attachments have been considered, which can be easily modeled as DC loads, as seen by the power source. The following section explains in detail what these loads are, and what approach has been taken to model such loads from an electrical perspective.

3.4.1. Types of DC Loads Used

For the purpose of this thesis, two common yet relevant DC loads have been used. These loads are as follows:

1. Snowblower

2. Battery Heater

Snowblower: The Snowblower is a commonly used machine in several farms, and it comes in handy when agricultural tasks must be accomplished in snowy conditions. In this study, a John-Deere SB11 Series Snowblower [8] has been considered. This machine

is compact, efficient, and ideal for low-to-medium load applications.

(a) Snowblower Implement   (b) Exploded View
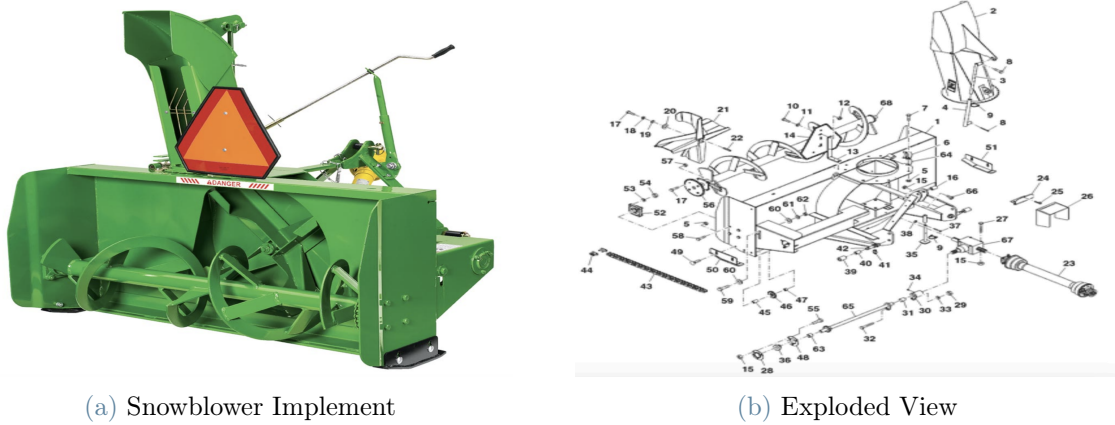
Figure 3.6: John-Deere SB11 Series Snowblower.

The John-Deere SB11 Series Snowblower is a very powerful machine, and employs a motor that runs at a constant speed of 540 RPM. From an electrical perspective, the Snowblower's motor can be seen as a fixed DC load. The real power drawn from the source remains constant, with the load vs time curve being flat.

Battery Heater: The other DC load considered for this study is the Battery Heater, which has the objective of heating up the tractor's battery in order to ease starting up the engine under severely cold conditions. A battery usually has a very limited working range of temperatures, and cold conditions can prevent the battery from producing enough voltage to fire the spark plugs, and as a result, the engine has difficulty starting. In this study, we have considered a hybrid tractor with its own HV battery pack. The use of the battery heater, in this situation, can be further extended to bring up the HV battery pack's temperature to optimum levels in order to work with the right amount of efficiency. Keeping this in mind, Kat's KH22200 battery heater has been selected [15].

(a) Battery Heater Blanket   (b) Thermal Wrap and LV Battery

Figure 3.7: Kat's KH22200 Battery Heater.

The KH22200 comes with a thermal blanket and produces heat when supplied by 0.8kW power. It is compact and easy to handle and therefore makes for an excellent choice for modeling a realistic and relevant DC load for our study.

3.4.2. DC Load Duty Cycles

Snowblower: In order to gain an understanding of the duty cycles of these tractor attachments, it is best to understand how they operate. The Snowblower works by driving [13] a double-stage blade system through engine power, which expels snow from a raised pipe. Theoretically, the blades can also be powered by an electric motor installed at the blade shaft.
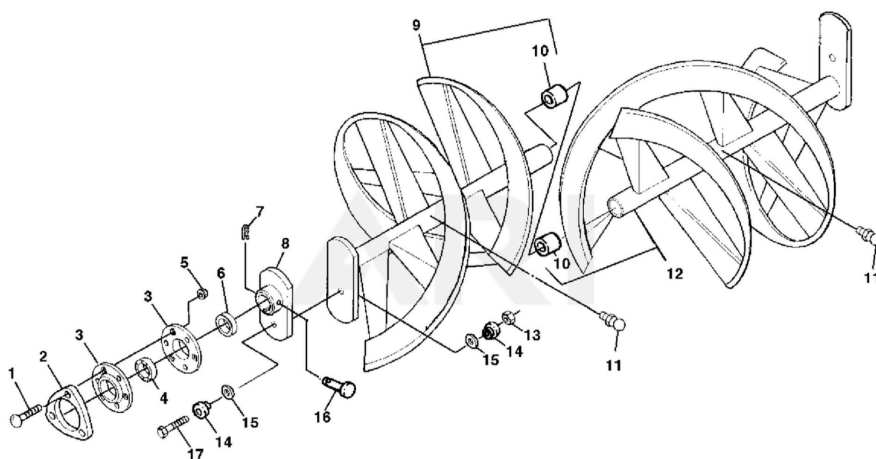
Figure 3.8: Snowblower Double-Blade Assembly.

As the Snowblower rotates at a fixed speed of 540 RPM, an electric motor with a constant

speed output can theoretically power this machine without the need of mechanical power from the engine. Assuming that the torque requirement for cleaning snow remains more or less constant, it can be assumed that the whole machine draws a fixed amount of power during the entire range of operation. This has been modeled in this next section.

Battery Heater: The Battery Heater, on the other hand, requires no mechanical power. Instead, it can draw power directly from the DC Bus to perform its operation. Much like the operation of an HVAC system [6], the heating operation of the Battery Heater can be simplified on the basis of a simple Hysteresis control, or ON/OFF action.
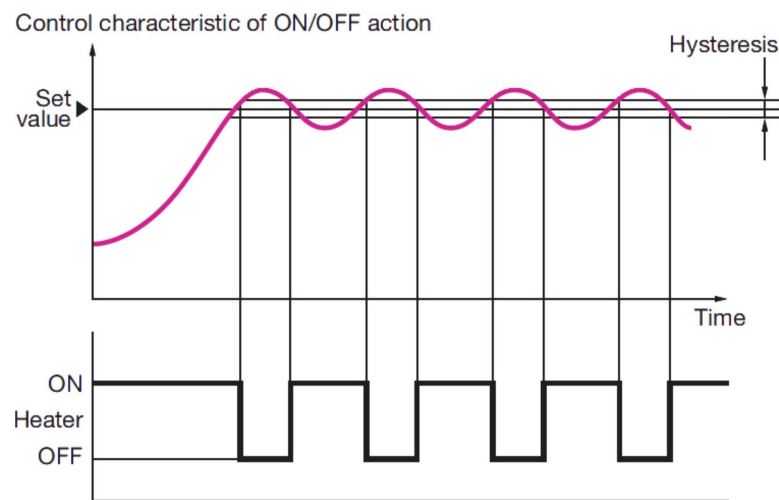
Figure 3.9: Control Characteristics of ON/OFF Control.

The objective is to keep the temperature within a range by sinusoidally increasing and decreasing the resistive load, depending on the thermal time constant of the material. In this thesis, a simplified model of the thermal requirements has been considered, where the set value of temperature does not change, and has been kept constant. As explained in this next sub-section, only the load resistance is varied with time, such that the duty cycle follows a sinusoidal trend.

3.4.3. DC Load Duty Cycle Modeling

For this thesis, the change in power drawn by the tractor implement has been modeled in the form of a constantly varying resistance. In the model, this has been achieved by using Variable Resistors, which change their values in Ohm, based on control signals designed to mimic the actual duty cycle of the selected load. As explained in the previous section, the load drawn by the Snowblower must remain constant over the entire range of operation. Therefore, the resistance of the load, which essentially models the power drawn from the

source, does not change with time. The following graph highlights the change in value of resistance with time for the Snowblower.
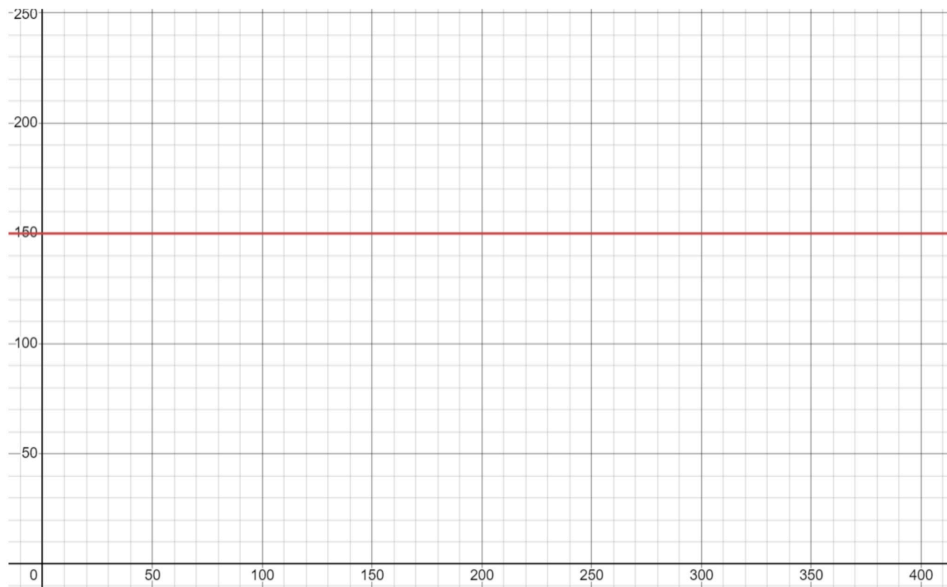
Figure 3.10: Snowblower Load Function.

The curve shown in Figure 3.10 has been easily realized using a basic mathematical equation.

$$R_{Snowblower}(t) = 150 \tag{3.1}$$

The variation of resistance of the snowblower with time being simple and straightforward, the load can easily be modeled as a DC value set at 150Ω, and fed into the Load Selector unit, which has been explained in later sections. The following image highlights the modeling of the Snowblower load curve.
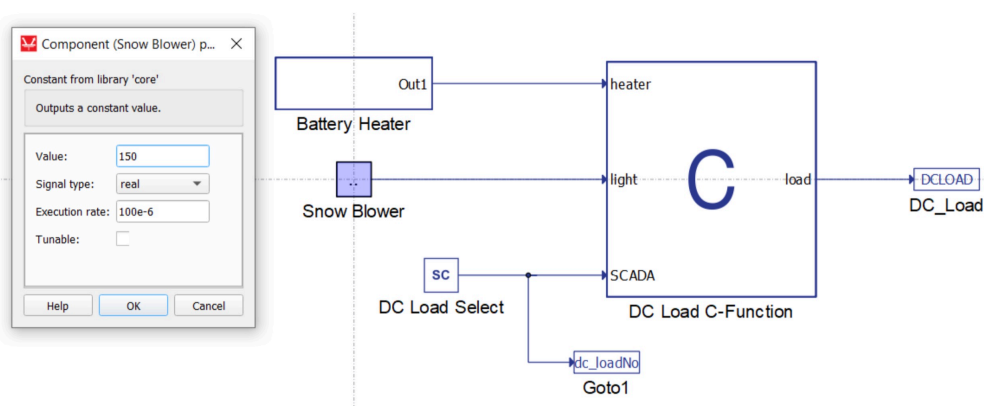
Figure 3.11: Snowblower Model Characteristics.

For the Battery Heater, the modeling approach is different. As highlighted in the previous section, the Battery Heater must operate based on an ON/OFF [6] control scheme. This means that the temperature must go up and down sinusoidally, after reaching steady state. In order to model this, the load resistance has been set to follow a sinusoidal trend, as heat dissipated is governed by the fundamental equation:

$$H = I_{DC}^2 Rt \tag{3.2}$$

However, for the sake of simplicity, only the steady state has been used for the model, and the transient state has been neglected. The following curve shows the change in resistance with time, for the Battery Heater.
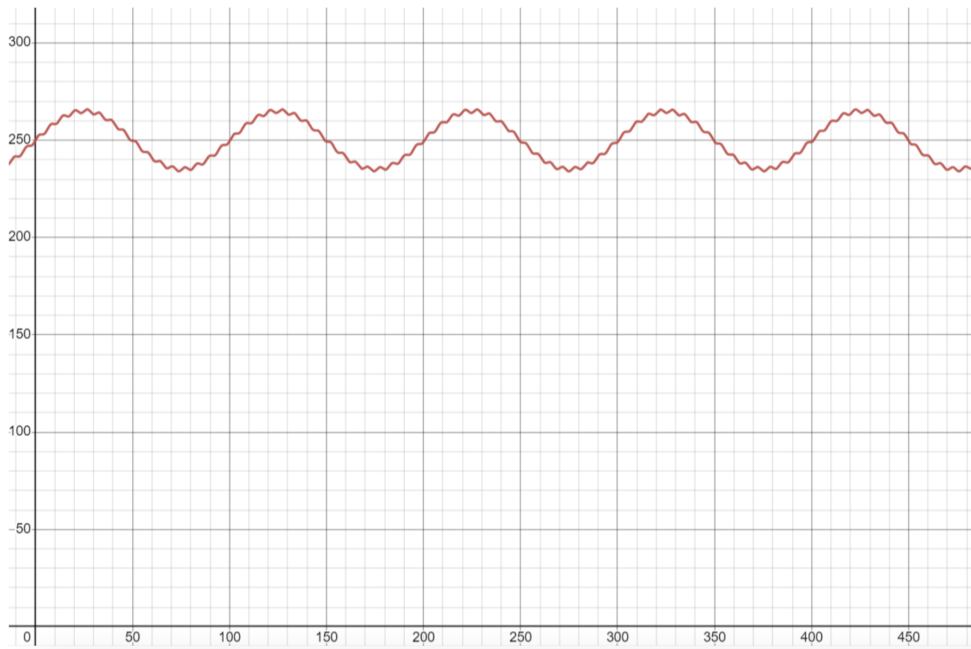
Figure 3.12: Battery Heater Load Function.

Finally, to model a bit of realism into the duty cycle curve of the Battery Heater, minor harmonics have been introduced to model inconsistencies in resistance. The following schematic explains how the load function has been modeled using fundamental signal blocks.
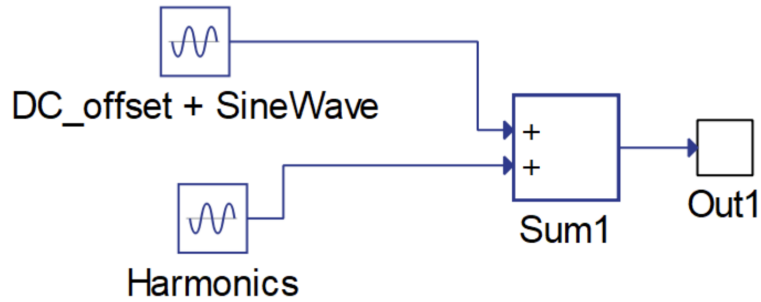
Figure 3.13: Modeling of Battery Heater Load Function.
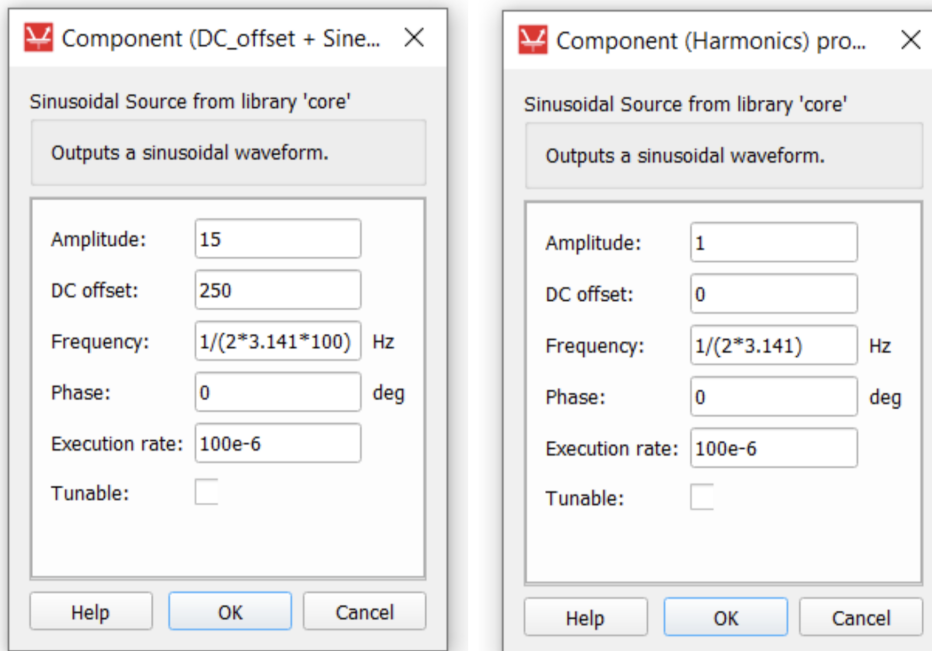
Figure 3.14: Battery Heater Model Characteristics.

The output from these sets of blocks is identical to the graph illustrated in Figure 3.12, and is achieved by employing the following mathematical function:

$$R_{BatteryHeater}(t) = 250 + 15[sin(\frac{2\pi}{100})t] + sin(t) \tag{3.3}$$

The next section illustrates some simulations that have been carried out for both the electrified implements. The current and voltage waveforms have been explored and compared, which give insights into how the Battery Heater and the Snowblower operate in the electrical system.

3.4.4. DC Load Duty Simulations

The following schematic highlights the modeling of the DC load. The DC load has been installed in parallel to the DC bus, and has been modeled as a simple variable resistor that receives the value of resistance from the Load Selector block, which governs the change in resistance as per the load modeling conditions shown in the previous section. The user must select which of the DC loads must be used, and the system varies the load of the variable resistor in real-time as per the modeled duty cycle curve.
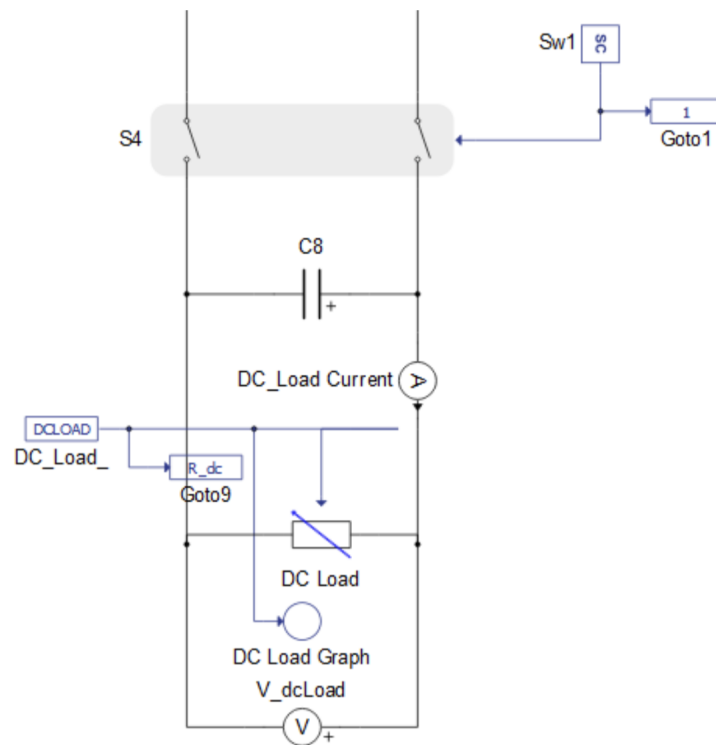
Figure 3.15: Electrical Model of the DC Load.

The DC load has been installed with a simple capacitive filter to cancel out higher order harmonics which might otherwise appear on the load and may potentially cause damage. Voltage and current measurement devices have been installed to gauge the electrical conditions during loading conditions for both the implements.

As highlighted in the previous sections, the loads under test here are the Battery Heater and the Snowblower. For the purpose of carrying out the DC Load simulations, the following conditions have been imposed:

- The voltage on the DC Bus is a steady 235V, being fully supplied by the generator.

- The speed of the Generator has been fixed at 101.5 rad/sec.

- A capacitive filter has been installed at the DC Load, with a capacitance of $5\mu F$.

- All signals have been sampled at 1 MSPS.

The first simulation result is that of the **Battery Heater**. The following graph shows the voltage and current characteristics when the Battery Heater is connected and power is supplied. As can be observed in the graph, after a small transient that lasts about 0.05s, the load voltage stabilizes at 235V, and remains steady. The current follows a similar trend, stabilizing at roughly 2.2A after undergoing a transient which lasts a few milliseconds.
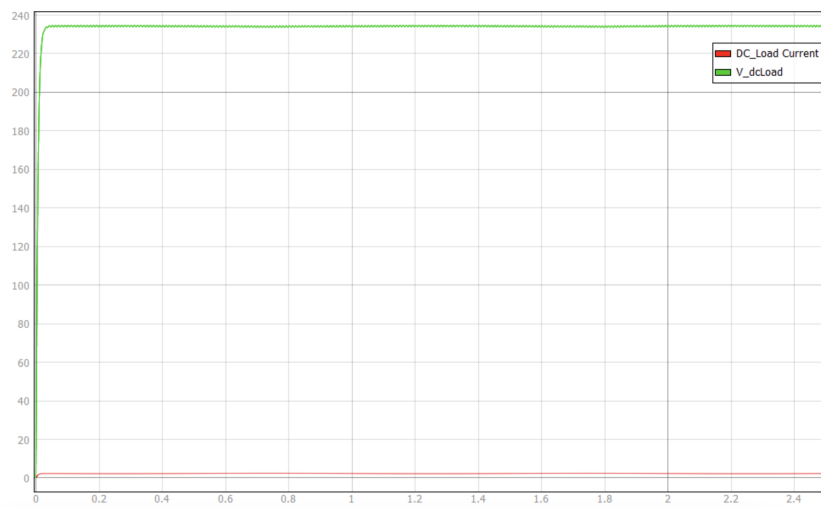
Figure 3.16: Voltage and Current Simulation of Battery Heater.

The following graph shows a closer look into the characteristics of the Battery Heater voltage. As observed, the voltage is not perfectly DC. Despite the filter, small ripples in the voltage exist, but of very small magnitude. The peak-to-peak ripple in the voltage comes out to about 0.45%, which shall be considered acceptable in this study.
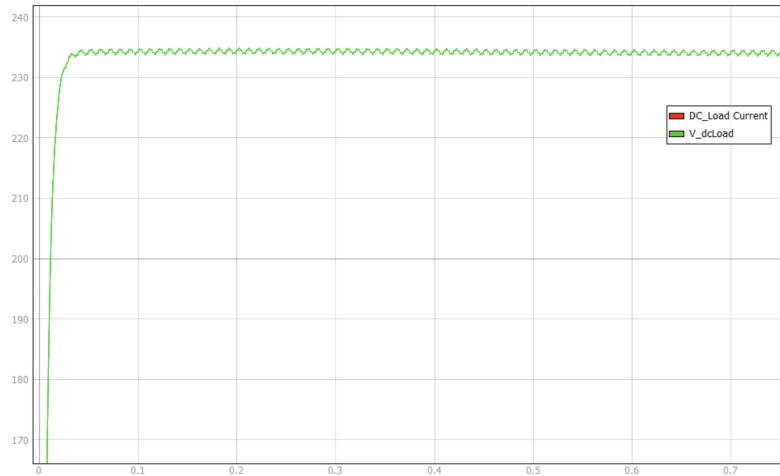
Figure 3.17: Voltage Simulation of Battery Heater.

The next graph shown is a closer look at the DC current in the Battery Heater. The current averages at a DC value of about 2.2A, and has small low order harmonic distortion. However, the peak-to-peak ripple in the current waveform is about 2.90%, which shall, again, be considered acceptable for the purpose of this study.
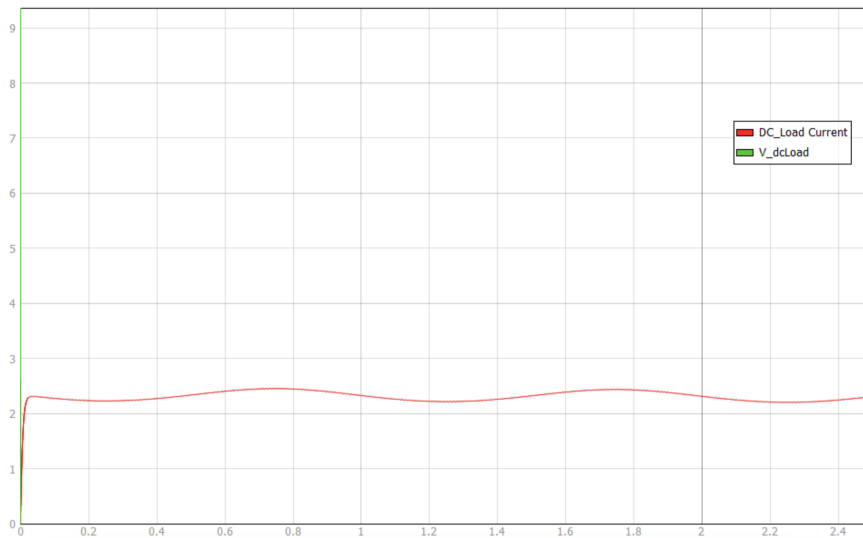
Figure 3.18: Current Simulation of Battery Heater.

The next set of results shown is that of the **Snowblower**. The output waveforms for this implement are much like that of the Battery Heater, in a way that the voltage waveform follows a similar transient that lasts about 0.05s, and then saturates at a DC value of 235V. The current follows a similar trend, and steadies at 1.95A.
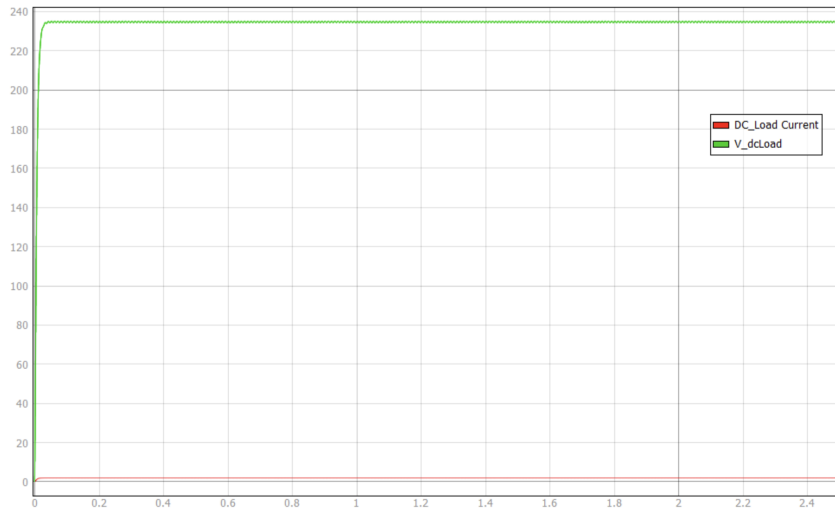
Figure 3.19: Voltage and Current Simulation of Snowblower.

The following graph highlights the voltage characteristics further in detail. In this case, the voltage waveform is not completely DC either, but has a small peak-to-peak ripple of 0.41%.
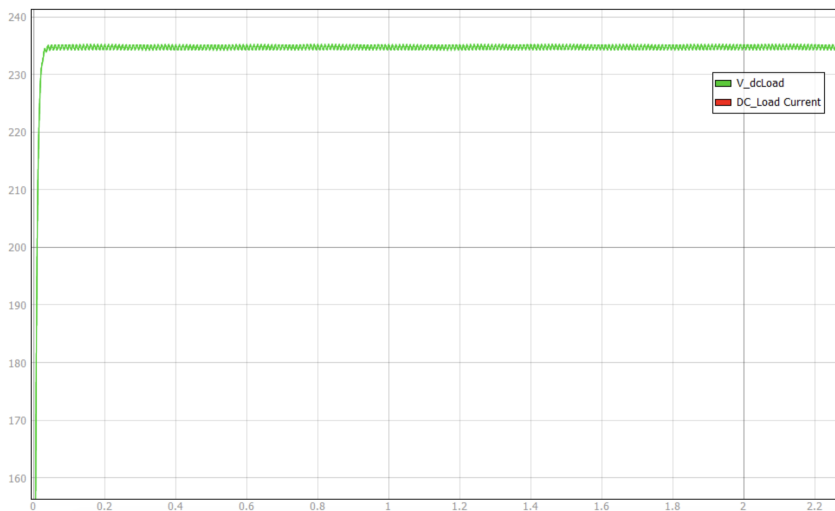
Figure 3.20: Voltage Simulation of Snowblower.

The current waveform for the Snowblower has been shown in the following graph. Unlike the Battery Heater, the Snowblower operates at a lower current value, and experiences a much lower peak-to-peak ripple. The value of the current ripple comes out to be 0.39%.
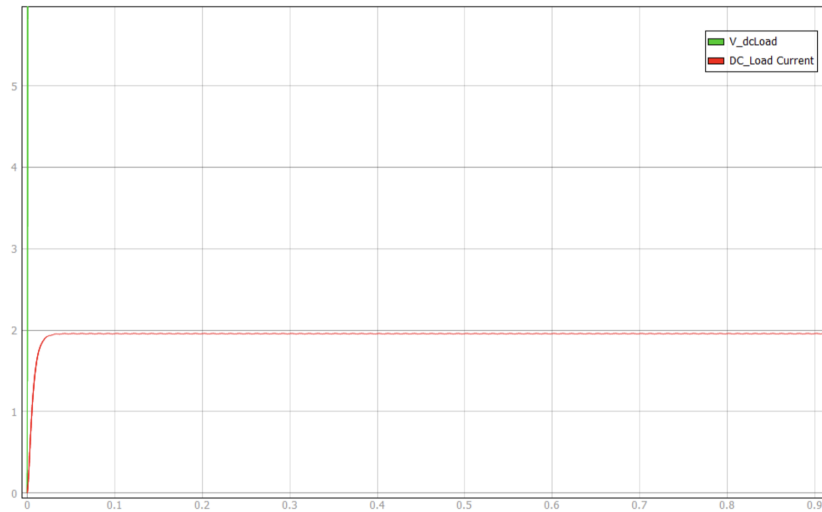
Figure 3.21: Current Simulation of Snowblower.

3.5.   1∼AC Loads

There are several types of 1∼ AC loads that can be utilized as electrified tractor implements. One common example is a standalone electric motor, which can be used to power various components such as pumps, fans, or augers. Electric motors offer efficient and reliable operation, making them suitable for tasks that require rotational motion or the transfer of fluids.

(a) HVAC System

(b) Electric Winch

Figure 3.22: Types of 1∼ AC Loads.

Another type of 1∼ AC load is an electric HVAC system, which can be employed for applications like cabin heating or defrosting. Additionally, single-phase AC loads such as electric winches or actuators can be utilized to facilitate tasks such as lifting or positioning

heavy loads. These loads can be integrated with the tractor's electrical system, allowing for versatile and efficient operation.

3.5.1.   Types of 1∼AC Loads Used

In this thesis, the only 1∼ load that has been considered for modeling is a PLC. Programmable Logic Controllers have the potential to greatly enhance the operation and control of electrified tractor implements. By using a PLC, the tractor operator can program and automate various tasks such as turning on and off the implement, adjusting the speed and torque, and monitoring the status of the equipment.

Figure 3.23: Programmable Logic Controller (PLC).

The PLC can also provide real-time feedback to the operator, allowing for precise control and increased efficiency. Additionally, PLCs can be integrated with sensors and other electronic devices to provide advanced functionalities such as fault diagnosis and predictive maintenance. Overall, the use of PLCs can improve the productivity and reliability of electrified tractor implements, leading to increased agricultural output and reduced operating costs.

3.5.2.   1∼AC Load Duty Cycles

A PLC is often supplied by a 240V AC input, and has an output of usually 24V DC. The current rating of a PLC may vary, and entirely depends on several different factors. The current rating of a PLC is influenced by the specific load requirements of the system it is intended to control. This includes the type and number of devices connected to the PLC, such as motors, solenoids, relays, or lights. Each device has its own current draw, and

the cumulative load determines the current rating needed for the PLC.
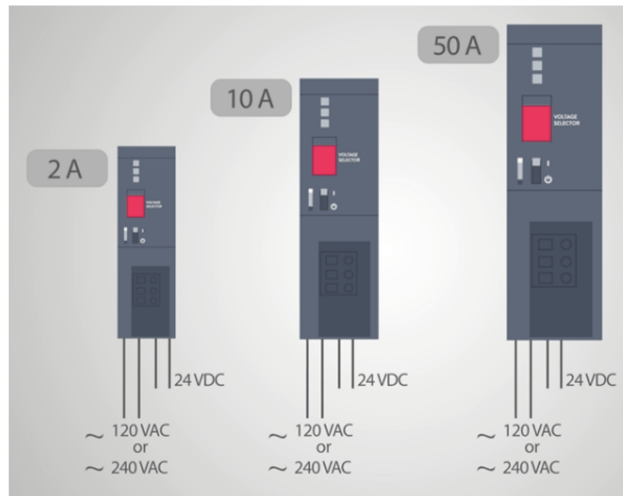
Figure 3.24: PLC Voltage and Current Ratings.

The nature of the application being controlled by the PLC also impacts its current rating. Industrial applications that involve heavy machinery, high-power devices, or complex processes may require a PLC with a higher current rating to handle the increased electrical load.
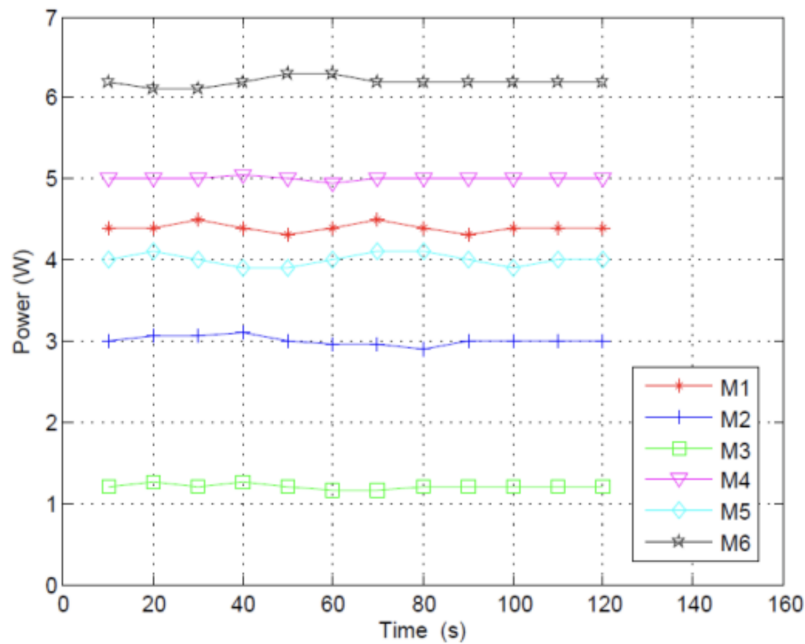
Figure 3.25: Power Consumption of different PLCs.

The graph above highlights the general trend of power consumption [4] of multiple PLCs,

under normal operating conditions. While the graph has been referenced from a paper discussing low-power PLC units, this trend in power consumption, and therefore, the modeled load can be mathematically described as a constant resistance.

3.5.3.   1∼AC Load Duty Cycle Modeling

As with the case of some of the other simpler implements, the load function of the PLC is simple, and does not vary with time. For the sake of simplicity, the value of the PLC resistance has been set to 100Ω, and does not change. The following graph highlights the curve implemented to model the load duty cycle of the PLC.
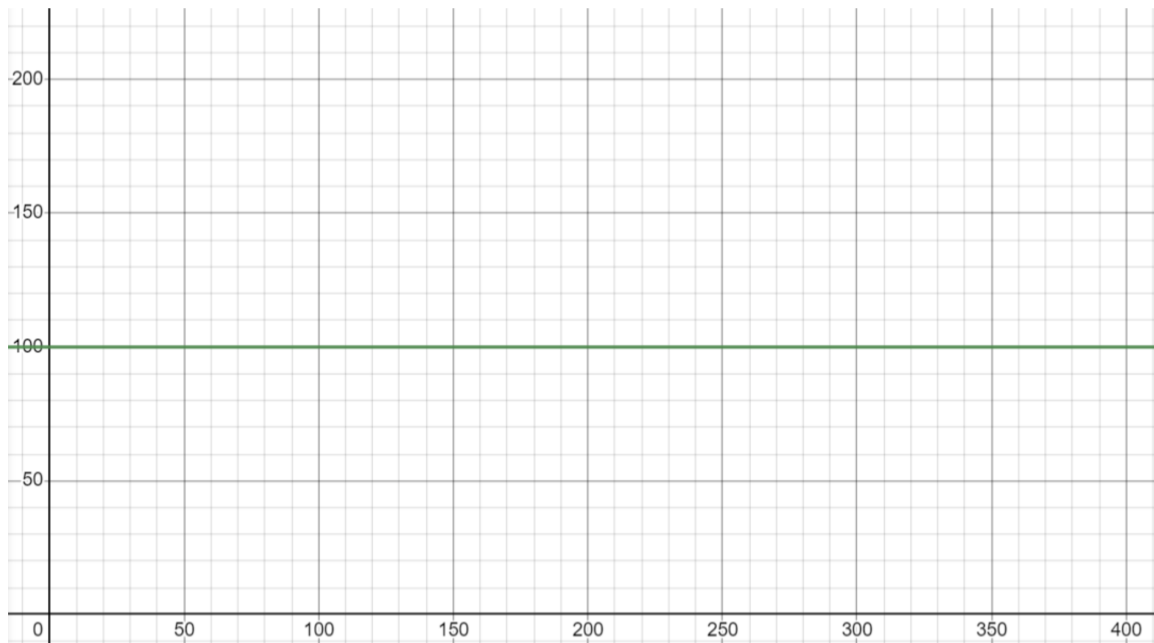
Figure 3.26: PLC Load Function.

The curve shown in Figure 3.26 has been easily realized using a basic mathematical equation:

$$R_{PLC}(t) = 100 \tag{3.4}$$

The next section highlights the result of some simulations for the 1∼ AC load. Aspects of current and voltage waveforms have been explored, along with the modeling of the load in Typhoon-HIL Schematic Editor.

3.5.4. 1∼ AC Load Simulations

For modeling the 1∼ load in Typhoon-HIL Schematic Editor, the following approach has been adopted, as illustrated in Figure 3.27. Voltage drawn from the DC Bus is fed into a single-phase voltage source inverter, which has been designed to produce a single-phase sinusoidal voltage of 220V peak. As shown in the model, the load receives a fixed value of resistance throughout the operation, which has been set at 100Ω. Suitable current and voltage measurement devices have been employed to measure corresponding waveforms during operation.
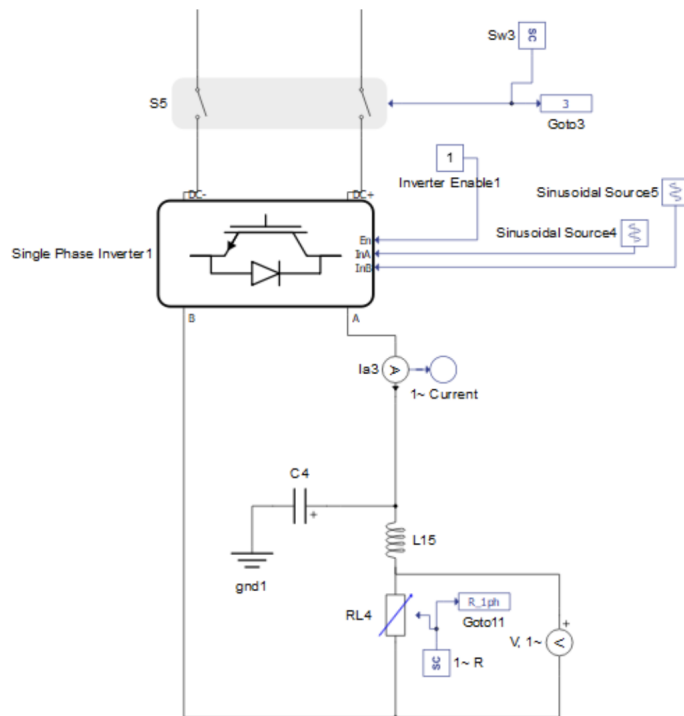
Figure 3.27: Electrical Model of the 1∼ AC Load.

The 1∼ load has been installed with a basic low-pass filter, which aims to filter out higher order harmonics which might otherwise cause distortion in the output waveforms. The following graphs illustrate the effect of operating the 1∼ AC load without using properly tuned filters, or inverter parameters. As can be seen, the bottom-right graph highlights the output waveforms of the 1∼ load, which show dominant harmonic distortions in both voltage and current waveforms. These harmonics, injected by the power electronics controller, enter the DC part of the circuit, thereby causing significant distortions in both the DC voltage, as well as the DC current. This behavior can be observed in the top-left graph in Figure 3.28.
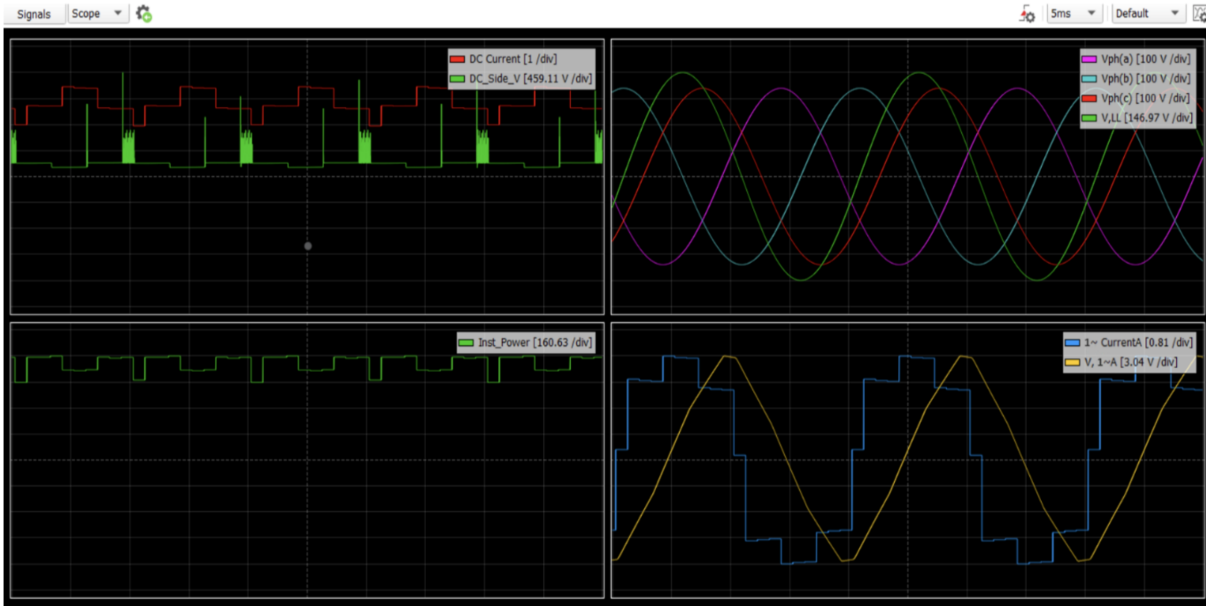
Figure 3.28: Harmonic Distortions in the Network without Filter.

For the purpose of carrying out the 1∼ load simulations of the PLC, the following conditions have been imposed:

- The voltage on the DC Bus is a steady 235V, being fully supplied by the generator.

- The speed of the Generator has been fixed at 101.5 rad/sec.

- A low-pass filter has been installed at the 1∼ load, with a shunt capacitance of 55μF, and a series inductance of 35 mH.

- The single-phase voltage-source inverter operates with a carrier frequency of 30 kHz, along with a dead-time period of 0.1 μs.

- All signals have been sampled at a rate of 1 MSPS.
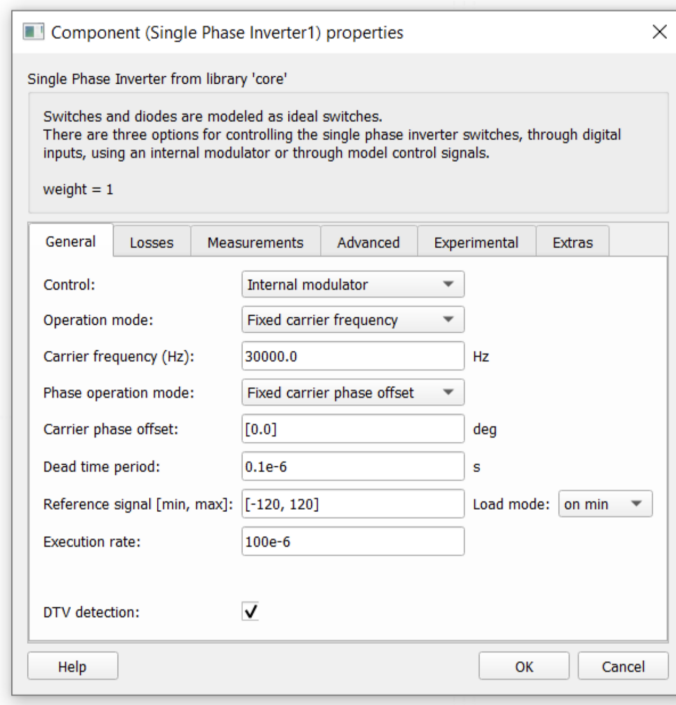
Figure 3.29: Model Properties of the Single-Phase Inverter.

The following graph shows the output waveform of voltage and current, when the 1 load is powered. As observed, the voltage and current undergo a short transient, after which they reach their steady state values. On comparison with Figure 3.28, both the waveforms have nearly no harmonic content, and behave as near-ideal waveforms. Additionally, it can be observed that there is almost zero phase delay between the current and voltage, which perfectly models the non-reactive behavior of the load.
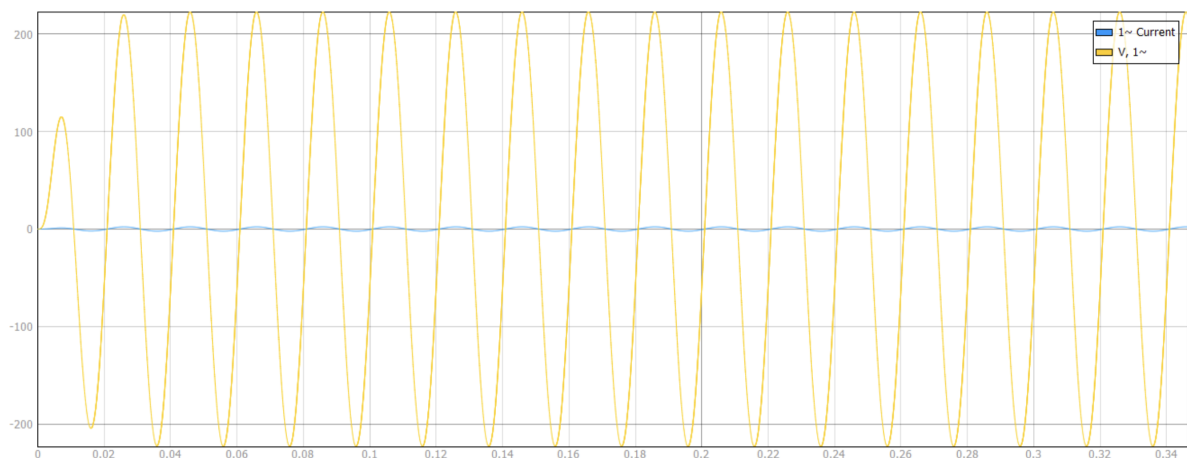
Figure 3.30: Voltage and Current Waveforms across the 1∼ Load.

The following curve illustrates the voltage waveform of the 1∼ load. The transient can be observed better. As mentioned, the voltage waveform is near-ideal, owing to properly tuned filters, high switching frequency, and a reduced dead-time period. On inspecting the voltage waveform further, no distortions can be observed, which is illustrated by Image 3.32. It can be seen that the transient lasts for only one time period, after which the voltage across the load reaches peak values of 220V.
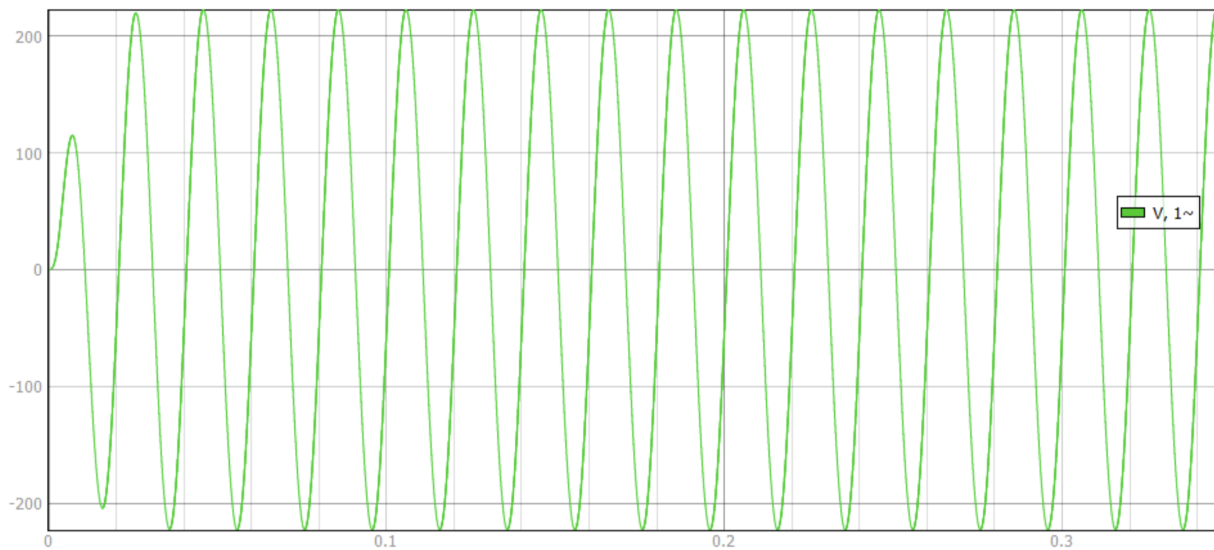
Figure 3.31: Voltage Waveform across the 1∼ Load.
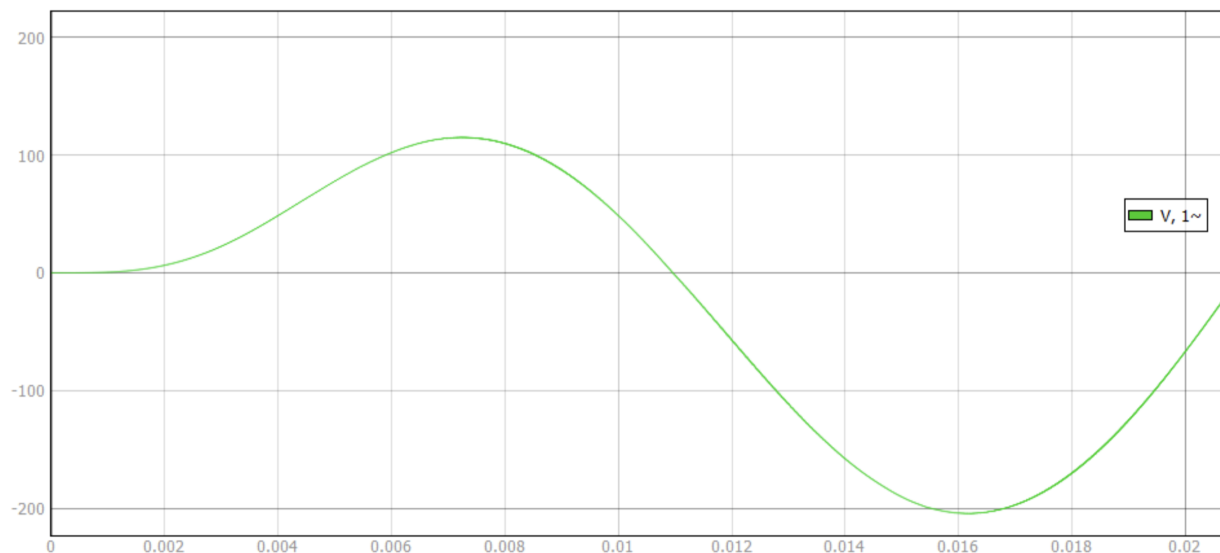
Figure 3.32: Close-up of the Voltage Transient at the 1∼ Load.

The following graphs illustrate the current output waveforms through the 1∼ AC load.

The transient can be better observed in these graphs, after which the load current reaches peak values of 2.2 A. As with the voltage output, the current waveform has little to no harmonic distortion, solely due to good circuit optimizations. However, on inspecting closely in Figure 3.34, it can be observed that the current waveform does come out slightly distorted, despite having a very high sampling rate of 1 MSPS. Regardless, this setback does not affect the performance of the overall system in any significant manner.
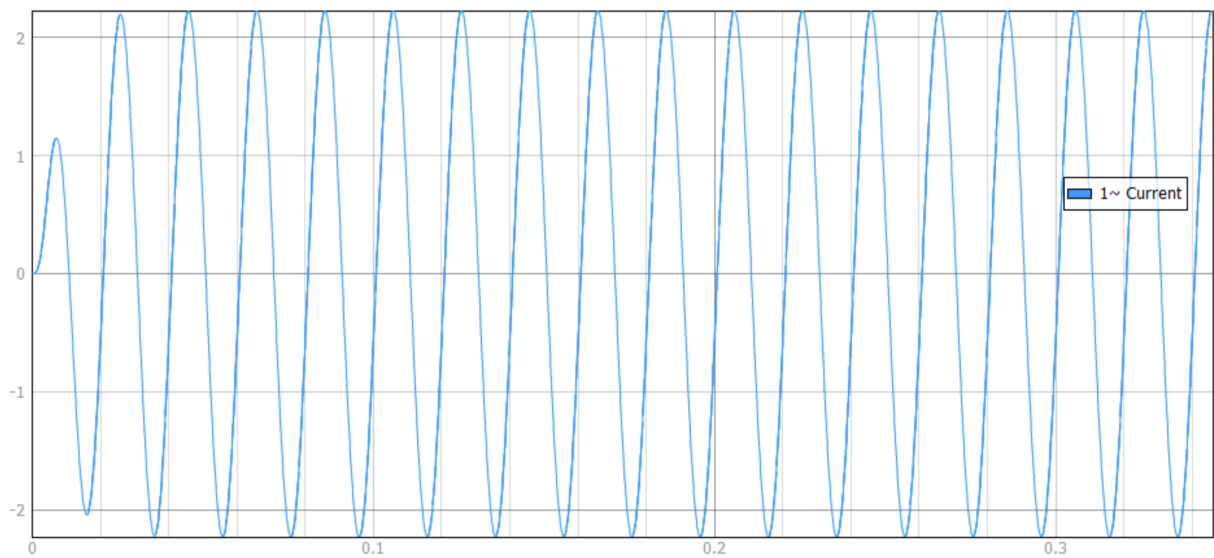
Figure 3.33: Current Waveform through the 1∼ Load.
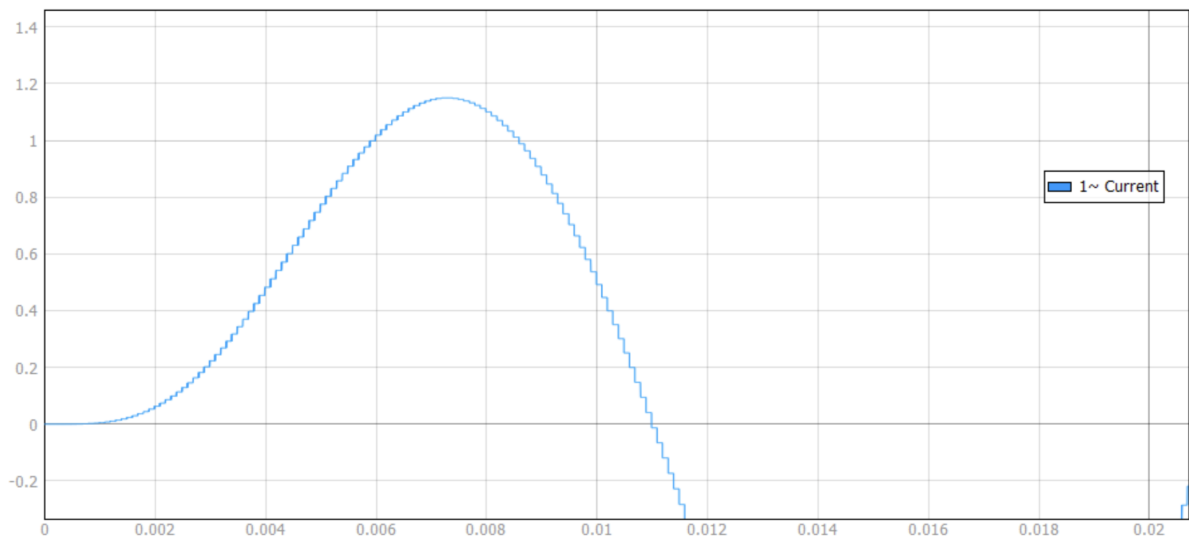
Figure 3.34: Close-up of the Current Transient through the 1∼ Load.

After having discussed the modeling and simulations of the 1∼ PLC load, the next section

covers some of the common 3∼ AC loads used for agricultural applications. The loads used for this study have been explored and explained in detail, along with the approach adopted for modeling and simulating electrical quantities.

3.6.   3∼AC Loads

There are several types of electrified tractor implements that can be implemented as 3∼ AC loads. One example is an electric plow, which uses an electric motor to power the plow blades. Another common example is an electric harrow, which uses electric motors to rotate the harrow disks. Electric seeders are also a common implement, which use electric motors to power the seed dispensing mechanism. Additionally, there are electric cultivators, which use electric motors to rotate tines and prepare the soil. Overall, the use of electrified tractor implements provides farmers with more efficient and sustainable options for their agricultural practices.

(a) Harrow   (b) Pesticide Sprayer

Figure 3.35: Types of 3∼ AC Loads.

One of the major advantages of electrified tractor implements over their conventional mechanical counterparts is that they are much quieter and emit zero emissions. This makes them ideal for use in urban or residential areas where noise and pollution are major concerns. Additionally, electric motors provide precise control over the speed and torque of the implement, allowing for more accurate and efficient operation. The next section covers the 3∼ AC loads that have been considered for this study, and the approach adopted towards their modeling and implementation.

3.6.1. Types of 3~AC Loads Used

Apart from some common farming implements that have been mentioned in the previous section, there are plenty of other devices that can be adopted as 3~ AC loads. Therefore, this thesis has considered the following implements for modeling, implementation and simulation:

- Manure Spreader

- Cultivator

- Atomizer

- Seed Spreader

Manure Spreader: A Tractor manure spreader implement is a useful agricultural tool that is used to distribute manure across fields. It typically uses an electric motor to power a conveyor belt or chain that moves the manure from the hopper to the spreader mechanism. This allows farmers to efficiently distribute manure across their fields, providing valuable nutrients to the soil.

One of the primary applications of an electrified tractor manure spreader implement is in crop farming. By spreading manure across their fields, farmers can improve soil fertility, increase crop yields, and reduce the need for synthetic fertilizers. This results in healthier plants and a more sustainable farming operation.

(a) Manure Spreader in Action

(b) Manure Spreader Side View

Figure 3.36: Manure Spreader.

For this study, the John-Deere MS12 Series Manure Spreader [9] has been used as reference. The MS12 Series employs a low-power spreading mechanism that efficiently discharges manure across the field. This implement was easy to model, and was found to be suitably relevant for use in the model.

Cultivator: A cultivator is a farming tool used to prepare soil for planting crops. It typically consists of a series of curved metal teeth or blades that are attached to a frame, which break up clumps and loosen the soil, creating a smooth and level seedbed. Cultivators are commonly used in farming operations where the soil needs to be tilled, aerated, or loosened in preparation for planting. They can be used for a variety of crops, including vegetables, grains, and fruits.

One of the advantages of a cultivator is that it is an efficient and cost-effective way to

prepare soil for planting. It is much faster and requires less labor compared to hand-tilling or using a hoe. Additionally, cultivators can be easily adjusted to fit the specific needs of different crops and soil types. Another advantage of cultivators is that they can help control weeds. By tilling the soil and breaking up weed roots, cultivators can help prevent weed growth and reduce the need for herbicides.

(a) Structure of the Cultivator

(b) Cultivator in Action

Figure 3.37: Cultivator.

In this thesis, the John-Deere 2230FH Floating Hitch Field Cultivator [10] has been modeled. The 2230FH is a highly sophisticated tilling machine that has multiple functionalities and offers excellent optimizations. It is a low-power device, and can be operated in tandem with a hydraulic system to fine-tune work output.

Atomizer: A tractor atomizer, also known as a sprayer or a crop duster, is a farming tool used to apply pesticides, herbicides, or fertilizers to crops. It typically consists of a

tank to hold the liquid, a pump to pressurize the liquid, and nozzles to disperse the liquid in a fine mist or spray. The implement is attached to a tractor and driven over the fields, spraying the crops evenly with the liquid.

One of the advantages of a tractor atomizer is that it allows for efficient and precise application of chemicals to crops. The spray can be adjusted to the appropriate concentration and coverage, reducing the risk of over- or under-application. This helps farmers control pests and weeds, and also ensures that crops receive the necessary nutrients for optimal growth.

(a) Atomizer in Action   (b) Tank and Nozzle of the Atomizer

Figure 3.38: Atomizer.

The John-Deere R4023 Sprayer [11] has been selected for this thesis, owing to its simple construction and impressive versatility. It is a low-power equipment that can be easily electrically reduced to a motorized pump, and has therefore been selected for modeling.

Seed Spreader: A seed spreader is a farming tool used to distribute seeds evenly across a field. It typically consists of a hopper that holds the seeds, and a mechanism that disperses the seeds onto the soil. One of the advantages of a seed spreader is that it allows for efficient and precise seeding of crops. The hopper can be filled with a specific quantity of seeds, and the mechanism can be adjusted to disperse the seeds at the appropriate rate and coverage. This ensures that the seeds are distributed evenly, which helps to promote healthy and uniform crop growth.

Another advantage of a seed spreader is that it is a time-efficient and cost-effective way to seed crops. It is much faster than hand-seeding, and can cover large areas of land quickly and efficiently. Additionally, using a seed spreader can reduce the amount of seed needed, which can lower the overall cost of production.

(a) Random Spray Pattern   (b) Radial Spray Pattern
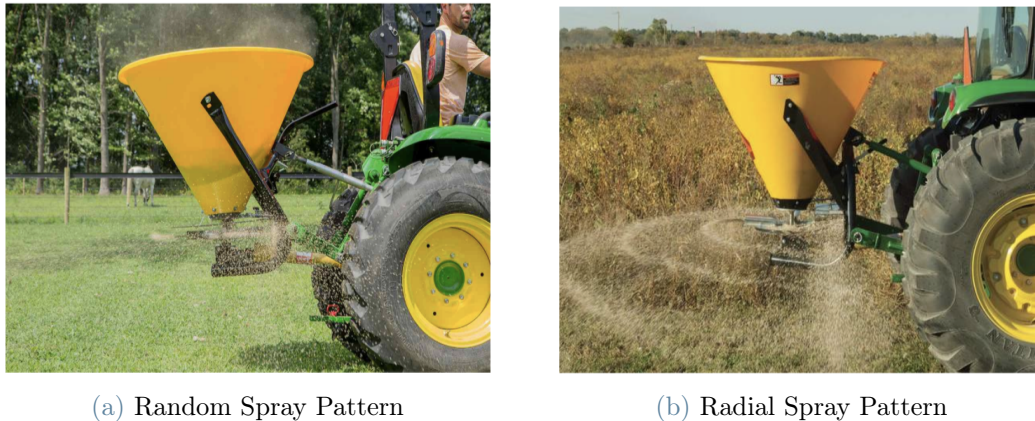
Figure 3.39: Seed Spreader.

The John-Deere SS20B Series Broadcast Spreader [12] has been chosen for this study, as it offers simple modeling, good operating conditions, along with great versatility with selection of seeds.

The next section ventures into the typical duty cycle characteristics of these implements. Unlike previously shown loads in this study, these heavy-duty attachments offer a wide variety of complexity in terms of power demand and usage. An attempt has been made to understand the modeling approach of these machines, and how they could possibly behave electrically.

3.6.2. 3~AC Load Duty Cycles

The implements used for this study undergo highly varied duty cycles, which have been studied and modeled according to real-world data. The power duty cycle of tractor implements depends on several factors, including the type of implement, the power that can be drawn from the source, the soil or terrain conditions, and the speed at which the tractor is operating.

Different implements require different amounts of power from the tractor, and some may require more power than others. For example, a heavy tillage implement may require more power than a light seeding implement. The duty cycles referenced for this thesis are carried out based on specific driving cycles, imposed by DLG (Deutsche Landwirtschafts-Gesellschaft).

Manure Spreader: The manure spreader is a relatively simple device that operates on low system power. The following graph [23] highlights the duty cycle of a Manure Spreader, operating on a standardized Z6MS Cycle. As illustrated in the figure, both the

PTO torque and the hydraulic power follow near-cyclic trends. The curve of interest here is the "Hydraulic Power", which is, in our case, supplied by the 3   system running the pump.
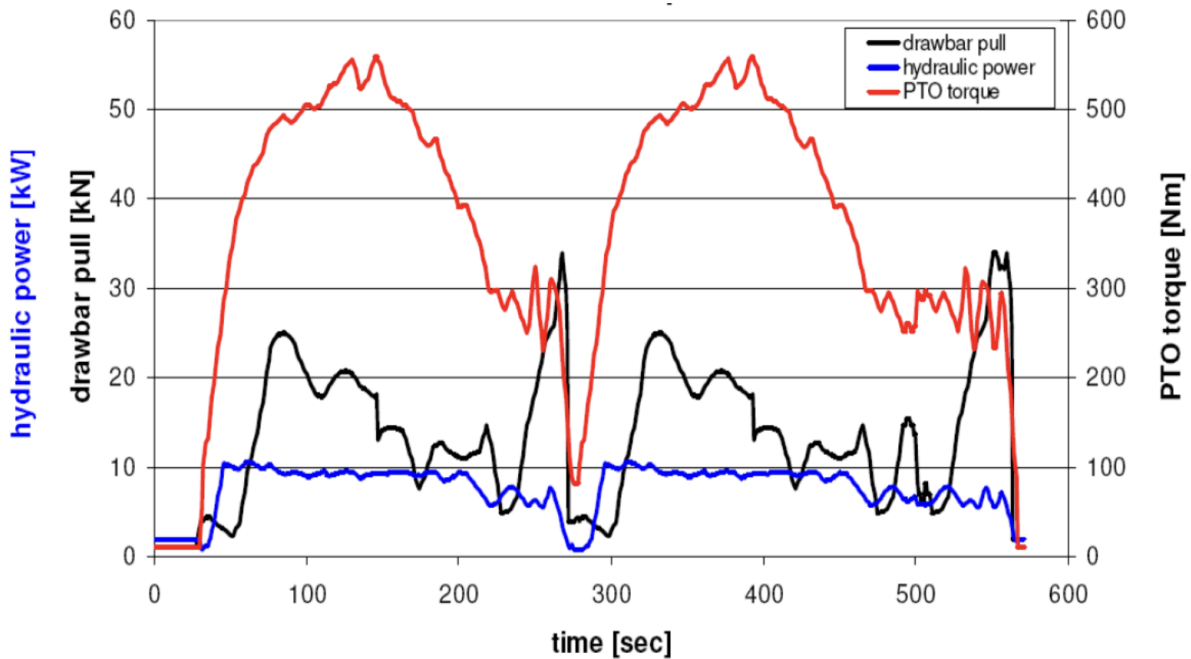
Figure 3.40: Real-World Duty Cycle of an Agricultural Manure Spreader.

It can be observed that the hydraulic power rises from zero, until an average DC value, around which the power oscillates for some time. Towards the end of the cycle, the power drops back to almost zero, after which, another cycle starts. As shown in the graph, it can be observed that the cycle period of operation is about 280 seconds.

Cultivator: The Cultivator operates on a much more complicated load cycle, as the power requirements for this device are relatively higher. The Cultivator's duty cycle is characterized by sharp spikes in power demand, [22] with intermittent drops in power, followed by a short period of low power consumption. The graph illustrated below is based on the standardized Z1G Cycle, and clearly highlights the cyclic but high power demand of the implement.
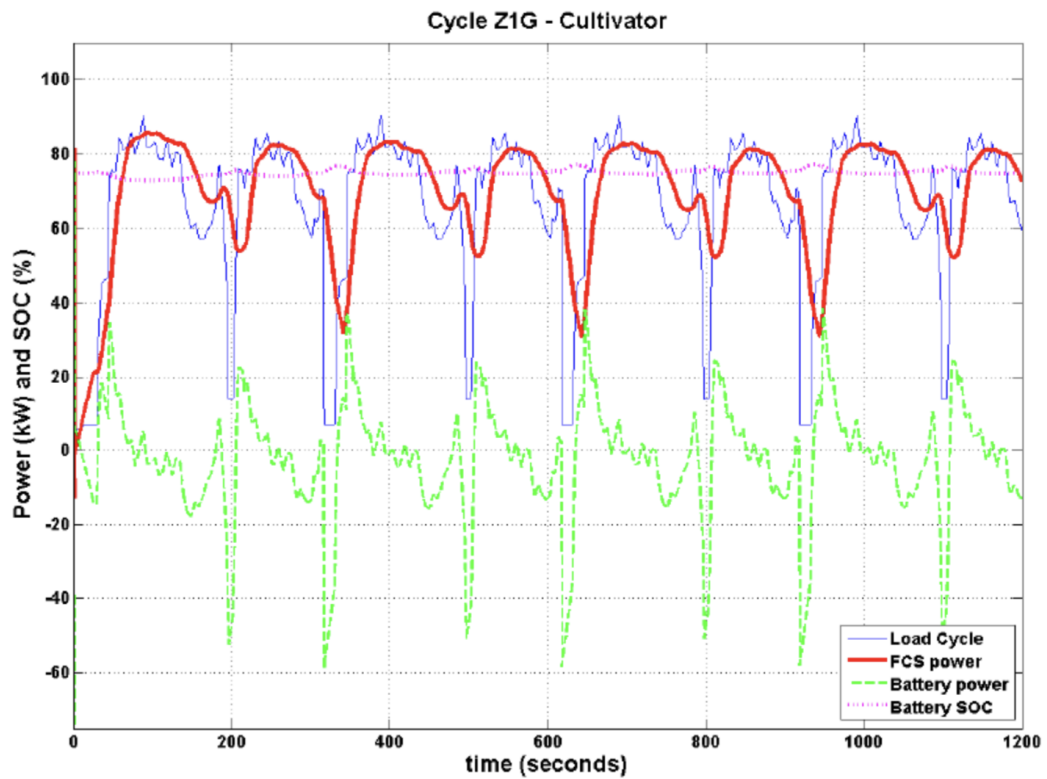
Figure 3.41: Real-World Duty Cycle of an Agricultural Cultivator.

The curve of our interest is the "Load Cycle", indicated in blue. As observed in the graph, the Cultivator's power demand can be interpreted as approximately cyclic, with a time period of about 310 seconds.

Atomizer: The Atomizer's duty cycle has been illustrated below, and this trend is in compliance with appropriate DLG cycles. In the graph shown, the blue curve is the PTO power, and is of interest to us. [24] It can be observed that the overall cycle of the Atomizer maintains a steady average DC value.
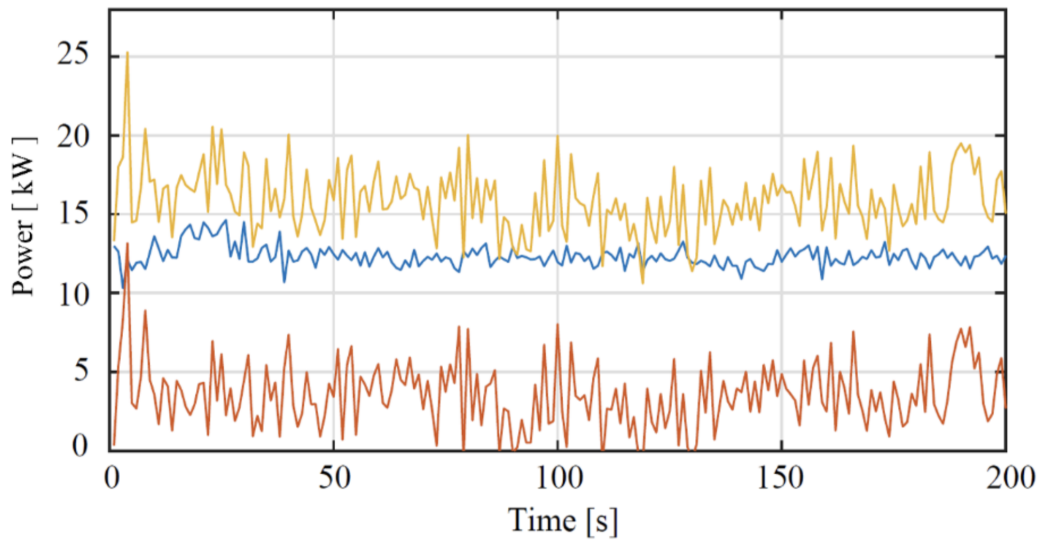
Figure 3.42: Real-World Duty Cycle of an Agricultural Atomizer.

There are sharp variations throughout the cycle, which deviate the power value away from the DC average. However, the amplitude of such deviations is small compared to the average DC value, and a significant variation is only observed at the start of the cycle. For practical purposes, this sharp deviation can be neglected, and we can assume that the load cycle follows cyclic but constant variations throughout the operating range.

Seed Spreader: The Seed Spreader is a simple device, but operates on a slightly complex duty cycle. As seen in the following graph, the operation of the Seed Spreader's load curve is characterized by somewhat sinusoidal curves, along with sharp variations of relatively smaller magnitudes.
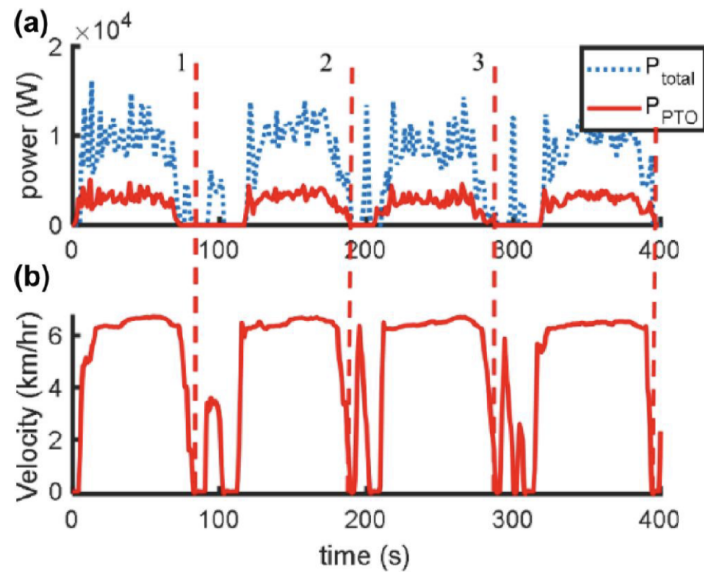
Figure 3.43: Real-World Duty Cycle of an Agricultural Seed Spreader.

As with other implements, the operation of the Seed Spreader can be estimated to be cyclic. In this case, the time period comes out to be approximately 100 seconds, which will be used for modeling this load. The next section takes a look into how these loads have been mathematically quantified, and the approaches adopted to model them into the overall system.

3.6.3.   3∼AC Load Duty Cycle Modelling

As the case with previously explained tractor implements, an attempt has been made to understand the duty cycle characteristics of the aforementioned 3∼ loads, and model them into a mathematical system. For the purpose of implementing those mathematical functions into the Typhoon-HIL schematic, several different types of signal processing blocks have been employed to achieve the desired characteristics. Explained below are the procedures adopted towards modeling the four selected 3∼ loads from the point of view of mathematics, as well as signal processing.

Manure Spreader: Referring to the actual real-world duty cycle of the Manure Spreader explained in the previous section, the following graph attempts to simplify, and to some extent, linearize the behavior of the load function.
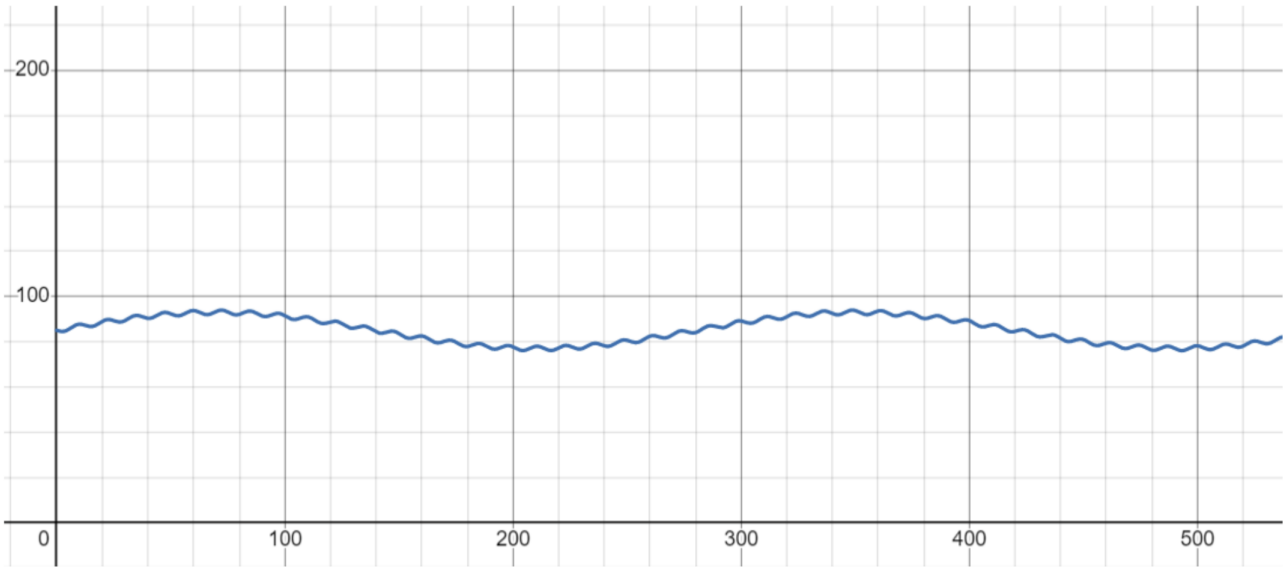
Figure 3.44: Modeled Load Function of the Manure Spreader.

As highlighted in the graph, the load function follows a cyclic trend, and has higher order harmonics to mimic the real-world characteristics of the Manure Spreader. Keeping the fundamental behavior of the function identical to the actual curve, the function has been designed with a period of 280s. The following mathematical function can be used to describe this curve:

$$R_{ManureSpreader}(t) = 85 + 8sin(\frac{2\pi}{280}t) - sin(0.5t) \tag{3.5}$$

It must be noted that this function is a simple attempt to mimic the behavior of the actual curve, and not replicate it exactly, which would otherwise require advanced signal processing beyond the scope of this thesis. However, the following explanation sheds more light into how this function could be approximated to be assumed practically similar to the actual load function.

The figure shown below illustrates two different sections of the load function, highlighted in yellow and orange. The yellow section in the modeled function attempts to mimic the average DC characteristics of the actual function, while compensating for the temporary "off" period.
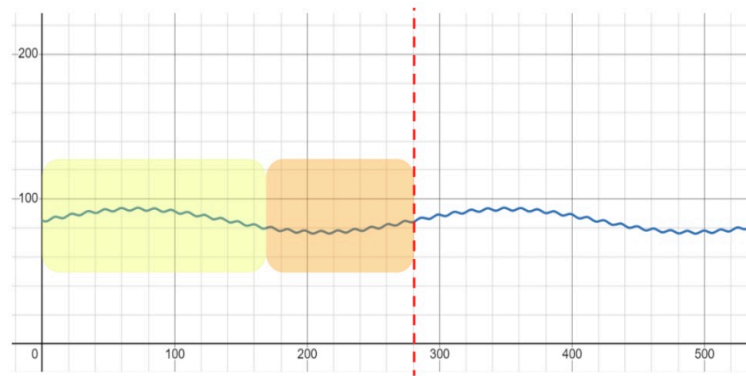
(a) Modeled Manure Spreader Load Function
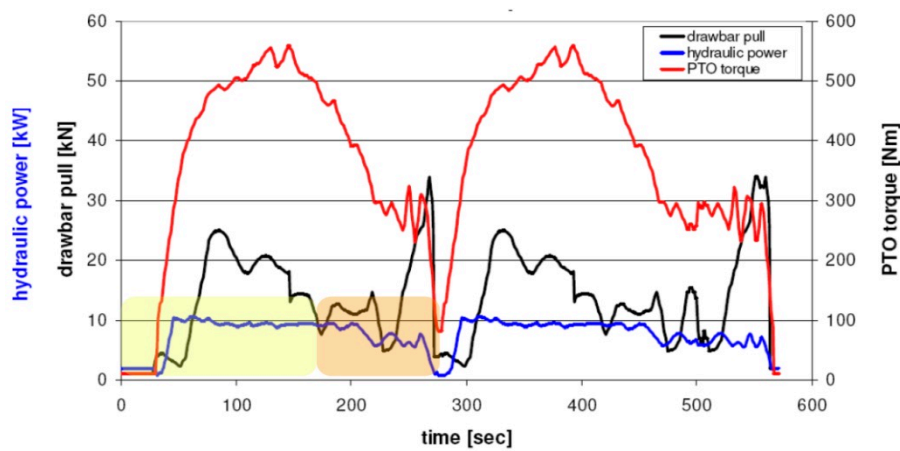
(b) Expected Duty Cycle in the Literature

Figure 3.45: Duty Cycle Mapping of the Manure Spreader.

Similarly, the section highlighted in orange tried to compensate for the dip in the actual curve, along with the temporary drop to "off" state. Over the entire period, the modeled function tried to keep up with the average trend of the real-world duty cycle.

This function has been implemented in Typhoon-HIL Schematic Editor using basic signal processing blocks, as shown in the image below. The main sinusoidal wave generator incorporates the properties shown in Figure 3.46, while the harmonics have been modeled using another sine-wave generator block.
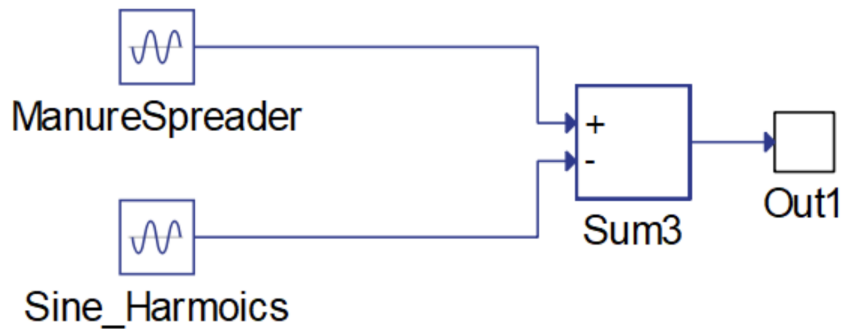
Figure 3.46: Modeling of the Manure Spreader.
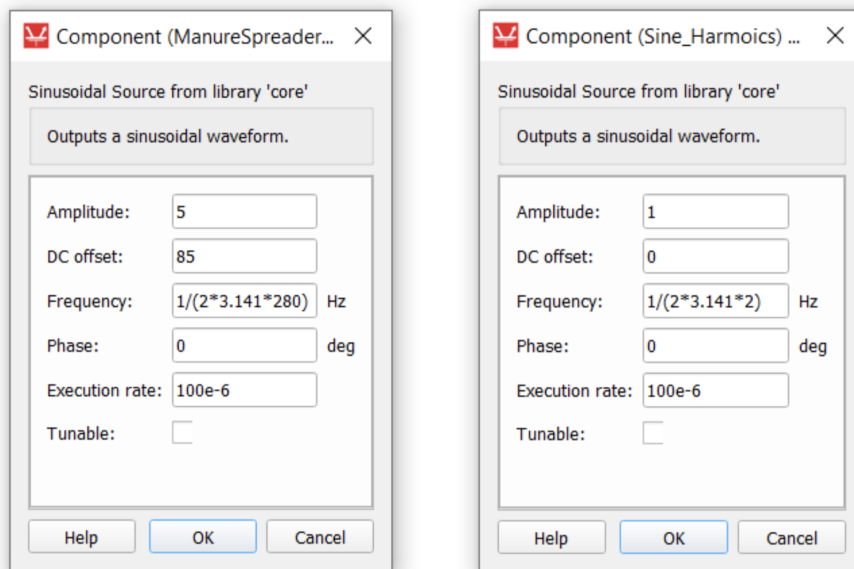
Figure 3.47: Manure Spreader Model Characteristics.

Both the signals are added into a sum block, and then fed into the Load Selector for further processing. The Load Selector has been explained in detail in later sections.

Cultivator: As observed from the duty cycle curve of the Cultivator, the trend of the curve is cyclic, but highly erratic and sharp. The following curve aims to model such a behavior in a mathematical context.
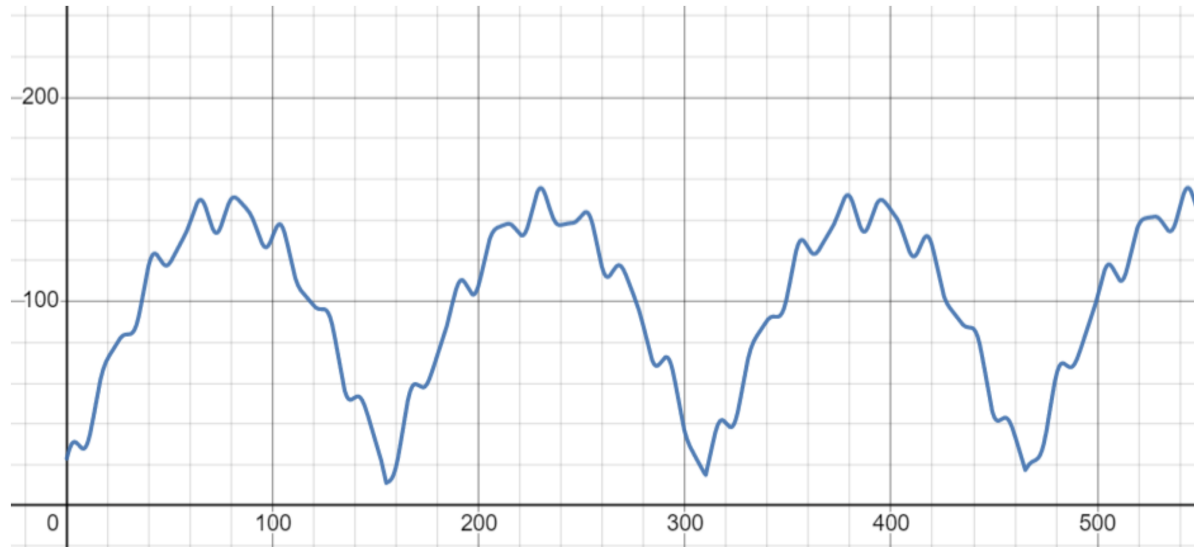
Figure 3.48: Modeled Load Function of the Cultivator.

While the load function does not exactly map the precise behavior of the Cultivator duty cycle, it is a fairly accurate estimation of its characteristics. The graph illustrates that the trend of the load function is cyclic, and has sharp higher order harmonic distortions. The function has been modeled to keep the fundamental properties identical to the actual duty cycle, and therefore, the period of this function has been set to 310s. This function can be expressed using the following mathematical function:

$$R_{Cultivator}(t) = 15 + 130|sin(\frac{2\pi}{310})t| + 3sin(0.5t) + 8cos(0.3t) \qquad (3.6)$$

The images shown below attempt to establish a correlation between the modeled function and the real-world duty cycle. The yellow parts in both the graphs correspond to the time period of one cycle, and it can be observed that there is a fair amount of similarity, and the designed function can be used to model this load in the electrical system.
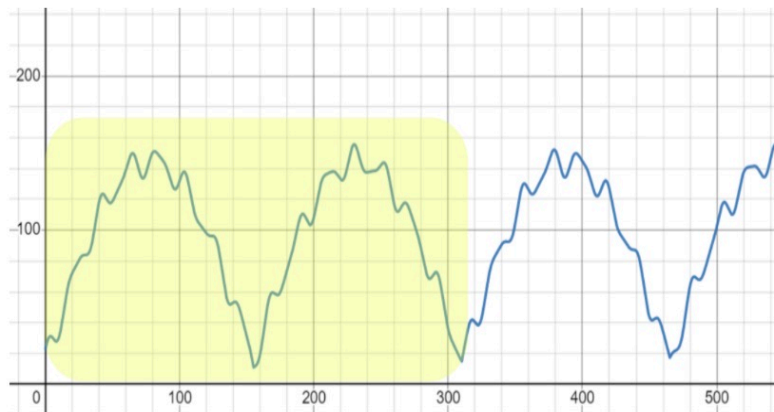
(a) Modeled Cultivator Load Function
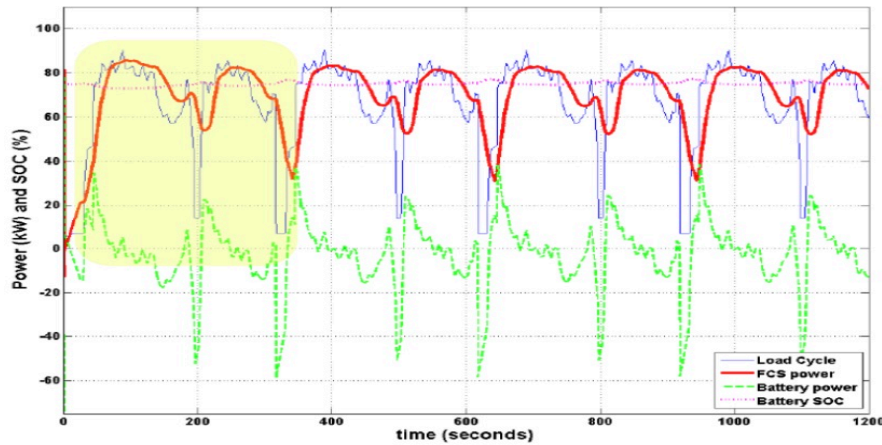
(b) Expected Duty Cycle in the Literature

Figure 3.49: Duty Cycle Mapping of the Cultivator.

In order to implement this load function in the Typhoon-HIL Schematic Editor environment, the following model has been employed using fundamental signal processing blocks, much like previous cases. The fundamental component of the function has been deployed by using a sine-wave generator, having a DC offset and sinusoidal characteristics shown in Figure 3.50.
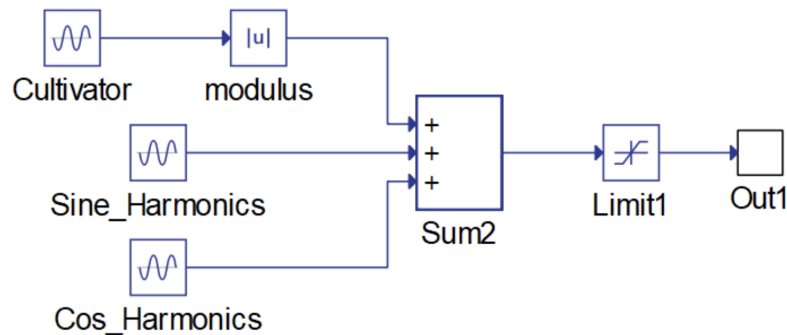
Figure 3.50: Modeling of the Cultivator.
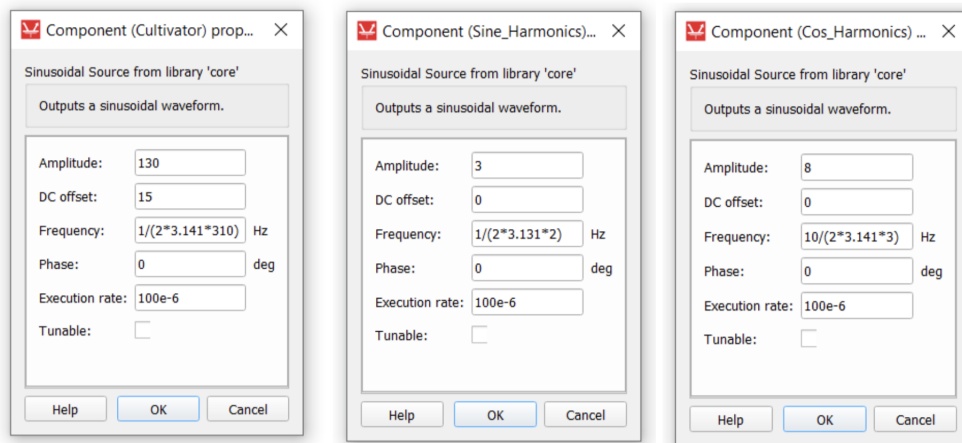
Figure 3.51: Cultivator Model Characteristics.

Two additional sine-wave generators have been used to mimic the harmonics in the load function, and have been realized using mathematical properties described in their corresponding settings windows in the figure above. All three signals are combined using a sum block, after which the signal is sent to a saturation unit, which ensures that the value of the load function does not fall below 15Ω at any given point during the cycle.

Atomizer: The duty cycle characteristics of the Atomizer are simple and easy to implement. The following figure shows how the load function for the Atomizer has been implemented. Although the actual load duty cycle curve does not have a sinusoidal trend, a small cyclic variation has been introduced to compensate for the sharper variations in the trend.
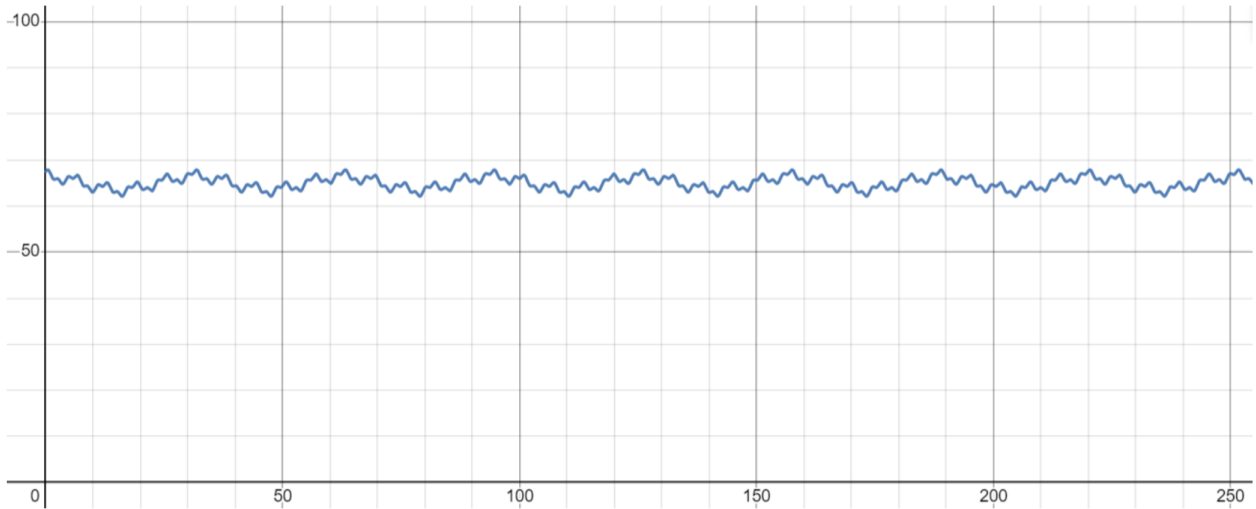
Figure 3.52: Modeled Load Function of the Atomizer.

Much like previous cases, the Atomizer's load function is also characterized by sharp and frequent harmonics, which have successfully been modeled into the equation. Therefore, the load function of the Atomizer can be modeled using the following mathematical equation:

$$R_{Atomizer}(t) = 65 + 1.5cos(0.2t) + cos(t) + 0.5sin(3t) \tag{3.7}$$

As there is not much variation between the actual duty cycle and the modeled mathematical function, it is safe to say that the modeled load function almost identically mimics the actual duty cycle of the Atomizer. This is made more evident by comparing both the trends, as illustrated in the figure below.
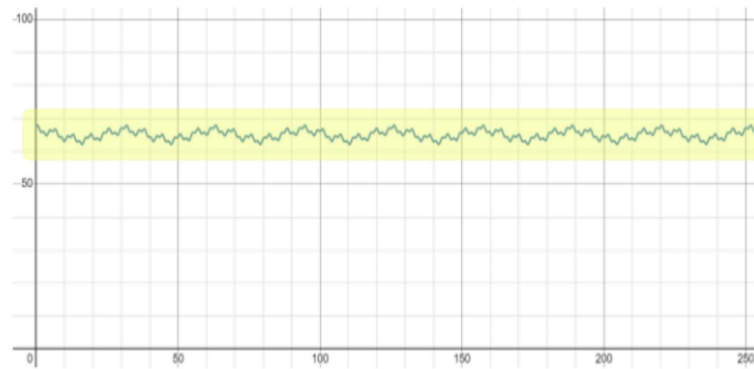
(a) Modeled Atomizer Load Function
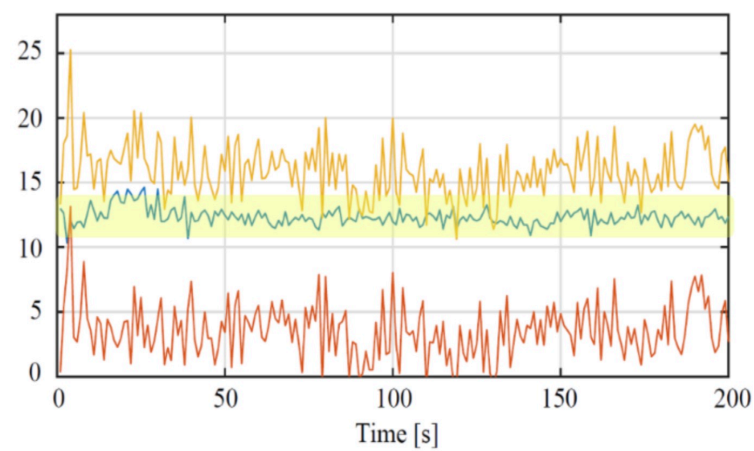
(b) Expected Duty Cycle in the Literature

Figure 3.53: Duty Cycle Mapping of the Atomizer.

The modeled equation has been implemented in Typhoon-HIL Schematic Editor using standard blocks. The following scheme highlights the approach adopted for generating the load function of the Atomizer.
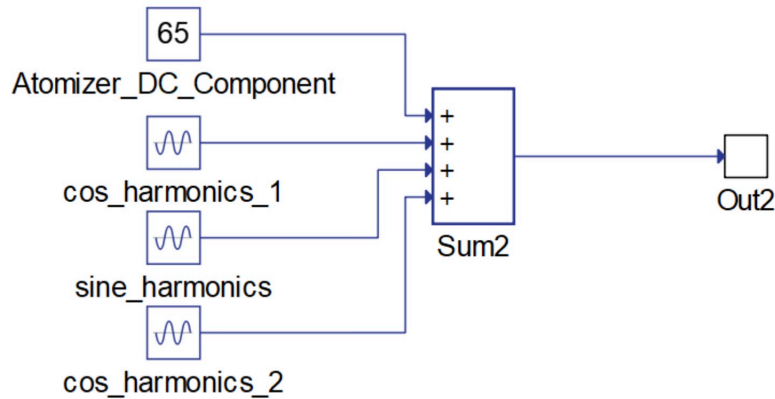
Figure 3.54: Modeling of the Atomizer.
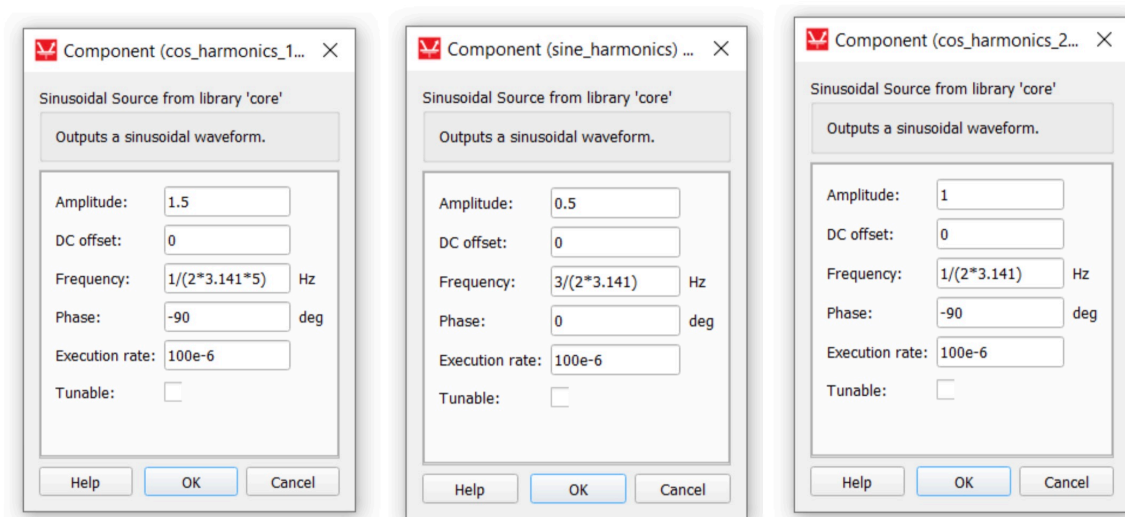
Figure 3.55: Atomizer Model Characteristics.

The model has been realized using one constant signal block, and three sine-wave generators, two of which model the cosine components, and the other, the sine harmonics. The image above illustrates the block properties of individual sine-wave generators.

Seed Spreader: The following graph illustrates the most feasible and actionable model of the actual duty cycle of the Seed Spreader. As studied in previous sections, the Seed Spreader's duty cycle is characterized by erratic changes in power demand, along with jumps in values. This is, however, difficult to implement mathematically in Typhoon-HIL, so a simpler yet reasonably accurate approach was adopted.
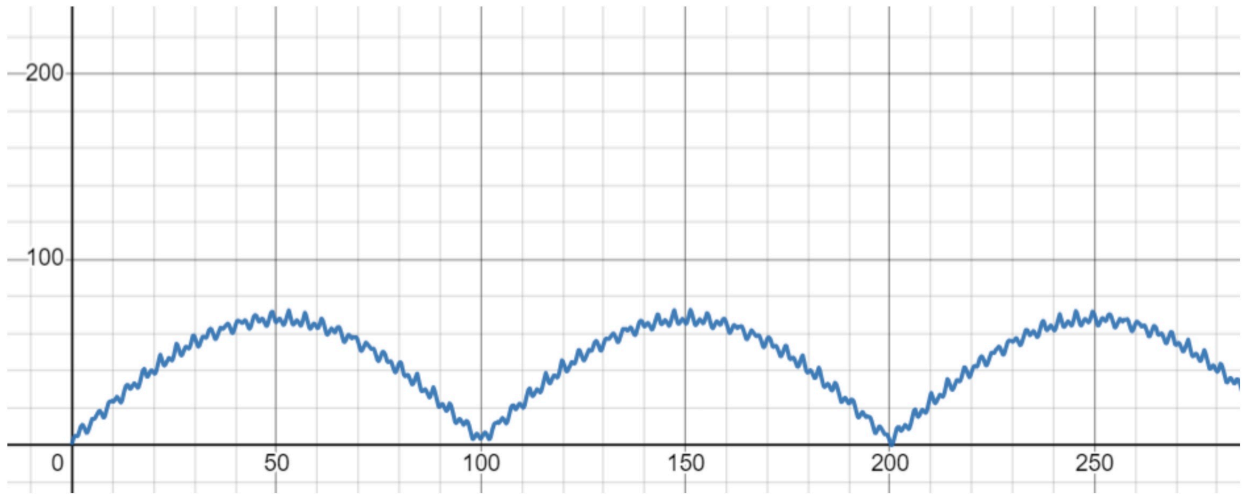
Figure 3.56: Modeled Load Function of the Seed Spreader.

The graph illustrated above attempts to mimic the real-world duty cycle of the Seed Spreader. While the mathematical function is not exact, it somewhat manages to accommodate some fundamental features of the duty cycle, such as a period of 100s, along with sharp harmonics seen in the actual curve. The modeled load function of the Seed Spreader can be expressed as the following mathematical function:

$$R_{SeedSpreader}(t) = 15 + 65|sin(\frac{2\pi}{200}t)| + 2sin(3t) - 5|cos(0.8t)| \qquad (3.8)$$

The images shown below attempt to showcase the similarities between the actual and modeled curve. It can be observed that the designed function appears to be fairly accurate in accommodating the sharp variations and dips in the actual duty cycle. For simplicity and practical purposes, this function has been assumed to be reasonably accurate for integrating into the electrical system.
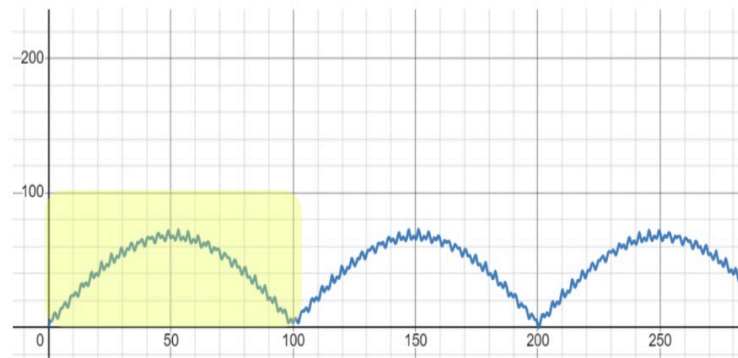
(a) Modeled Seed Spreader Load Function
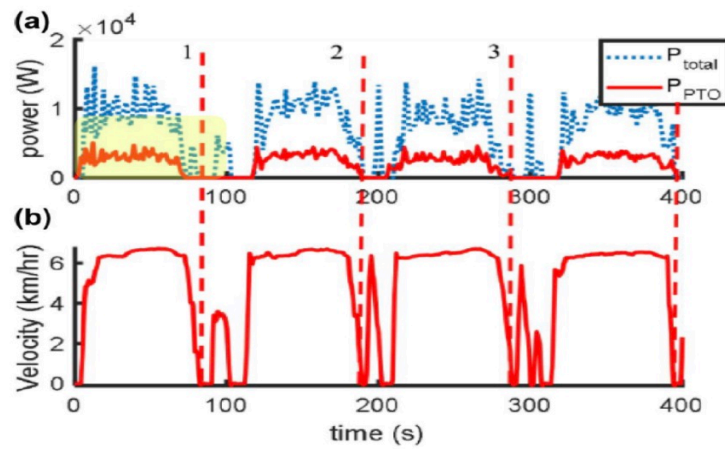
(b) Expected Duty Cycle in the Literature

Figure 3.57: Duty Cycle Mapping of the Seed Spreader.

Furthermore, the load function of the Seed Spreader has been realized by employing a constant signal, three sine-wave generators, and two modulus blocks. The values of individual signals are sent to a sum block, which adds all signals together to form the mathematical curve required for producing the Seed Spreader's load function.
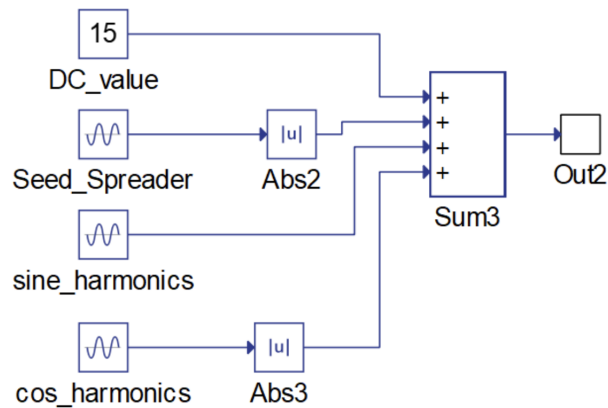
Figure 3.58: Modeling of the Seed Spreader.
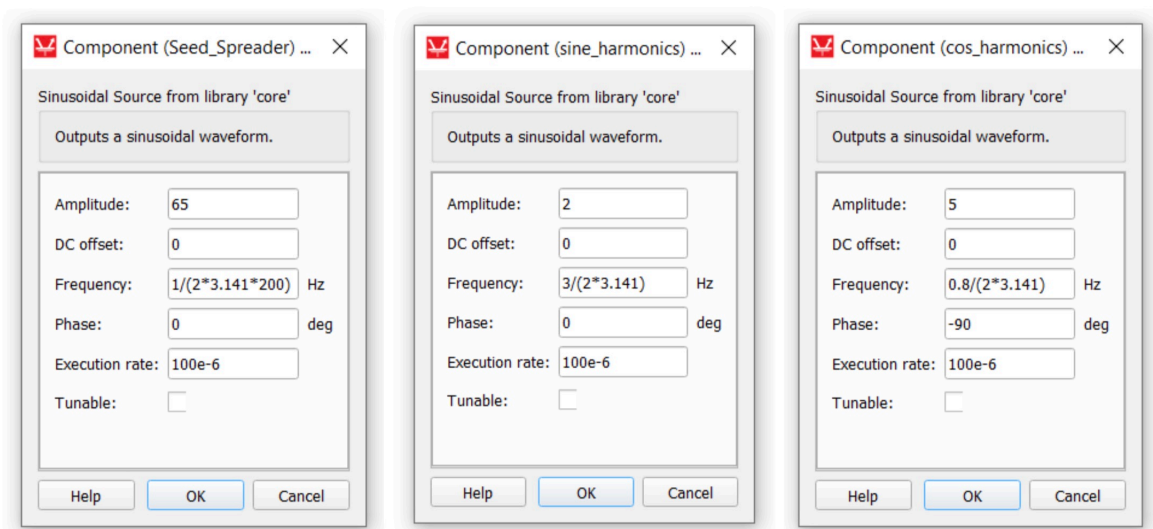
Figure 3.59: Seed Spreader Model Characteristics.

Finally, the processed signal is sent to the Load Selector, which then sets the value of the variable resistor of the 3∼ load depending on the instantaneous value of resistance. The image above illustrates the values fed into the sine-wave generators in order to get the desired function.

The next section will highlight the approach adopted to model the 3∼ load electrically, along with data and simulations of all the implements discussed in this section.

3.6.4.   3∼AC Load Simulations

In order to get a better understanding of the electrical behavior of the modeled loads
mentioned in the previous section, it is better to first understand how the 3∼ load itself
has been electrically modeled in the Typhoon-HIL Schematic Editor. The figure below
illustrates the approach adopted for modeling the 3∼ load. In the model, a three-phase
voltage source inverter draws DC power from the DC bus, and provides a steady 120V
sinusoidal output to three different phases. The inverter is controlled via fixed control
signals that help in generating suitable AC output voltages.
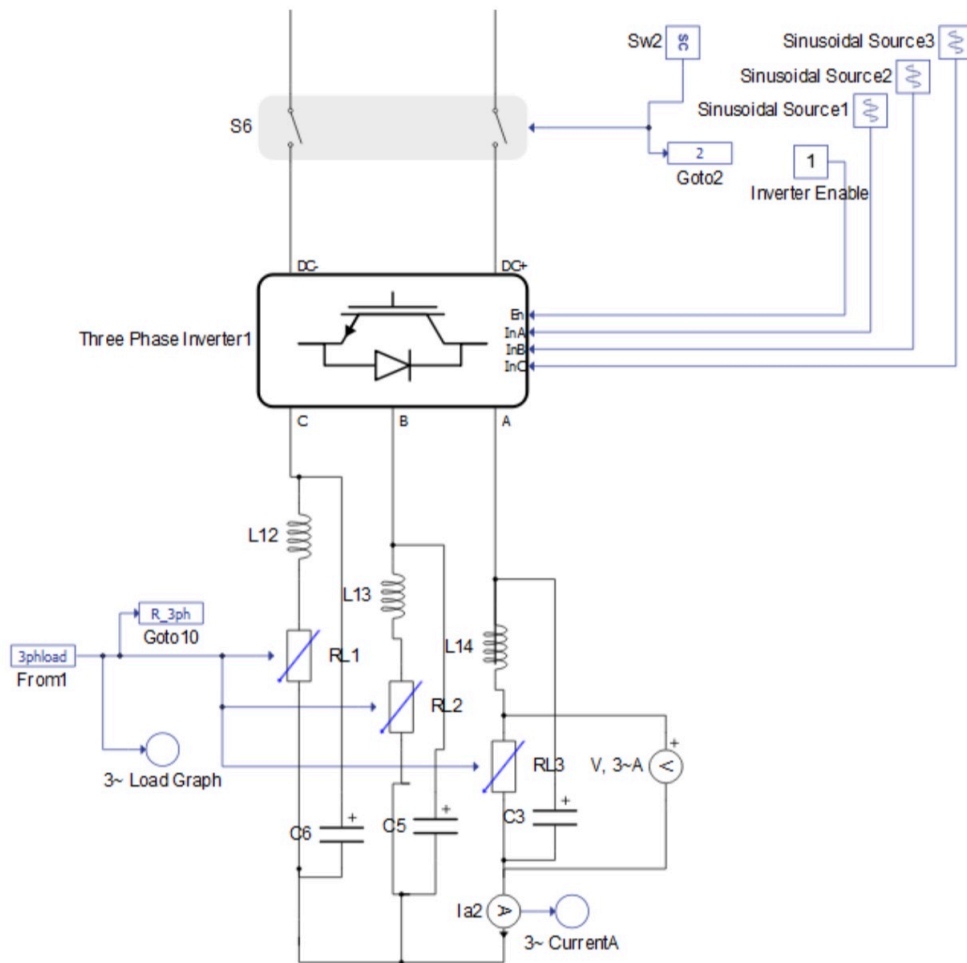
Figure 3.60: Electrical Model of the 3∼ AC Load.

On the load side, three variable resistors have been installed, whose instantaneous values
are dedicated by the load function of the implement selected by the user. A set of
voltage and current measurement devices have been installed for each phase, which help in
mapping the real-time electrical behavior of the load. The simulation has been conducted

and data has been observed for only Phase (A), as the load is symmetrical, and electrical properties of all three phases are identical, apart from a phase difference of 120°.

Additionally, three low-pass filters have been installed on each phase to eliminate high-order harmonics from the microgrid, as well as distortions generated due to the power converter. The following graph illustrates the effect of powering the 3∼ load without using appropriate filters. It can be observed that the harmonic distortion is evident in the 3∼ system (bottom right graph). The 1∼ system is also affected due to the harmonics, without appropriate filters. This causes major voltage surges on the DC bus (top left graph), which in turn causes erratic power demand from the source.
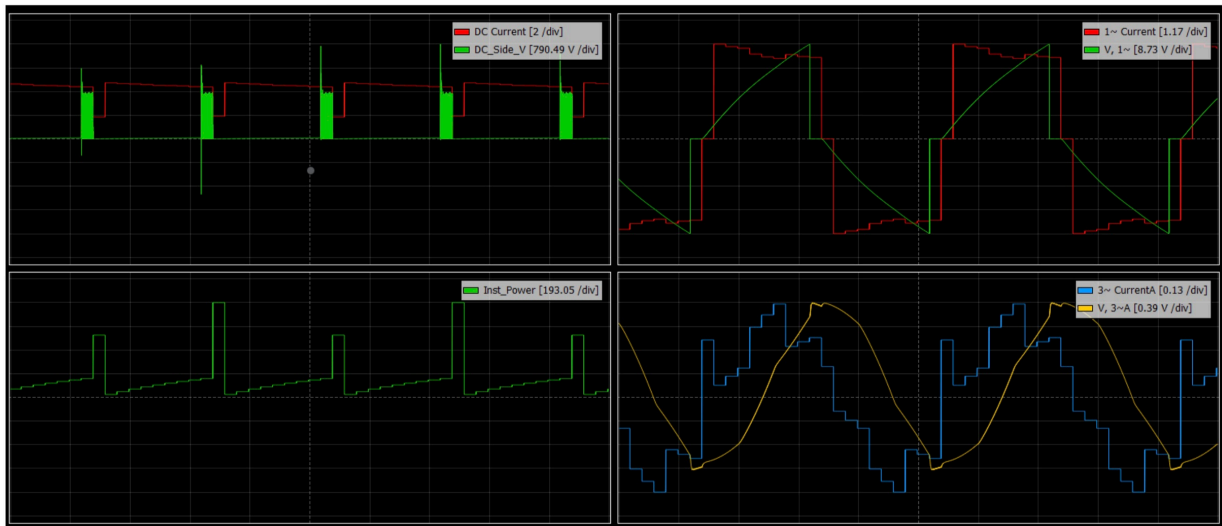
Figure 3.61: Harmonic Distortions in the Network without the 3∼ Filter.

For the purpose of carrying out the 3∼ load simulations of all the four implements, the following conditions have been imposed:

- The voltage on the DC Bus is a steady 235V, being fully supplied by the generator.

- The speed of the Generator has been fixed at 101.5 rad/sec.

- A low-pass filter has been installed at each phase of the 3∼ load, with a shunt capacitance of 45 μF, and a series inductance of 15 mH.

- The three-phase voltage-source inverter operates with a carrier frequency of 30 kHz, along with a dead-time period of 0.1 μs.

- Data for each implement has been observed for only 2.5s, as collecting data points for broader time horizons can be extremely processor-intensive.

- All signals have been sampled at a rate of 1 MSPS.
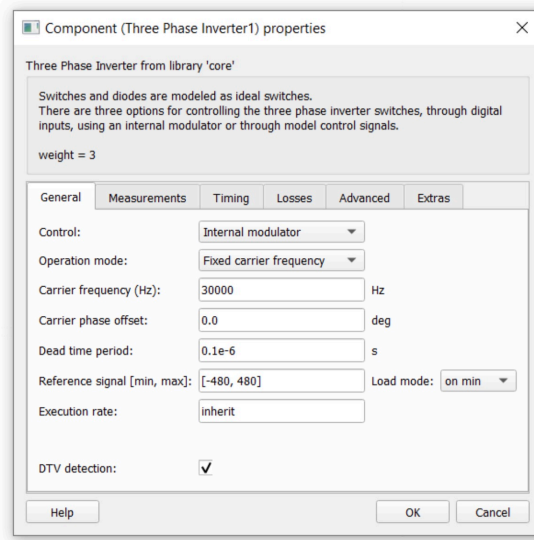
Figure 3.62: 3∼ Inverter Model Characteristics.

Manure Spreader: The following graphs illustrate the voltage and current characteristics through the load of the Manure Spreader. As observable, the voltage rises to a peak value of 120V, after undergoing a short transient that lasts about 0.02s. The load current follows a similar trend, undergoing a short transient, after which, it undergoes its normal operating cycle.
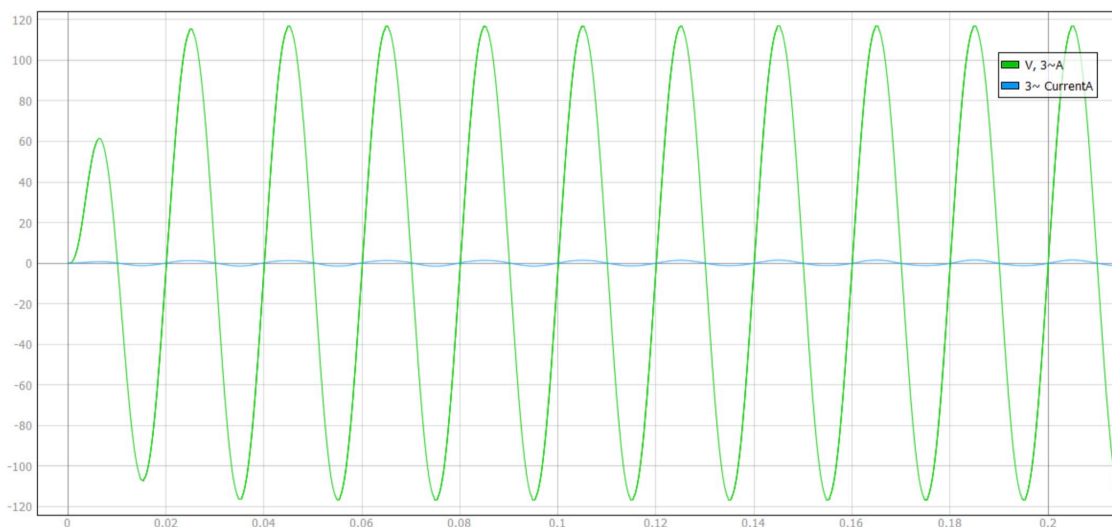
Figure 3.63: Voltage across the Manure Spreader.
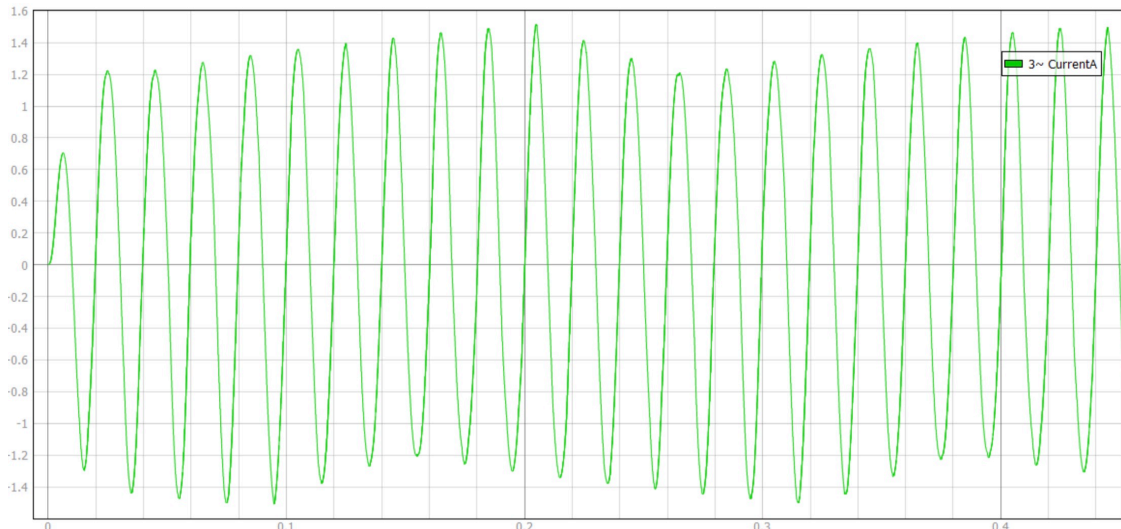
Figure 3.64: Current through the Manure Spreader.

It must be noted that the load function of the Manure Spreader produces varying resistance values in time. Additionally, the rate of change of resistance can be fairly high at certain points, which explains the sharp variations of current peaks over time. At any rate, the peak current varies between 1.22A and 1.58A within the observed time frame, but may show higher or lower peak values at much later time intervals. The trend, however, remains consistent with what has been illustrated in the graphs.

Cultivator: The voltage and current characteristics of the Cultivator have been highlighted in the following graphs. Much like the Manure Spreader, the voltage rises to a peak value of 120V, after undergoing a short transient that lasts about 0.02s. The load current then follows a similar trend, following its normal operating cycle after undergoing a short transient.
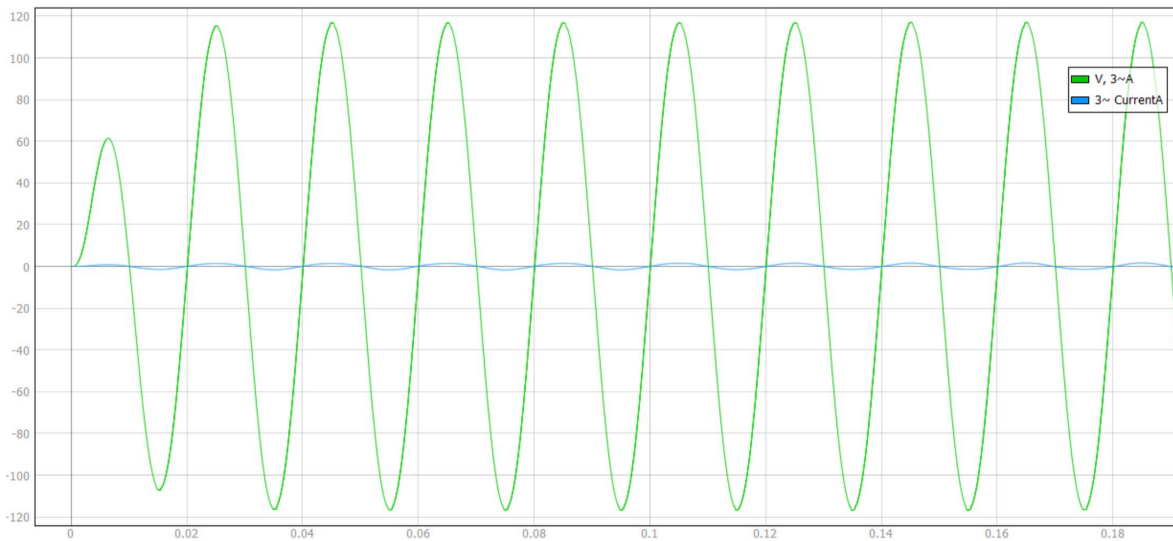
Figure 3.65: Voltage across the Cultivator.
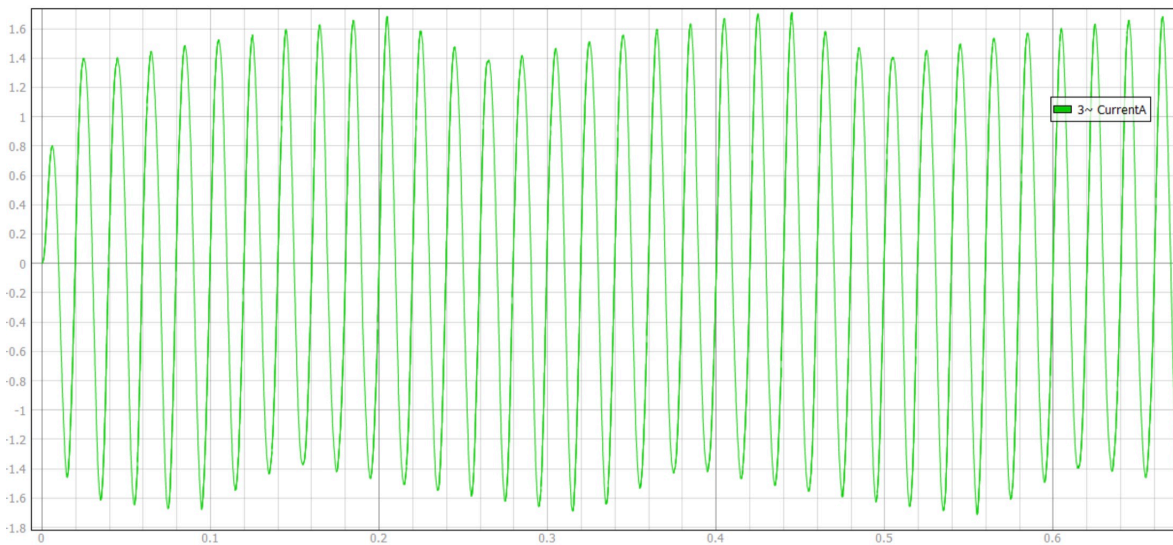
Figure 3.66: Current through the Cultivator.

It can be observed that the peak current variation is much more pronounced in the case of the Cultivator. This is because the load function of the Cultivator follows sharp variations in resistance, which result in a significant variation of power drawn over time. As a consequence, the peak load current changes considerably over time, and within the time frame of the shown simulation, can vary between 1.45A to 1.78A. As mentioned earlier, the current values may be higher or lower, depending on the time interval selected.

Atomizer: The graphs shown below illustrate the electrical behavior of the Atomizer. As shown, the voltage follows the same trend as it does in the previous cases. After

undergoing a short transient, it reaches its peak value and stabilizes. The current follows suit, undergoing its regular cycle after undergoing a transient phase.
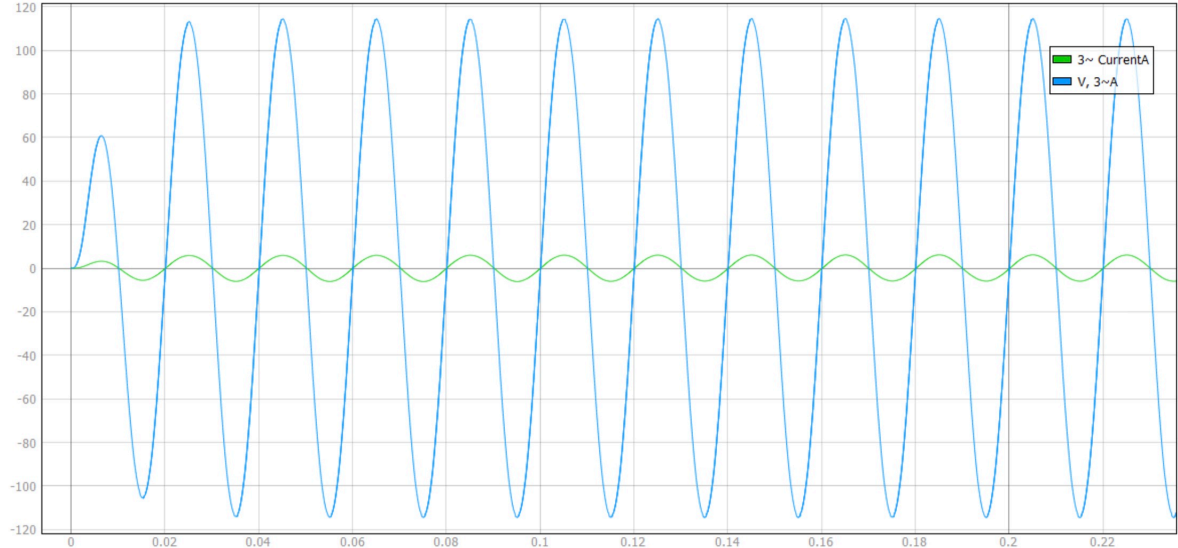
Figure 3.67: Voltage across the Atomizer.
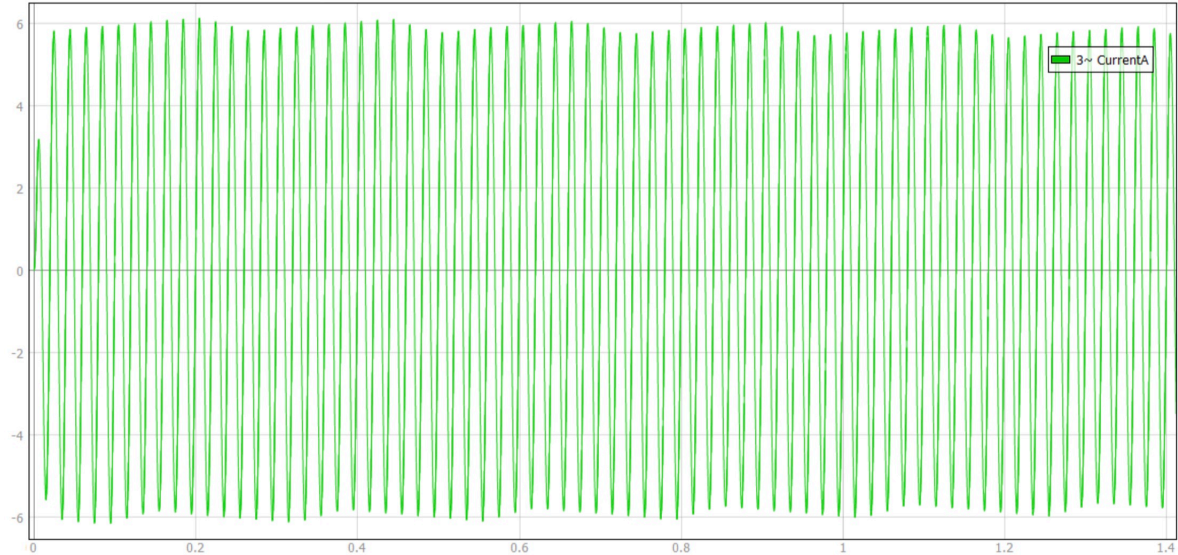
Figure 3.68: Current through the Atomizer.

It can be observed that the peak current variation is extremely limited in the case of the Atomizer. This can be attributed to its relatively steady duty cycle, which shows less variations in resistance values. As a consequence, the peak load current in the Atomizer varies between 5.85A to 6.00A, which is a relatively large value for load current, but stays more or less steady throughout operation.

Seed Spreader: The final simulation data shown is that of the Seed Spreader. As in the case with the other loads, the voltage follows the same trend of undergoing a transient for 0.02s, after which it stabilizes at 120V. The current follows suit, undergoing its natural working cycle after a short transient.
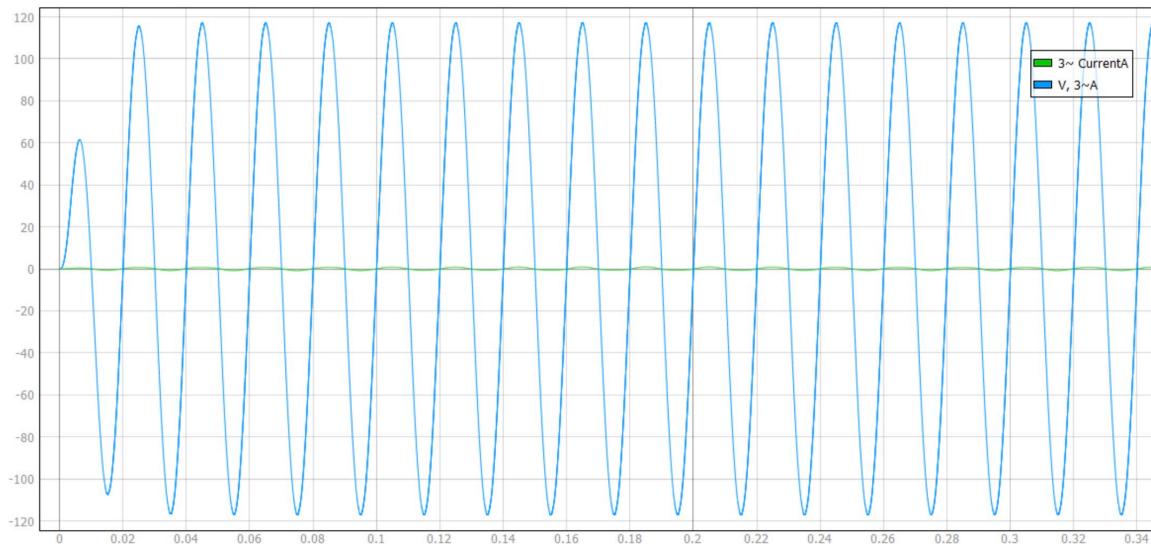
Figure 3.69: Voltage across the Seed Spreader.
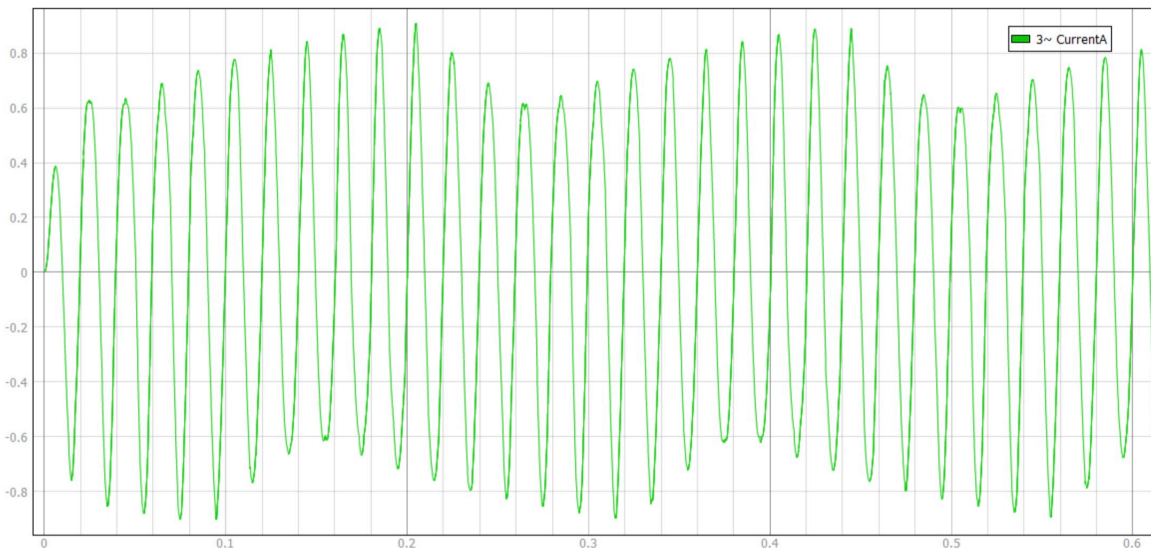
Figure 3.70: Current through the Seed Spreader.

Due to the heavily variable nature of the Seed Spreader load function, the current is also observed to have sharp relative variations. While the overall value of load current is small, the percentage variations are high. In the time frame of the simulation shown in

this section, the current varies between 0.62A and 0.92A, while its values may reach much higher figures during later stages of operation. The trend, however, remains consistent.

3.7.   Load Selector

The Load Selector serves as one of the key subsystems in this thesis. The user has the option of selecting the DC and AC loads of their choice, through the SCADA panel designed specifically for this purpose. The Load Selector takes in selected values from the user, and controls the output of corresponding loads, based on their load functions. These values are then reflected electrically at the loads while running a simulation in real-time.
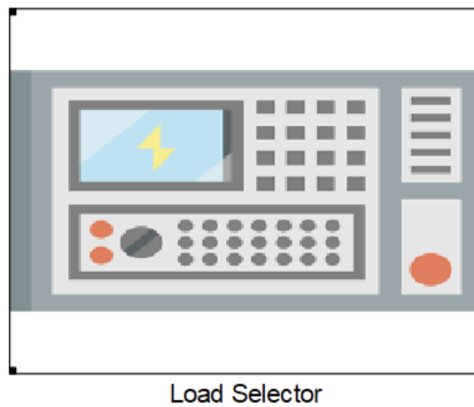
Load Selector

Figure 3.71: Load Selector.

The following image illustrates the SCADA panel utilized in this thesis. It can be observed that two large sections, (boxes in blue and green) have been dedicated for the selection of loads. In the case of DC loads, the user can select either the Battery Heater or the Snow Blower by typing in their corresponding numbers. Similarly, the user can select any of the four available 3$\sim$ AC loads by writing the corresponding number in the text box.
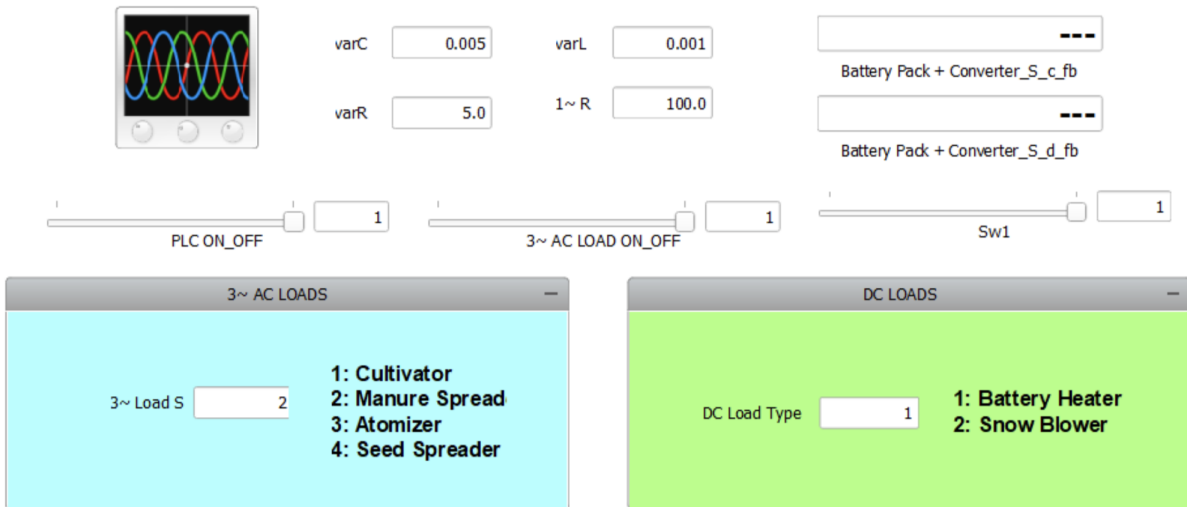
Figure 3.72: SCADA Panel designed for the Thesis.

The user also has the option of coupling or decoupling any of the three loads, which changes the power drawn from the source. This is achieved via Single Pole Double Throw Switches (SPDT) switches installed before each of the three types of loads in the model. This feature can be observed in Figure 3.15, Figure 3.27, and Figure 3.60. The user also has the option of fine-tuning some of the circuit parameters, such as the DC-Side capacitance, "varC", DC-Side inductance, "varL", the DC-Side resistance, "varR", along with the load resistance of the 1∼ AC PLC load. These values, however, shall remain unchanged throughout the study of this thesis.

Shown in the image below is the schematic inside the Load Selector block. The load selected by the user in the SCADA interface is received at the "DC Load Select" and "3∼ Load Select" SCADA Input blocks, and are then fed into the DC Load C-Function and 3ph Load C-Function blocks, respectively. Meanwhile, the DC Load C-Function block receives two more inputs: the load function of the Battery Heater and the Snow Blower in real-time. Similarly, alongside the load selected by the user, the 3ph Load C-Function receives additional signals in the form of load functions of the Cultivator, Manure Spreader, Atomizer, and the Seed Spreader.
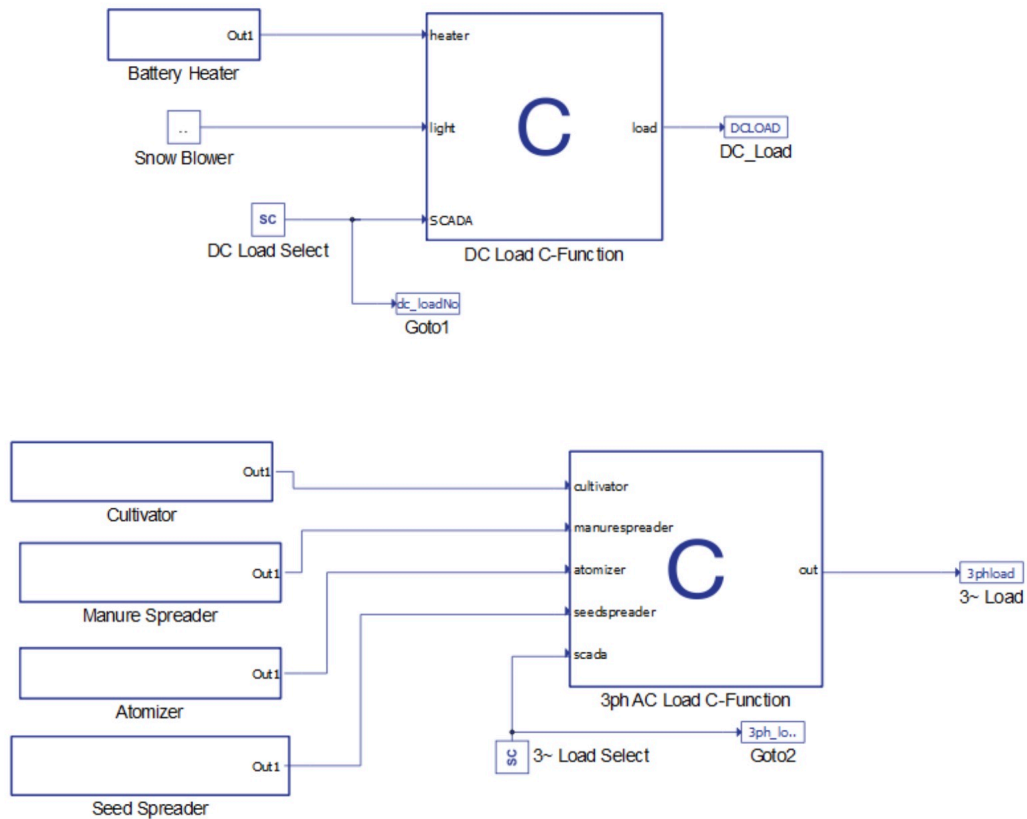
Figure 3.73: Inside the Load Selector Subsystem.

The DC and 3ph Load C-Functions are coded using the simple logic illustrated in the following images. Depending on the implement selected by the user, the C-Functions only allow the output blocks, "DCload" and "3phload" to receive the load functions corresponding to those specific implements.

These values are then sent to the actual variable resistors at the load, as seen in Figure 3.15 and Figure 3.60 , which then dictate the electrical behavior of the implement in the modeled circuit. This approach successfully models the selection of various different types of agricultural implements by the user, and manages to change the loading behavior on demand, and in real-time.

4 | Battery Pack

The objective of installing a battery pack is to provide power independently, whenever the involvement of the IC engine is intended to be reduced. The battery pack, for supporting power requirements, must therefore be installed in series with the DC Bus. For the time being, the energy management aspect of the battery pack shall not be discussed, as this section only aims to explain the installation and modeling of the battery pack. Since the objective is to install the battery pack in series with the DC bus, there are only two possible locations where the battery pack can be installed in series, location A and location B, shown in the following figure.
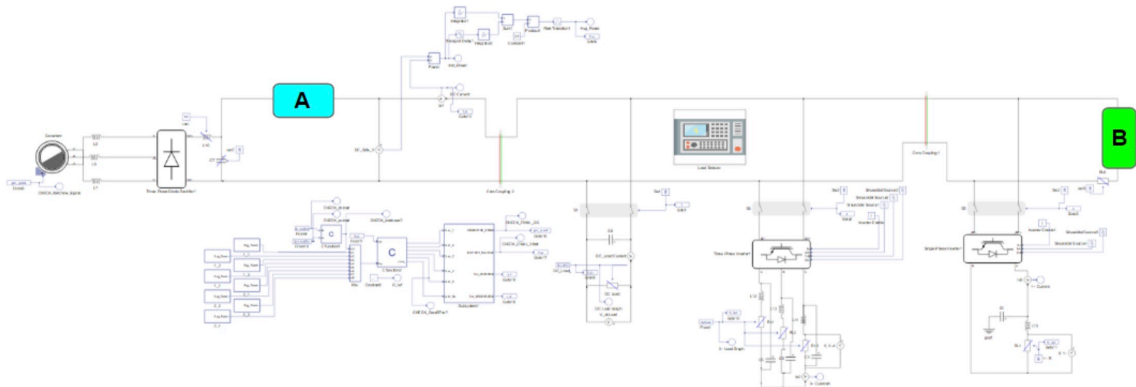
Figure 4.1: Possible Locations for Installing the Battery Pack.

It must be noted that modeling on Typhoon-HIL Schematic Editor has its limitations. This schematic has been created while keeping the HIL 404 as the primary board for system modeling. Therefore, the entire model must strictly follow restrictions laid out by the processing limitations of this board. Depending on the type of configuration selected, the maximum converter weight that can be allowed per core comes out to be 4. However, the model designed for the thesis has been based on the utilization of 3 cores, and therefore, the maximum converter weight has been restricted to 3.

HIL Device HIL404 ▼	Configuration 1	Configuration 2	Configuration 3	Configuration 4	Configuration 5	Configuration 300
Number of SPCs	3	4	2	3	3	3
Machine solvers	1	0	1	2	0	1
DC-DC converter solvers	0	0	0	0	1	0
Signal generators	12	12	12	12	12	12
Look Up Tables	8	8	8	8	8	8
PWM modulators	12	12	12	12	12	12
PWM analyzers	4	0	0	0	0	4
SPC peak processing power [GMACS]	1.12	1.12	1.12	1.12	1.12	1.12
SPC matrix memory [KWords]	16.0	16.0	16.0	16.0	16.0	16.0
SPC output memory size [variables]	512	512	512	512	512	512
Max converter weight (ideal switches) / SPC	3	3	4	3	4	3
Contactors (ideal switches) / SPC	6	6	6	6	6	6
Non-ideal switches / SPC	0	0	32	0	32	0
Time varying elements / SPC	16	16	16	0	16	16
Nonlinear machine support	yes	no	yes	no	no	yes
Nonlinear machine LUT size [KWords]	32	0	32	0	0	32
Converter power loss calculation	yes	yes	yes	no	yes	yes
Converter forward voltage drop	yes	yes	yes	yes	yes	yes
Switch-level GDS oversampling	no	no	yes	no	yes	no

Figure 4.2: Model Configuration Options for HIL 404.

Employing an actual Battery and a Boost Converter at location A would contribute to a weight of 1, and since core 1 already has a diode bridge, which has a weight of 3, installing the Boost Converter block would violate these limits. Therefore, the only place available for installation of the battery and the converter is location B, which is on core 3. However, installing the blocks in location B would not allow us to apply the battery voltage in series with the DC bus, as the DC line resistor has been placed there, which prevents us from measuring the DC Side voltage from the DC Bus and the Battery combined.

4.1. Modeling Approach Adopted

Keeping the points mentioned in the previous section in mind, the best option forward for integrating a battery pack was to model one. This approach not only reduces the computation cost of the model and simplifies the unnecessary complexity of the system, but also ensures the same expected behaviour of the battery impact on the grid. The Battery Pack + Converter subsystem block has been modeled in Typhoon-HIL Schematic Editor using this innovative approach, and has been installed at location A. Additionally, it has been implemented only using fundamental electrical and signal processing blocks to mimic the actual behavior of the battery pack.

Figure 4.3: Battery Pack + Converter.

The following schematic illustrates the modeling approach behind designing the Battery Pack + Converter block. Much like an actual battery pack, the Battery subsystem block has a positive and negative terminal, connected in series with the DC Bus.
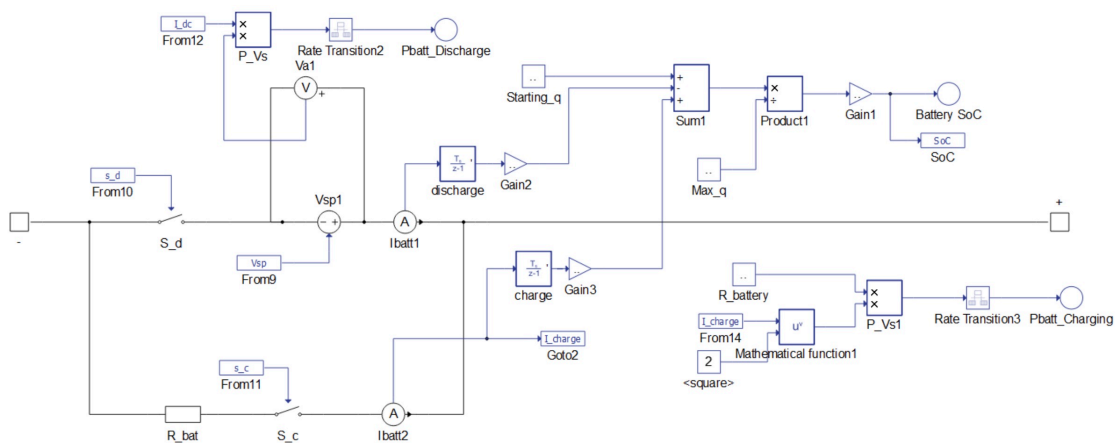
Figure 4.4: Inside the Battery Pack + Converter Subsystem.

Highlighted in the following figure is the core element of the battery pack, the Signal Controlled Voltage Source. On receiving the value of the required voltage from an external control signal, the Signal Controlled Voltage Source, "Vsp1", changes its terminal voltage to the value set by the control signal. This value can be increased or decreased, and can be set within a range of acceptable voltage values. In practice, this essentially behaves as a battery and boost converter setup, where the control signal is used to adjust the duty cycle of the boost converter, such that the output is the voltage value desired at the terminals. This approach helps us model the battery and converter without actually having to use a Boost Converter in core 1 of the model. Shown in Figure 4.6 is a Simulink model of a Boost Converter, whose duty cycle is controlled via an external signal source.
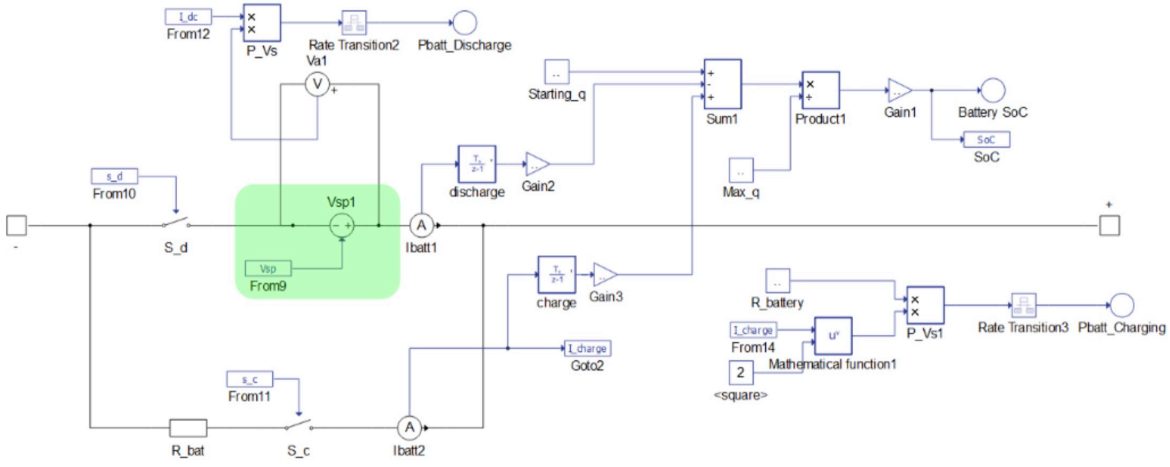
Figure 4.5: Signal-Controlled Voltage Source.
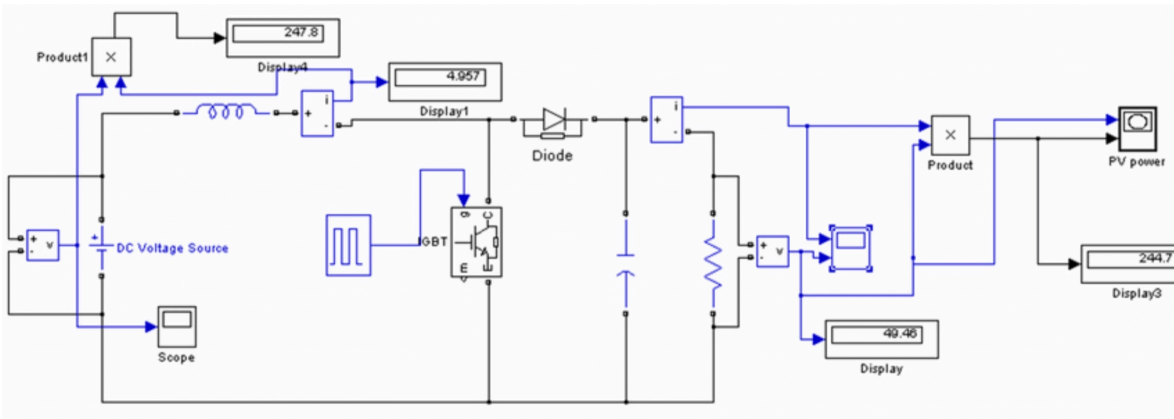
Figure 4.6: Schematic of a Generic Boost Converter.

The next part within the Battery subsystem worth mentioning is the section which calculates the total discharge power in real time. This unit multiples the battery voltage along with the DC line current to obtain the power delivered by the battery pack whenever it is discharging. The formula used is as follows:

$$P_{discharge} = V_{batt} \times I_{dc} \tag{4.1}$$
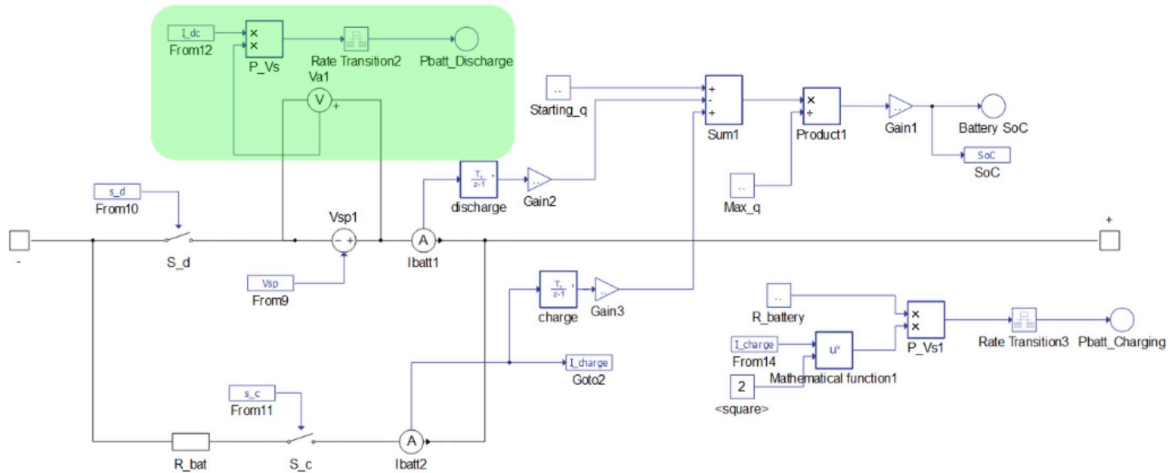
Figure 4.7: Discharge Power Calculator.

Similarly, the following image highlights the section of the subsystem responsible for calculating the power consumed by the battery pack during charging. The power drawn by the battery pack from the DC Bus is calculated in real time, during which the Battery behaves as a load, rather than a source. The battery resistance has been set to 0.75Ω. This is achieved by installing a line parallel to the voltage source, and disconnecting the primary line via switches when the battery is intended to behave as a load. The switching logic has been explained in detail in later sections. The power absorbed by the battery is calculated using the following formula:

$$P_{charge} = I^2_{charge} \times R_{batt} \tag{4.2}$$
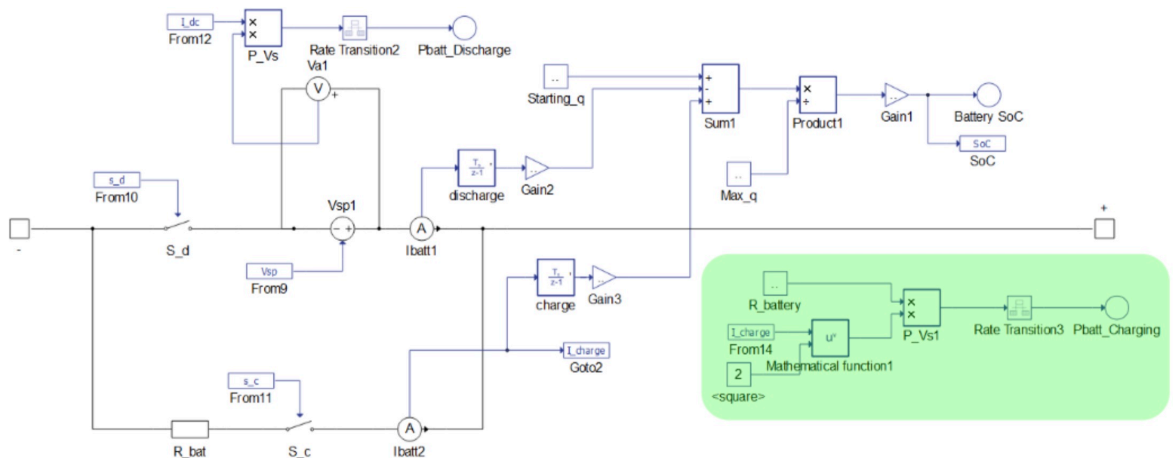
Figure 4.8: Charging Power Calculator.

The final section of the Battery subsystem worth highlighting is the SoC calculator. This section utilizes a basic Coulomb Counting logic to estimate the SoC of the battery pack in real time. The discharge and charging currents are integrated over time using Integrator blocks which calculate the amount of charge leaving or entering the battery pack during operation, at any given time. These values are either subtracted from, or added to the initial charge of the battery pack, "starting_q", which has been set to 7000mAh. The total value of real-time charge is calculated at "Sum1", and is then divided by "Max_q", which is set to 7500mAh, then multiplied by 100 to give the real-time SoC value in percentage.
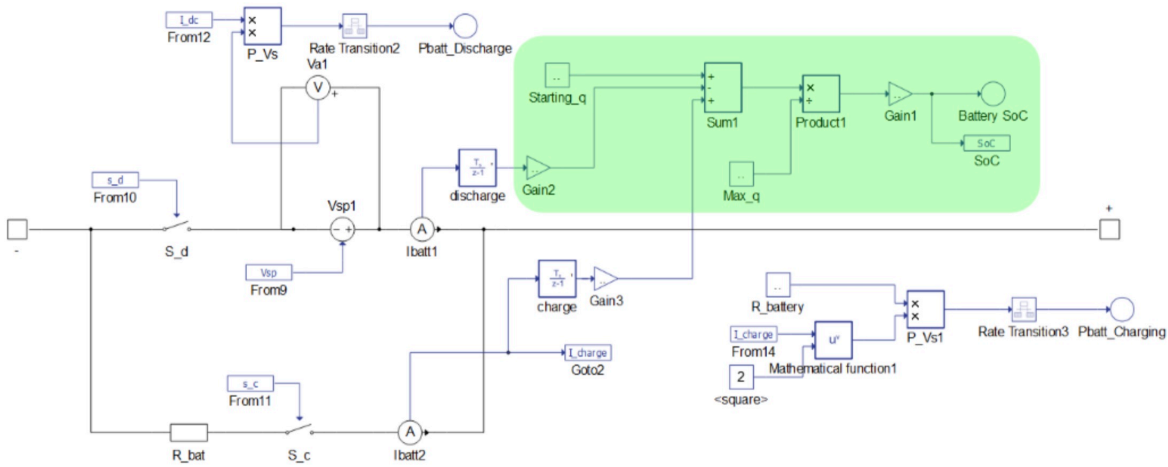
Figure 4.9: State-Of-Charge Calculator.

Throughout the subsystem, various gain blocks have been employed to fine tune parameters and add system noise wherever required to model non-ideal behaviors and losses. For the purpose of the thesis, these values have been optimized in order to get tangible readings and actionable values for the model.

4.1.1.   Battery Simulations

This section explores some Battery simulations, and covers examples showing how the battery discharges, and how the SoC behaves. The Battery pack has been programmed to discharge under very specific conditions, and its delivered power largely depends on its SoC. The algorithm and power deliver logic has not been covered in this section, but has been explained in detail in later stages of this thesis.

However, for understanding the simulation results, it is good to know that the Battery is programmed to discharge power when the average power demand of the system exceeds a certain threshold. If this condition becomes true at any given point during the simulation,

the amount of power delivered by the Battery will depend on its SoC, where a high percentage of SoC corresponds to a higher delivery of power.

Shown in the following figure is a preliminary simulation that was run during the initial stages of the Battery design. It is an exemplary simulation, intended for the reader to understand what the following simulations in this section intend to illustrate.
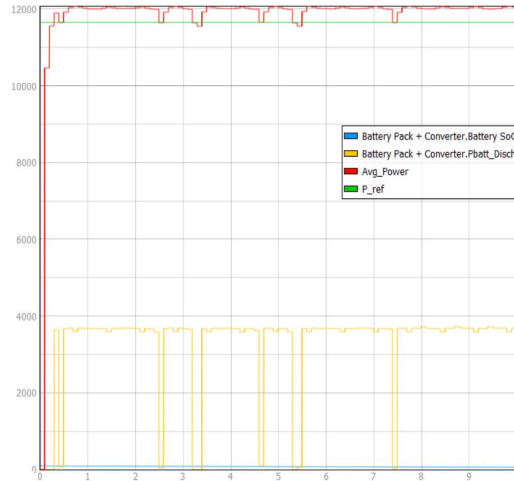
(a) Battery Pack Discharge Power, Average Power, and Reference Power
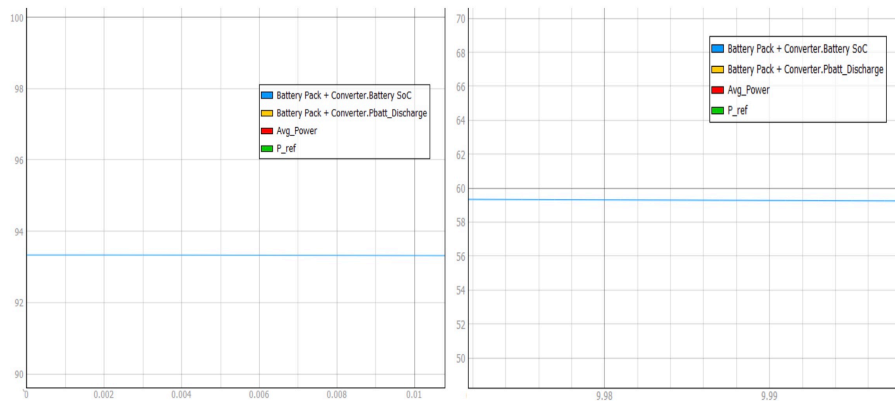
(b) Battery Pack SoC at the Start and End of the Simulation

Figure 4.10: Generic Simulation of the Battery Pack.

The graph in Figure 4.10 (a) illustrates four curves, namely, the Average Power, the Reference Power, the Discharged Power by the Battery, and the Battery SoC. At the start of the simulation, the Average Power quickly rises to its operating values, and varies with time, as the simulation proceeds. The Reference Power marks the threshold beyond which the Battery pack must deliver power, whenever the Average Power exceeds this value. It can be observed that the Battery discharges and delivers power to the load whenever

Average Power exceeds the Reference Power. However, the Battery's contribution is only about 30% of the total requested power. Figure 4.10 (b) illustrate the SoC of the Battery at the start and at the end of the simulation, indicating depletion in charge.

Case No. 1: Snowblower and Cultivator, starting_q = 3500 mAh

The image shown in figure illustrates the average power demand when the Snowblower and the Cultivator have been engaged. It can be observed that the battery delivers power to the loads, at instances when the average power exceeds the reference power. Additionally, since the starting charge, "q", has been set to 3500 mAh, the starting SoC is about 46.6%, because of which the Battery only delivers about 40% of the requested power.
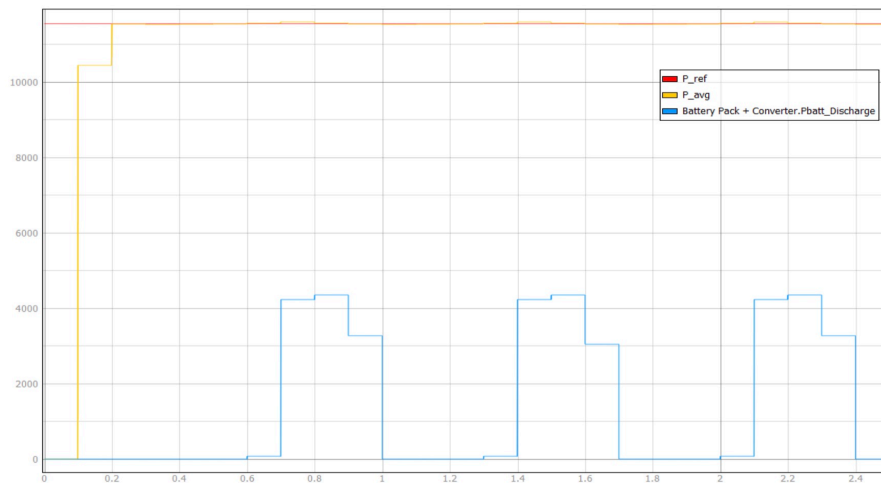
(a) Power Discharged by the Battery Pack, Case 1
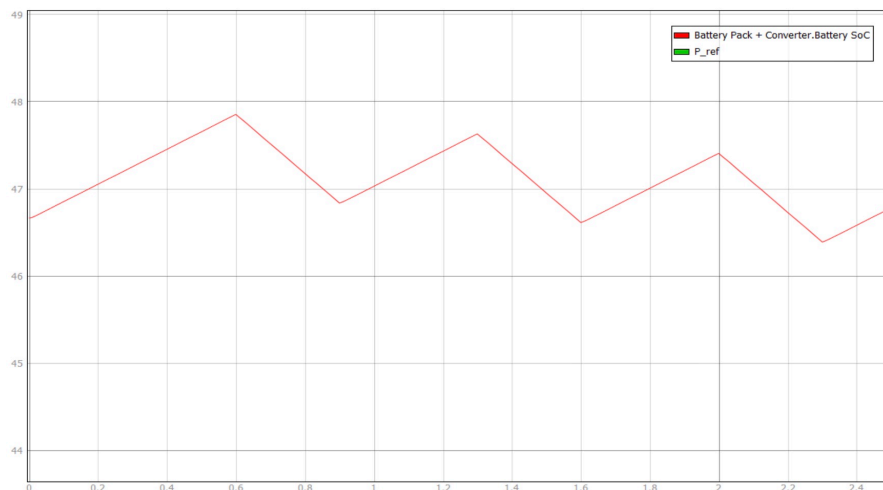
(b) Battery Pack SoC Variation, Case 1

Figure 4.11: Simulation of Snowblower and Cultivator, q = 3500 mAh.

Figure 4.11 (b) shows the variation in SoC of the Battery. The SoC increases (charging)

whenever the Battery is not delivering power, and is therefore acting as a load, getting charged in the process. The SoC decreases (discharges) whenever the Battery is expected to deliver power to the load. Over the course of the simulation, the average SoC trend is tending towards depletion.

Case No. 2: Battery Heater and Atomizer, starting_q = 3500 mAh

In this case, the average power demand crosses the reference value of power nearly at the beginning of the simulation, and maintains values higher than the reference. It can be observed that the battery delivers power to the load by discharging, almost throughout the simulation interval. This is different from the previous case where the battery was providing power on an intermittent basis.
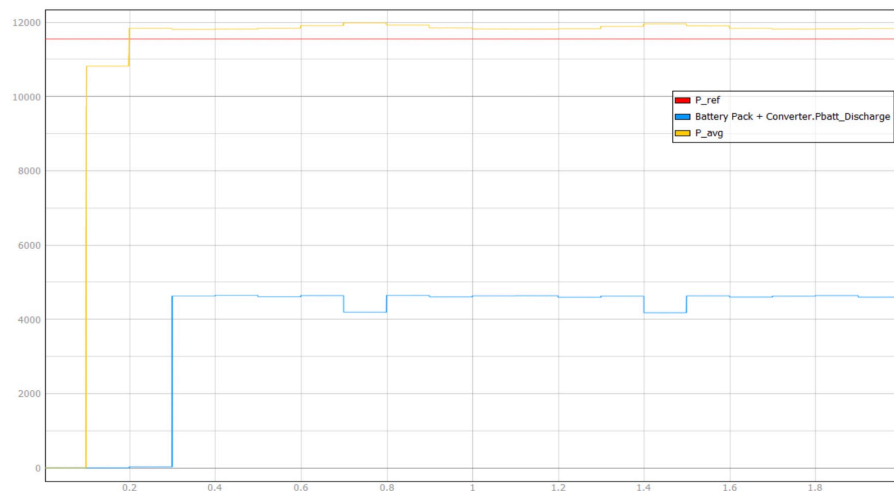
(a) Power Discharged by the Battery Pack, Case 2
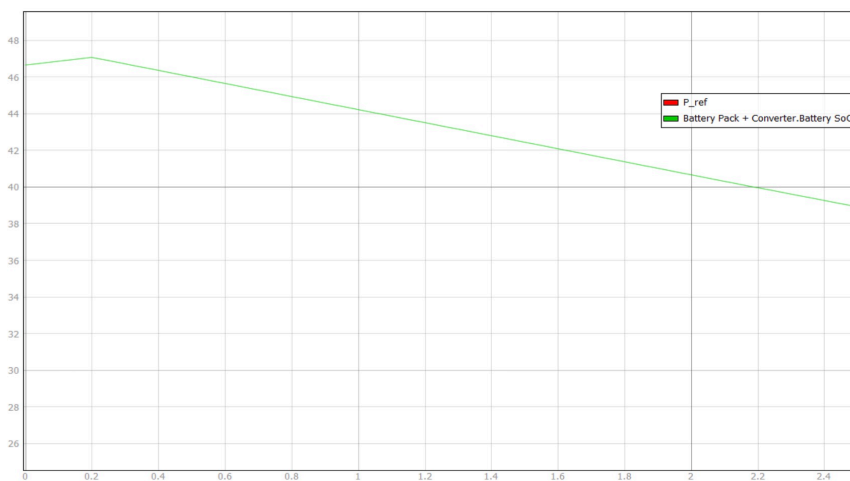
(b) Battery Pack SoC Variation, Case 2

Figure 4.12: Simulation of Battery Heater and Atomizer, q = 3500 mAh.

The SoC of the Battery increases during the initial few milliseconds of the simulation
when the Battery is not delivering any power. Once the average power demand exceeds
the reference value, the Battery consistently starts delivering power, and the SoC starts
decreasing rapidly.

Case No. 3: Battery Heater and Cultivator, starting_q = 5500 mAh

The starting SoC is about 73.5% in this case, and it can be observed that the Battery
delivers nearly 100% of the requested power whenever the average power exceeds the
reference value. This stays true until about t = 1.4s, after which the Battery delivers
about 75% of the requested power.
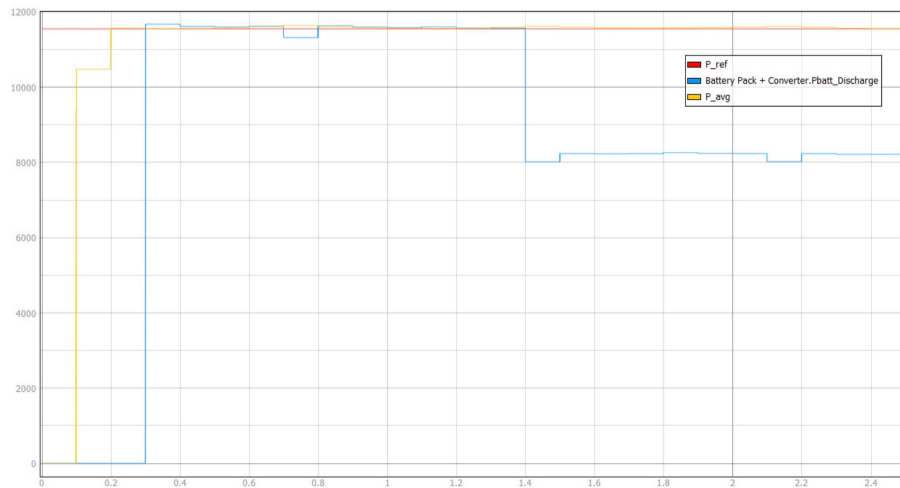
(a) Power Discharged by the Battery Pack, Case 3
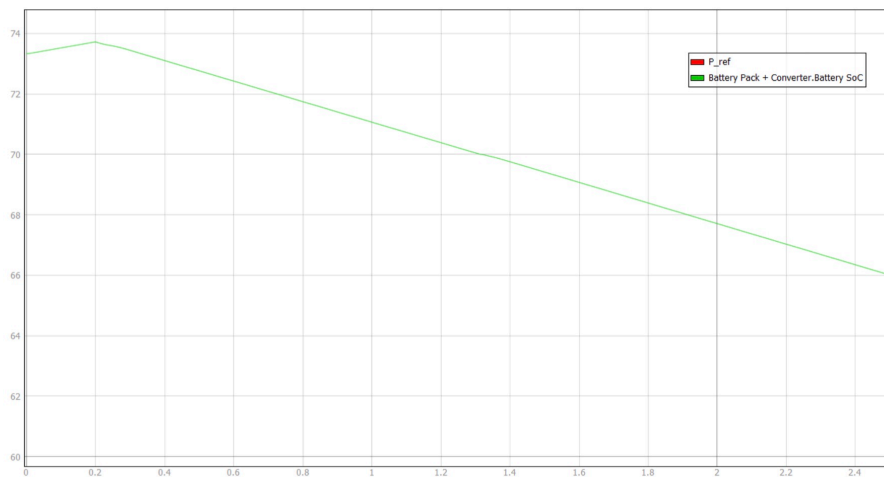
(b) Battery Pack SoC Variation, Case 3

Figure 4.13: Simulation of Battery Heater and Cultivator, q = 5500 mAh.

This happens because, as shown in Figure 4.13 (b), the SoC drops below 70% just before

t = 1.4s, because of which, the Eower Management algorithm follows a slightly different logic for the battery pack, in order to conserve charge. It must be noted that the next section will discuss how these average power curves have been obtained, and what threshold value has been selected for reference, as none of this has been illustrated in this particular section.

Moreover, it is worth mentioning that the Battery charging and discharging has been greatly exaggerated by tweaking coefficients, just to show the upward or downward trend of the SoC more easily. Judging from the graph, it is obvious that a correctly sized battery for automotive applications should not have its SoC down by 15% within 5 seconds of operation.

5 | Power Calculation

Since the central theme of this thesis is to devise an Energy Management algorithm for the hybrid powertrain, it is exceedingly important to collect, understand, and manage power data. As our system has two DC loads and four AC loads, we have a total of 8 different load combinations possible. Actually, the total number of possible combinations comes out to be 14, including 4 cases where only one of the four $3\sim$ AC implements is active, and none of the DC implements are active, and 2 more cases where one of the DC implements are active and none of the $3\sim$ AC implements are active. It has been assumed that the $1\sim$ AC load, ie, the PLC always stays on, as long as there is a DC or a $3\sim$ AC load active.

Power data is later used in the Energy Management algorithm for predicting the load's power demand, and managing the energy exchange between the loads, the IC Engine and the Battery Pack. It is therefore of paramount importance to measure the power demand, peak values, and most importantly, the fluctuations in the drawn power from all possible load combinations. This would not only safeguard the Energy Management system against sharp load variations, but also help in developing a robust system that can optimize power flow between the two primary power sources. As far as calculating power is concerned, there are two approaches that can be adopted for using the Energy Management algorithm. Both have been discussed in this section.

5.1. Instantaneous Power Calculation

The most basic approach towards calculating power drawn by the loads is by gauging the voltage and the current at the DC Bus. The following equation is employed:

$$P_{total} = V_{DCbus} \times I_{DC} \tag{5.1}$$
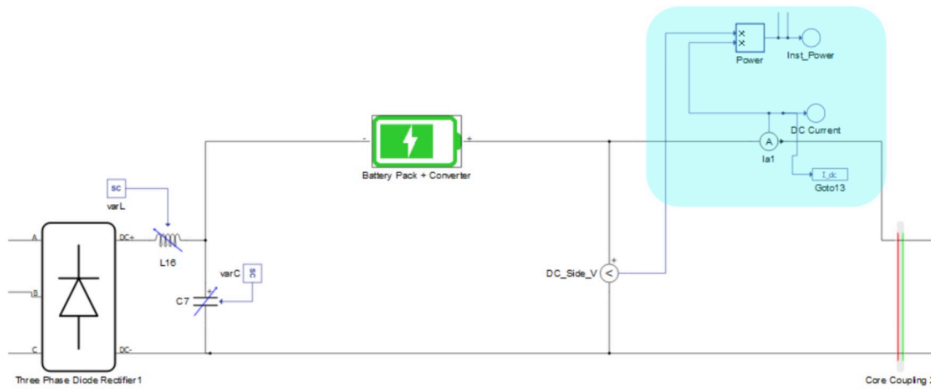
Figure 5.1: Instantaneous Power Calculation in the main Schematic.

This approach is simple, and gives a clear measure of how much power is being drawn by the load. It's implementation can be observed in Figure 5.1. The primary DC Side voltage and the DC current values are measured and multiplied, to get the Instantaneous Power being drawn by the system. This curve varies with time, and can follow very different characteristics, solely based on the combination of loads selected by the user.

5.1.1. Instantaneous Power Load Cases

The following graphs illustrate the variation in Instantaneous Power drawn by different load combinations. The data collection has been carried out by choosing all the possible 8 load combinations, and running simulations one after the other. The observed results have been shown below.

(a) Battery Heater + Cultivator

(b) Battery Heater + Manure Spreader

(c) Battery Heater + Atomizer

(d) Battery Heater + Seed Spreader

(e) Battery Heater + No 3∼ AC Load

(f) Snowblower + Cultivator

(g) Snowblower + Manure Spreader

(h) Snowblower + Atomizer

(i) Snowblower + Seed Spreader

(j) Snowblower + No 3∼ AC Load

(k) No DC Load + Cultivator

(l) No DC Load + Manure Spreader

(m) No DC Load + Atomizer

(n) No DC Load + Seed Spreader

Figure 5.2: Instantaneous Power Curves for all Load Cases.

	Cultivator		Manure Spreader		Atomizer		Seed Spreader		No 3ph Load	
	Pmax	Pmin	Pmax	Pmin	Pmax	Pmin	Pmax	Pmin	Pmax	Pmin
Battery Heater	12.85	11.15	12.83	11.21	13.95	11.29	12.62	11.08	12.47	10.95
Snowblower	12.76	11.20	12.72	11.15	13.83	11.24	12.53	11.03	12.38	10.81
No DC Load	12.31	10.73	12.28	10.69	13.37	10.80	12.12	10.57	-	-

Table 5.1: Maximum and Minimum Instantaneous Power (kW) variation for all 14 Load Cases.

It can be clearly seen that all of the 8 load cases exhibit sharp variations in power demand, which can cause steep fluctuations in the Energy Management control system. Additionally, due the high sampling rate of the Instantaneous Power signal, it could potentially be challenging for the Energy Management algorithm to keep up with the dramatically changing power requests, and make optimized adjustments.

Table 5.1 highlights the maximum and minimum power drawn by all 14 load cases, including the combinations where either the DC load or the 3∼ loads are inactive. The case where both the loads are inactive has not been considered, as it does not make technical sense. Due to the reasons mentioned earlier, it was best to consider a case where the power signal sampling was lower yet accurate, and in a manner in which the control system of the Energy Management Unit could keep with the requested optimizations without sacrificing performance or robustness. The most efficient way forward was to employ Average Power measurement, which has been explained in the next subsection.

5.2.   Average Power Calculation

As explained in the previous section, the steadier approach towards estimating the real-time power demand of the loads is to take into account the Average Power. Instead of measuring power drawn at every 1μs, the objective is to get a broad idea of how much power is being drawn by the loads over a longer time period, and optimize power management accordingly. By measuring the Average Power demand over a time range of 0.1s, the Energy Management control system has a better idea of how to manage the IC Engine and the Battery Pack, thereby significantly reducing switching instances and offering far more stability to the electrical network.
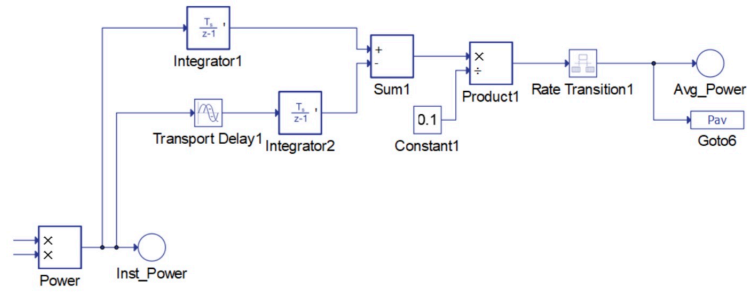
Figure 5.3: Average Power Calculation in the main Schematic.

Figure 5.3 highlights the modeling approach towards calculating the Average Power in Typhoon-HIL Schematic Editor. From the Instantaneous Power calculated using the approach explained in the previous section, two signals are taken out. One of these lines contains the power values in real time, and the other line has been introduced to a Transport Delay of 0.1 seconds. Both these values are integrated, and their difference is calculated. During the first 0.1 seconds of the simulation, the output of the Transport Delay has been set to zero. The difference of these values gives the area under the power curve, which is then divided by the set time step of 0.1 seconds. A Rate Transition converts the sampling time step from $1\mu s$ to 0.1s, which makes plotting this function easier. The obtained output is much more usable for the control system.

5.2.1. Average Power Load Cases

The following group of curves highlights Average Power curves for all of the 14 load cases. From the graphs, it can be observed that peak variations have been drastically limited, and this data can be further used for employing in the Energy Management algorithm.

(a) Battery Heater + Cultivator

(b) Battery Heater + Manure Spreader

(c) Battery Heater + Atomizer

(d) Battery Heater + Seed Spreader

(e) Battery Heater + No 3∼ AC Load

(f) Snowblower + Cultivator

(g) Snowblower + Manure Spreader

(h) Snowblower + Atomizer

(i) Snowblower + Seed Spreader

(j) Snowblower + No 3∼ AC Load

(k) No DC Load + Cultivator

(l) No DC Load + Manure Spreader

(m) No DC Load + Atomizer

(n) No DC Load + Seed Spreader
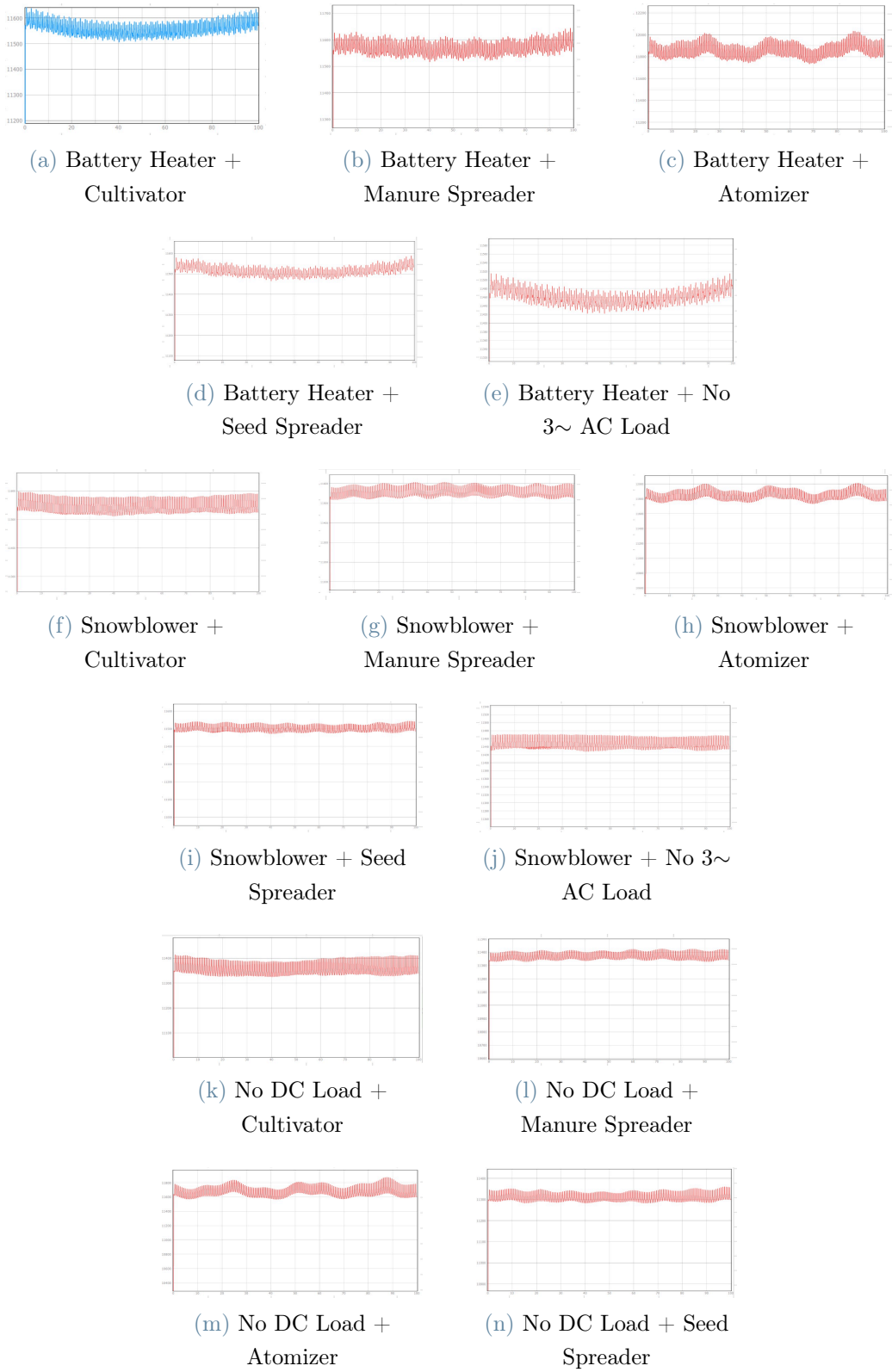
Figure 5.4: Average Power Curves for all Load Cases.

	Cultivator		Manure Spreader		Atomizer		Seed Spreader		No 3ph Load	
	Pmax	Pmin	Pmax	Pmin	Pmax	Pmin	Pmax	Pmin	Pmax	Pmin
Battery Heater	11.64	11.50	11.64	11.51	12.03	11.73	11.57	11.46	11.52	11.42
Snowblower	11.59	11.51	11.60	11.52	12.01	11.73	11.54	11.47	11.47	11.42
No DC Load	11.42	11.32	11.42	11.32	11.87	11.56	11.36	11.28	-	-

Table 5.2: Maximum and Minimum Average Power (kW) variation for all 14 Load Cases.

Table 5.2 illustrates a summary of the data collected, and tabulates the maximum and minimum Average Power drawn from the source, over a simulation time of 100 seconds.

Observing the data shown in the previous table, a value must be selected that represents the approximate average of these varying figures, such that it can serve as a reference value for the Energy Management algorithm. Keeping this in mind, the reference value of power was set to 11.55kW, as it represents a good average value.

6 | Energy Management System

This section explains in detail, the most critical part of the thesis, which is the Energy Management System. The Energy Management System brings all other modeled systems together, and optimizes system-level performance. As explained earlier, the objective of the Energy Management System is to gauge when the load demand is high, and distribute power delivery responsibilities between the Generator (I.C. Engine) and the Battery Pack.

The following schematic has been developed and implemented from the ground-up, and is a functional representation of how the Energy Management Logic operates. The entire system comprises several different types of signal processing blocks, which work together to ultimately govern the speed of the Generator, and decide the Battery voltage at any given point.
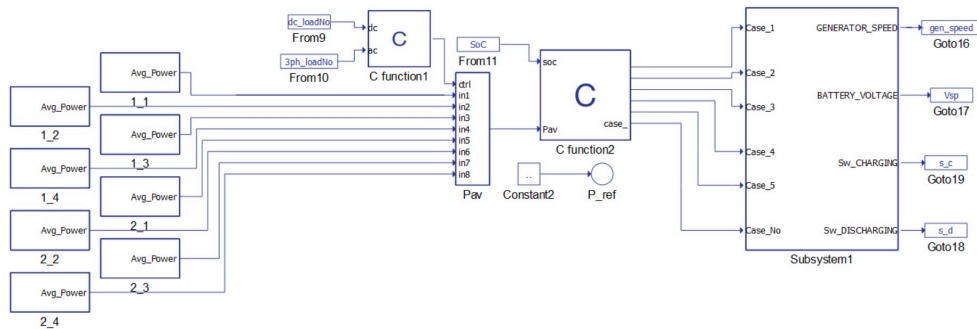
Figure 6.1: Full Schematic of the Energy Management System.

Eight Dynamic Tables have been installed, which set the reference curves for the Average Power demand for all load combinations. Based on which two loads the user selects, only the Average Power curve of that particular combination is forwarded to the main C-Function. Depending on the real-time SoC of the Battery Pack, the system decides the percentage involvement of the Battery in providing power. This is represented in the form of a "Case Number", which is forwarded to the main Switching Signal subsystem. The entire Energy Management System is governed by the following algorithm:
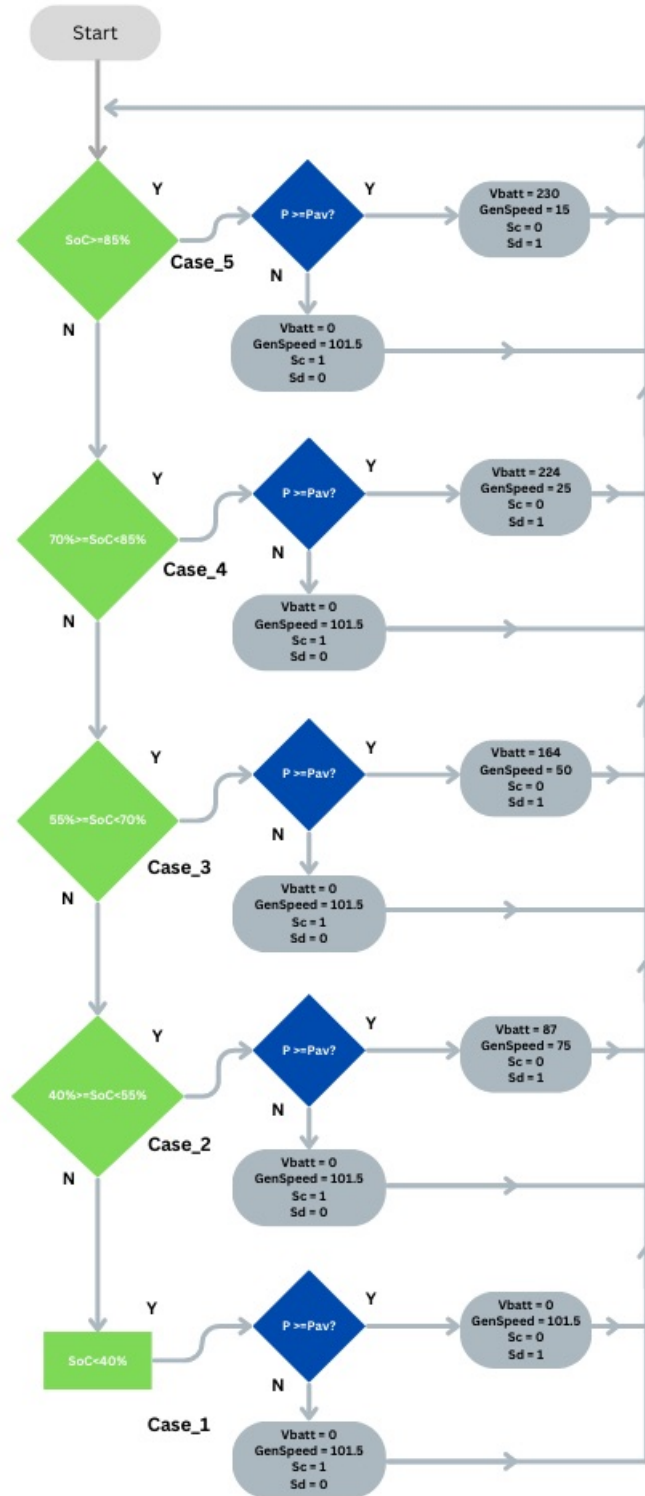
Figure 6.2: Energy Management System Algorithm.

6.1. Dynamic Tables

From the above schematic and algorithm, it should be noted that the system controls the Battery voltage and Generator speed by checking the demand of Average Power. Additionally, by changing the Battery voltage and Generator speeds, there is a small voltage fluctuation at the DC bus during the switching transients. This, in turn, affects the real-time values of Average Power, which is being measured to control the Battery and Generator. Therefore, the system must not take Average Power reference from real-time measurement, as it undergoes variations during the switching transients. The system should, therefore, have an ideal set of values for Average Power demands under different loading conditions. This is where Dynamic Tables in Typhoon-HIL Schematic Editor come in handy.
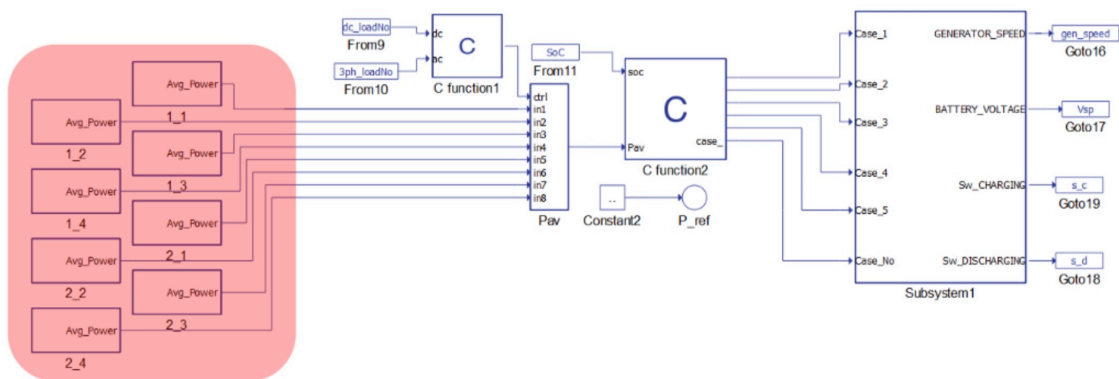
Figure 6.3: Dynamic Tables within the Energy Management System.

As shown in the figure above, the Dynamic Tables contain 8 different sets of values of Average Power versus time, for all 8 key implement combinations. These values are based on the same simulation outputs explained in the Average Power Measurement section, and illustrated in Figure 5.4. Once installed, any of these 8 Dynamic Tables can be accessed by the control system, as well as the user, to look up Average Power values at any given point in time, during the simulation.
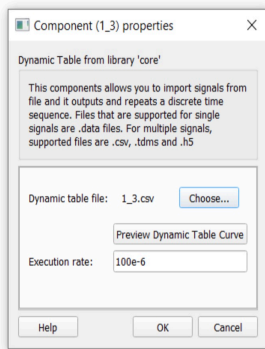
(a) Model Properties of a Dynamic Table "1_3"
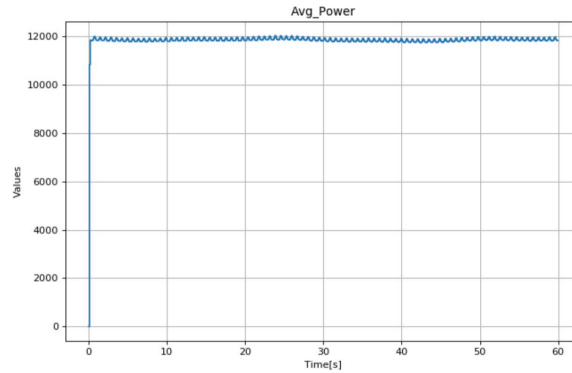
(b) Average Power Curve mapped within the Dynamic Table

Figure 6.4: Features within each Dynamic Table.
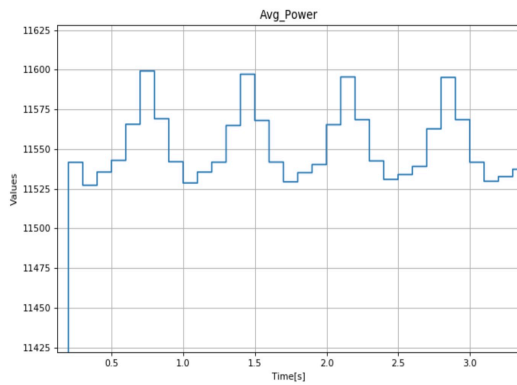
(a) "2_1": Snowblower and Cultivator
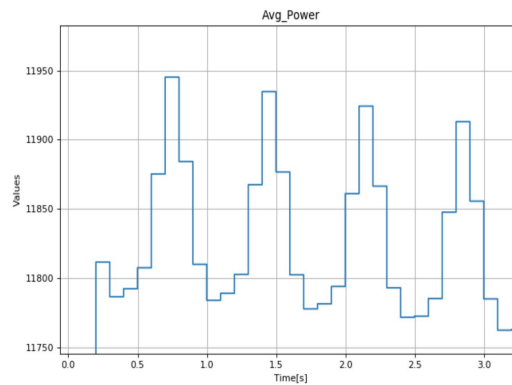
(b) "2_3": Snowblower and Atomizer

Figure 6.5: Load Functions within Dynamic Tables.

As illustrated in the figures above, the Average Power values can be accessed and observed in time intervals of 0.1 seconds, which is the set time interval for maintaining control system stability, as highlighted in previous sections. The value from these 8 Dynamic Tables is accessed by the system throughout the simulation duration, but only one table gets forwarded, depending on the implements selected by the user. This is achieved using a Signal Switch block, which is explained in the next section.

6.2. User-Input C-Function

The User Input C-Function plays a key role in deciding which Dynamic Table to use as reference for Energy Management. As illustrated in the figure below, the User Input

C-Function takes inputs: the DC load selected by the user (either 1 or 2), and the 3 AC load (either 1, 2, 3 or 4), as previously shown in the HIL SCADA layout of the model.
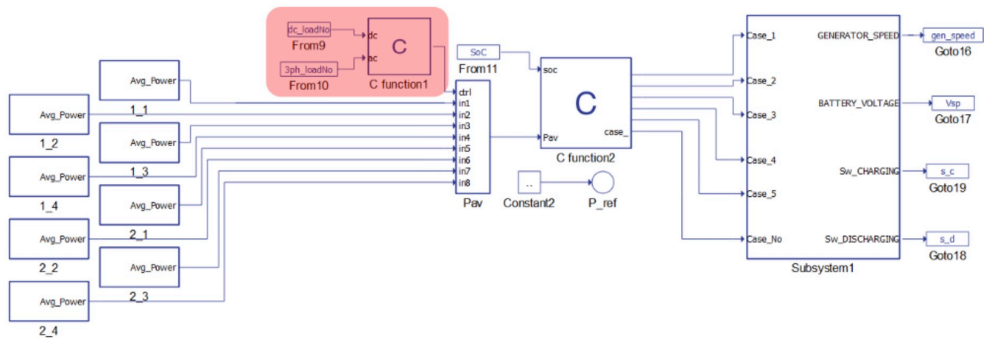
Figure 6.6: User-Input C-Function within the Energy Management System.

Depending on the values of the input received, the User Input C-Function then employs a code which helps in allotting a specific number. For example, when DC = 1, and AC = 1, then Load = 1. Similarly, when DC =1, and AC =2, then Load = 2, and so on. The following image illustrates the code that has been employed for allotting a specific number to each load combination, therefore resulting in an output, which ranges from 1 to 8.

Based on which two loads the user has selected, the User Input C-Function gives an output ranging between 1 and 8. This value is then fed into the Signal Switch, which is the block highlighted in the following image.
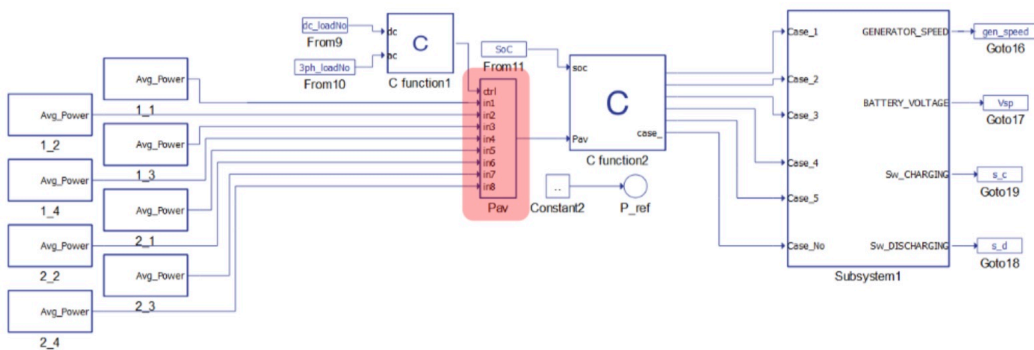
Figure 6.7: Dynamic Table Signal Switch within the Energy Management System.

The Signal Switch, in this case, has 9 inputs and 1 output. 8 out of those 9 inputs are the Average Power curves from all the Dynamic Tables, and these values are received in

real-time at the Signal Switch. Based on the input value received from the User Input
C-Function, the Signal Switch only passes the Average Power curve of that specific load
combination, and the rest of the signals are blocked. For example, if the User Input C-
Function sends a value of 5 to the Signal Switch, only the Average Power curve of "2_1"
will be forwarded, as this is the power curve when DC = 2, and AC = 1. The power curve
is then forwarded into the Decision C-Function.

6.3.   Decision C-Function

The next block in the logic sequence is the Decision C-Function, which receives 2 inputs,
and has 6 outputs values. The inputs of the Decision C-Function are the real-time Battery
SoC, and the Average Power curve received from the Signal Switch block. The following
image illustrates the position of the Decision C-Function.
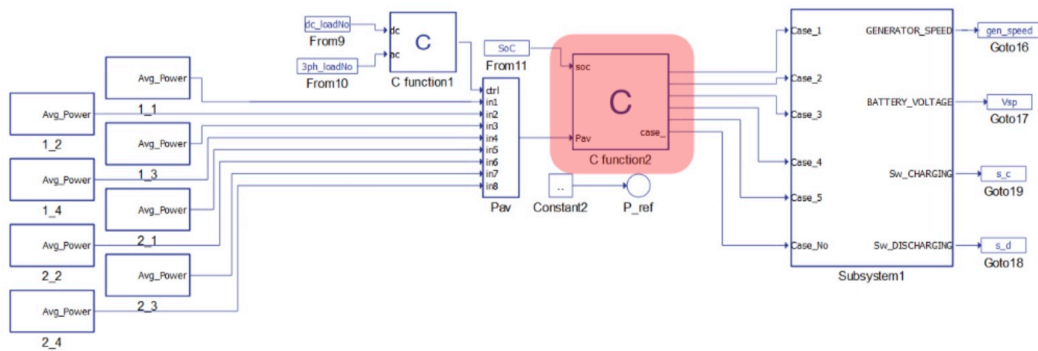
Figure 6.8: Decision C-Function within the Energy Management System.

The objective of the Decision C-Function is to decide the contribution of the Battery Pack
in power management, based on the SoC of the Battery. If the Battery is low on charge,
ie, if the SoC is low, then the percentage contribution of power from the Battery will
be low, and if the SoC is high, the Battery can deliver a higher percentage of the power
demand. The Decision C-Function partly follows the logic of the algorithm shown in
Figure 6.2. Based on the SoC of the Battery Pack, the Decision C-Function must allocate
a case number, ranging from 1 to 5, as the Energy Management algorithm is based on 5
different SoC cases. The following image illustrates the code that has been employed for
governing the Decision C-Function.

Depending on the value of SoC, the Decision C-Function allots a case value. The C-
Function also forwards the Average Power curve values to only one of the five output
ports, depending on the case number. It must be highlighted that 5 different switching

patterns have been designed for the Generator and the Battery Pack, and depending on the SoC of the Battery, one of these switching patterns must be employed to ensure optimized performance. The Decision C-Function essentially checks the value of SoC, and forwards the Average Power curve to the port that is assigned the switching role (in the next subsystem) at that SoC. The remaining ports are assigned a value of zero, and remain inactive, as they do not fall in that SoC range.

6.4.   Energy Management Controller

The Energy Management Controller is the last and main subsystem responsible for governing all switching actions. It mainly controls four elements: the Generator Speed, the Battery Voltage, the Battery Discharge Switch, and the Battery Charge Switch. The following image highlights the Energy Management Controller subsystem.
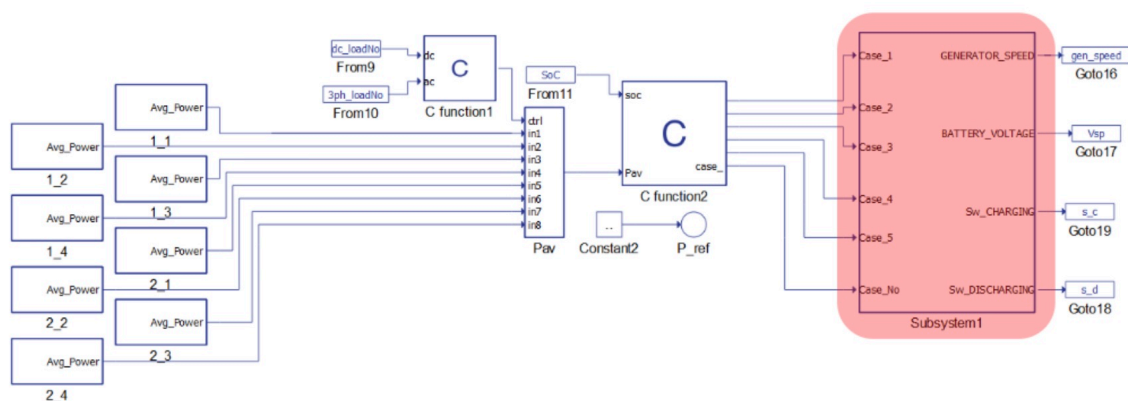
Figure 6.9: Energy Management Controller within the Energy Management System.

The Energy Management Controller is a complex subsystem, housing 5 cases designed for different control patterns. Only one of these cases becomes active at a time, and that case is determined by the SoC of the Battery. Figure 6.12 illustrates the signal processing network employed inside the Energy Management Controller subsystem. The Decision C-Function sends the Average Power data to these five ports, which then sets the value of Generator Speed and Battery Voltage. For each case, there are two conditions: If the Average Power is less than, or greater-than/equal-to the Reference Power, which has been set at 11.55kW. Depending on if the previous condition has been satisfied, the Energy Management Controller then sets different values of Generator Speed and Battery Voltage, only selectively ensuring the involvement of the Battery Pack in order to meet peak power demands.

All the 5 cases pass 4 outputs at all times: the Generator Speed, the Battery Voltage, the

position of the Battery Discharge Switch, and the position of the Battery Charge Switch. However, the values of only the active case are valid, since all other cases receive zero as input. All the four control outputs are received from all the five cases, and are met at four different Signal Switches, each dedicated to selecting the Generator Speed, Battery Voltage, and the two Switch Positions, respectively. The "case_no" received from the Decision C-Function is used to pass only the values of the active case, and the values of the remaining cases are blocked. These values are then sent directly to the Generator, the Battery Pack, and the switches, with no further signal processing required.
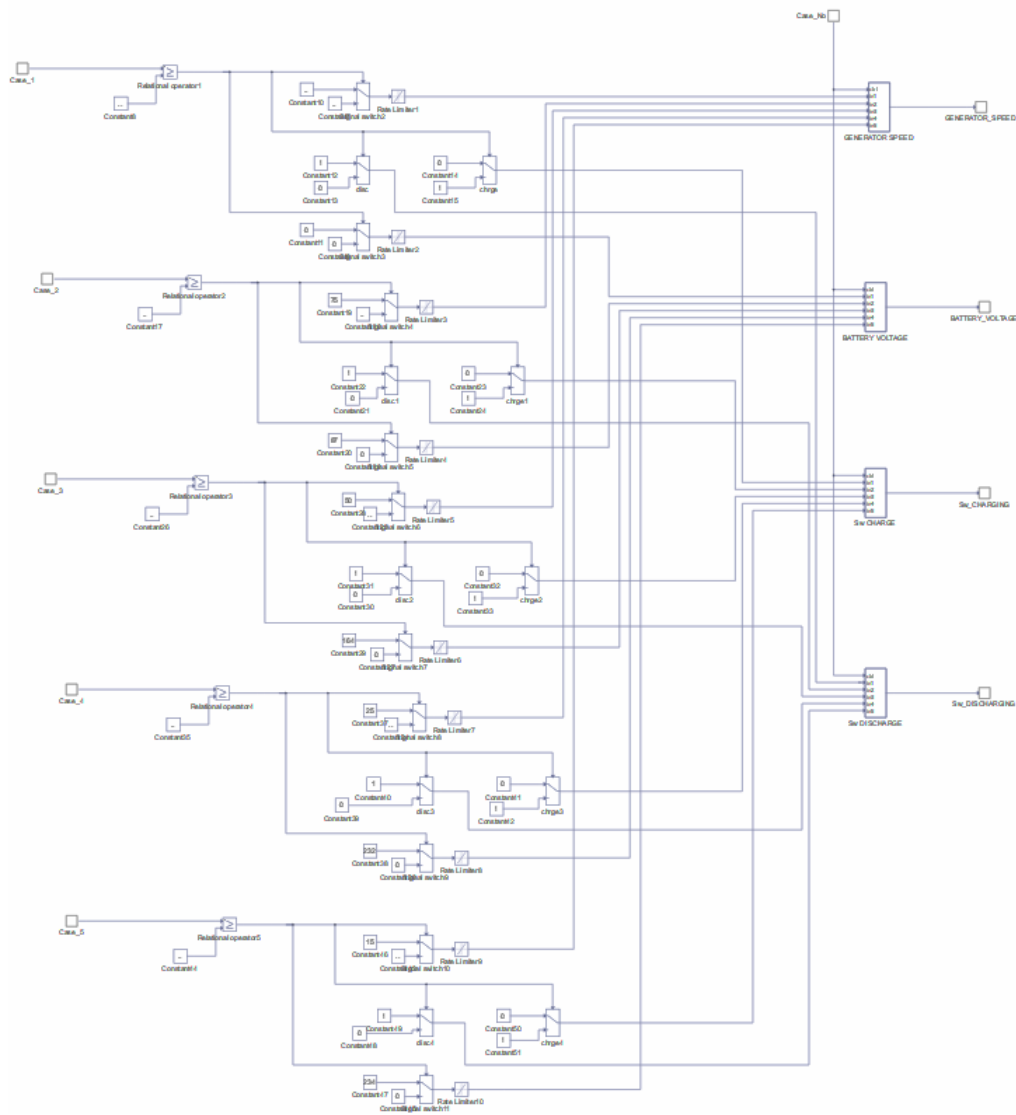
Figure 6.10: Signal Processing Schematic within the Energy Management Controller.
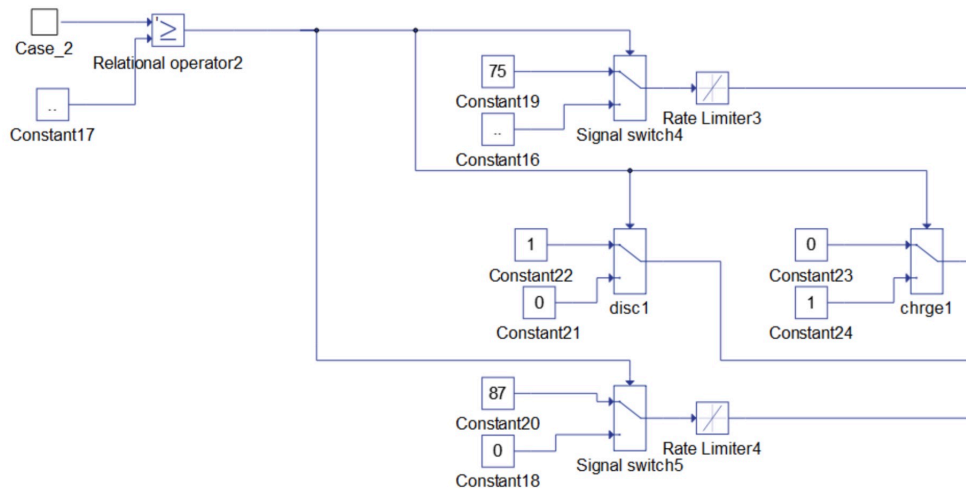
Figure 6.11: Close-up of one of the cases inside the Energy Management Controller.

Figure 6.12 illustrates a closer look into one of the five cases inside the Energy Management Controller. In the image, Case 2 has been highlighted. It can be observed that each case consists of common blocks. Individual cases follow the logic of the algorithm illustrated in Figure 6.2, and implement the signal processing using basic comparison blocks and Signal Switches. It must, however, be noted that the change in values of the Generator Speed and the Battery voltage is not instantaneous. This has been ensured in the model by the usage of Rate Limiters, which play a highly critical role in keeping the system dynamics stable. The impact of Rate Limiters has been illustrated in the next section.

6.5.   Rate Limiter Tests

Rate Limiters have been installed for regulating the change in Generator Speed and Battery Voltage values. It is certain that making critical voltages jump from one value to another can cause significant instabilities in the system, or might introduce sharp spikes in system voltages. This section aims to illustrate the process of selecting the ideal Ramp value, through trial-and-error methods.
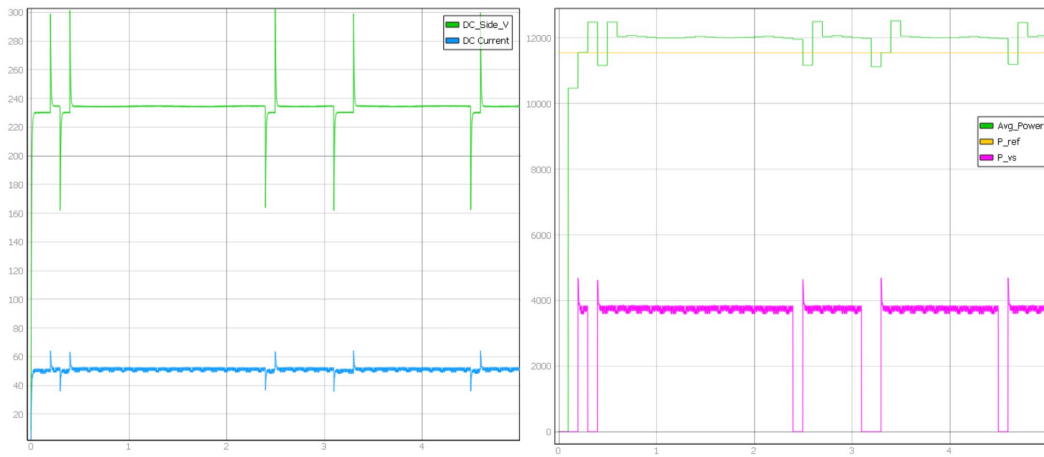
Figure 6.12: Voltage Spikes (Green) at Ramp = 0.
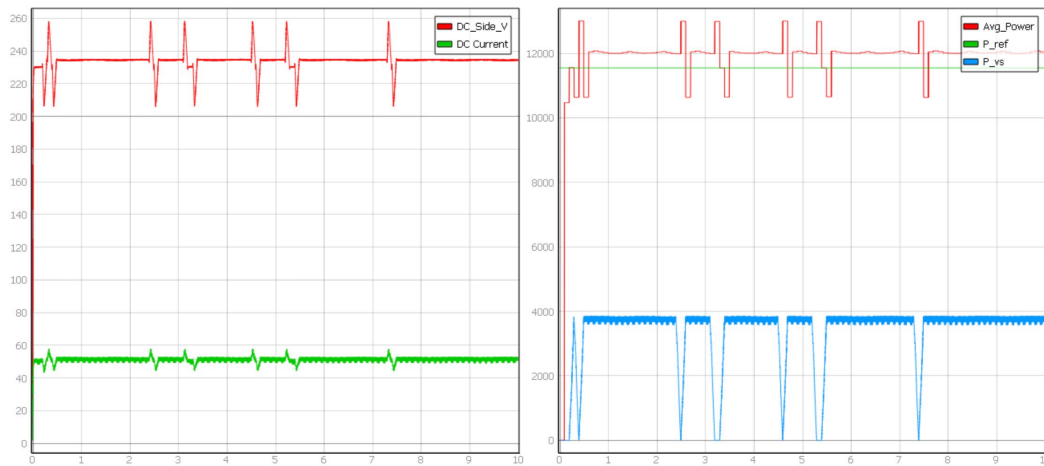
Figure 6.13: Voltage Spikes (Red) at Ramp = 750.
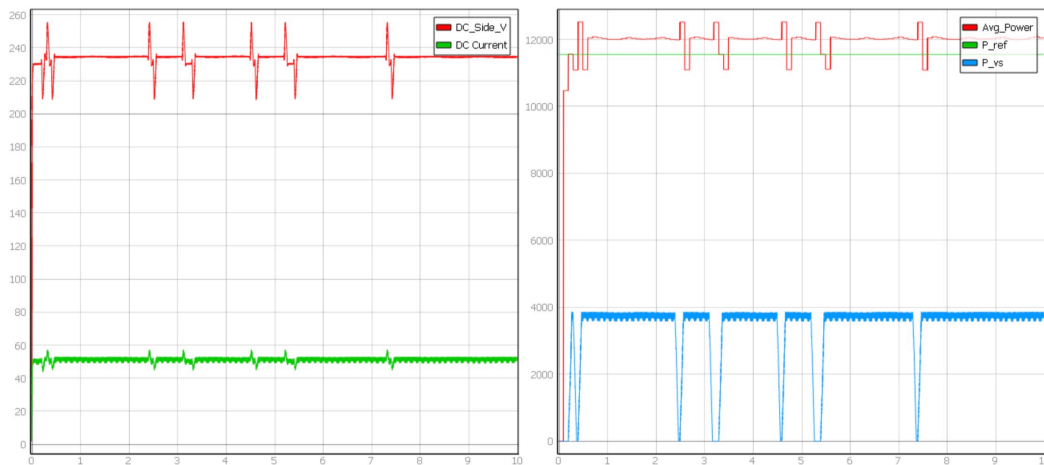
Figure 6.14: Voltage Spikes (Red) at Ramp = 1000.
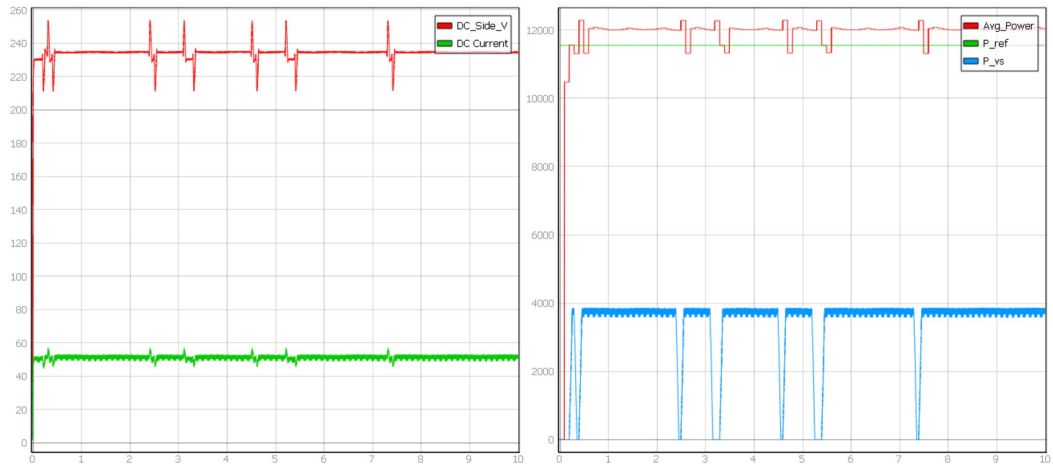
Figure 6.15: Voltage Spikes (Red) at Ramp = 1200.
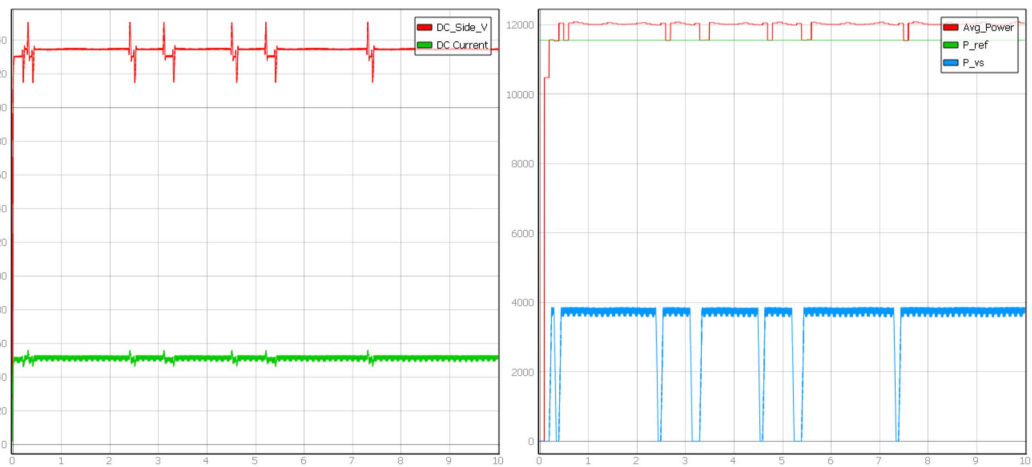
Figure 6.16: Voltage Spikes (Red) at Ramp = 1500.
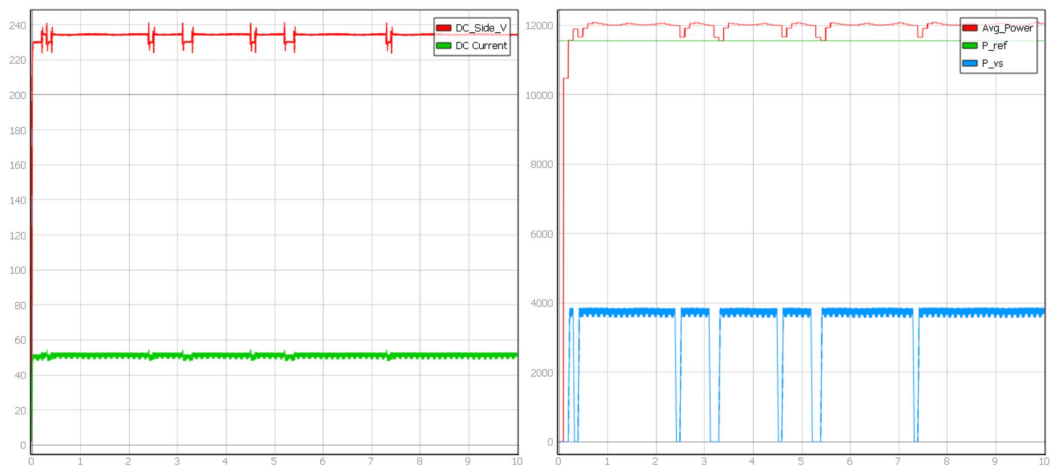
Figure 6.17: Voltage Spikes (Red) at Ramp = 2000.

It can be observed from the graphs that the DC Side voltage experiences extremely sharp spikes of high magnitude when no Ramping is employed during switching. The DC voltage ripple is very high, and measures around 59.57%, which is completely unacceptable. On introducing a Ramp value of 750, the ripple is limited to 21.27%. As the Ramp value is increased gradually, and the signals are allowed to change at a slower pace, the ripple comes down to 12.76% for a Ramp value of 1200, and then finally to an acceptable value of 4.25% at a Ramp of 2000. The limiting of the ripples gets saturated after this Ramp value, and very little gains are observed even after large changes in Ramp value, which is why this value has been selected as the final Ramp value. The target was to bring the oscillations below 5.00%, which was successfully achieved.

6.6.　Energy Management Simulations

This section explores some of the simulations run using the Energy Management System. This section aims to highlight the successful implementation of the Energy Management algorithm, where the graphs illustrate the change in Generator Speed and Battery Pack voltage changes when the Average Power exceeds the reference value during the course of the simulation.
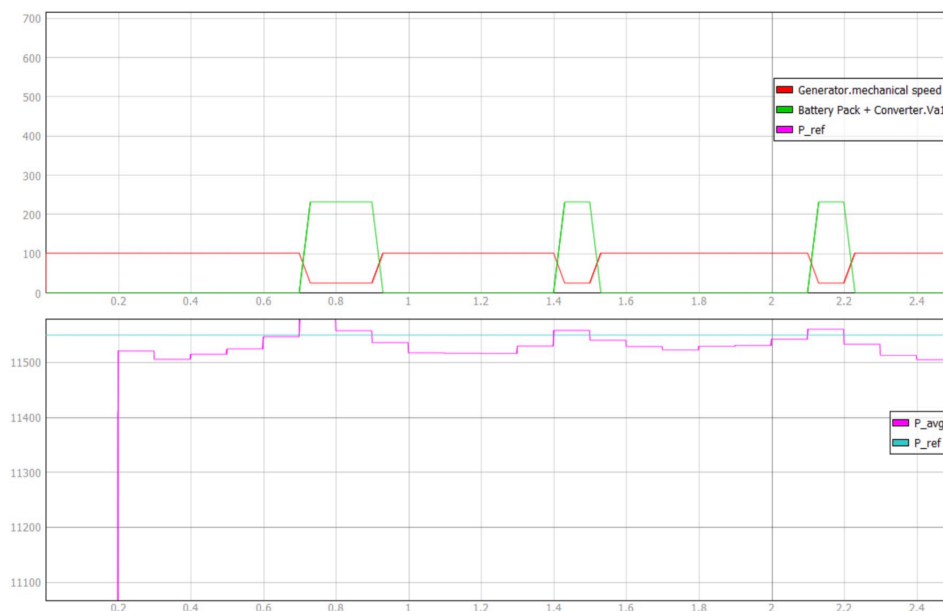
Figure 6.18: Generator Speed and Battery Voltage variations for Battery Heater and Seed Spreader, at Starting SoC of 73%.

The graph above illustrates the simulation of the Battery heater and the Seed Spreader, when the starting SoC of the Battery Pack is at 73%. It can be observed that when Pav

> Pref at t = 0.7s, 1.4s, and 2.1s, the Generator Speed comes down from its peak value of 101.1 rad/sec to 25 rad/sec. This is where the involvement of the Battery Pack begins, supplying an additional 224V to the DC Bus.
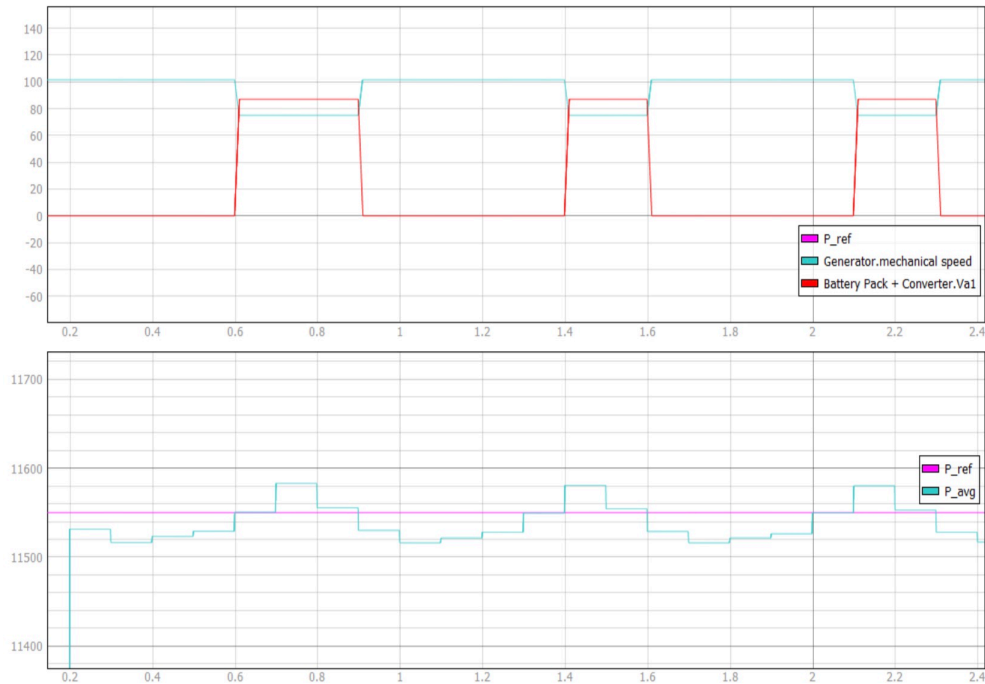
Figure 6.19: Generator Speed and Battery Voltage variations for Snowblower and Manure Spreader, at Starting SoC of 46%.

The case above illustrates the simulation of the Snowblower and the Manure Spreader, at a starting SoC of 46%. It can be observed that the contribution of the Battery Pack is much lower when the SoC is low. As Pav crosses the Pref mark at t = 0.6s, 1.4s, and 2.1s, the Generator Speed goes from 101.1 rad/sec to 75 rad/sec, thereby only partially reducing its output. The Battery Pack, on the other hand, supplies only 87V to support the Generator, which is the case specifically designed for low SoC conditions.
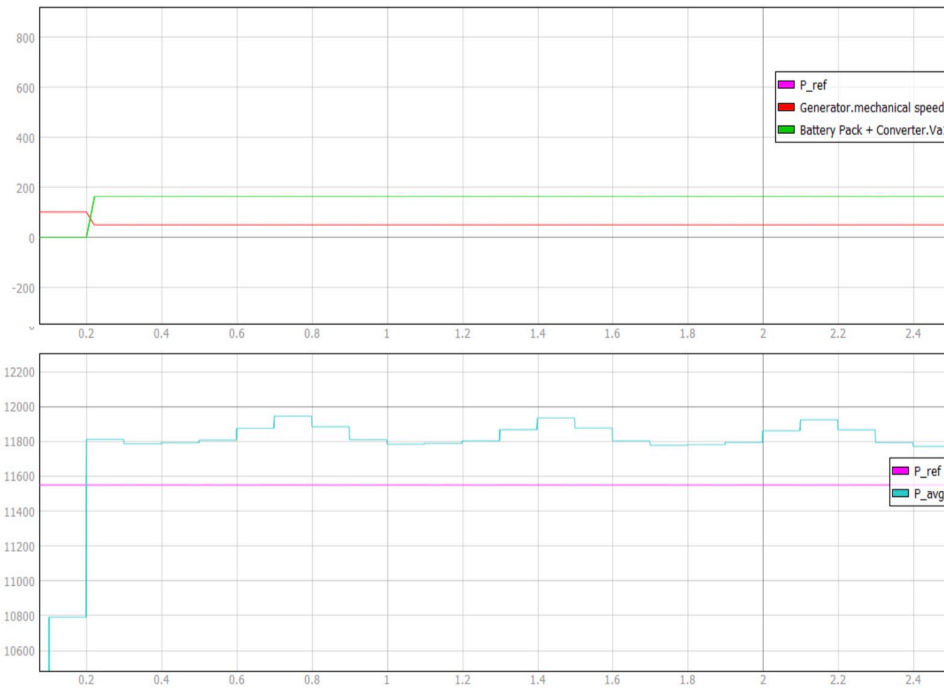
Figure 6.20: Generator Speed and Battery Voltage variations for Snowblower and Cultivator, at Starting SoC of 68%.

The final simulation illustrated in this section is that of the Snowblower and the Cultivator. In this case, Pav > Pref becomes true at t = 0.2s, and the condition is maintained throughout the length of the simulation. During this time, since the SoC is at a high enough value, the Generator Speed goes down from 101.1 rad/sec to 50 rad/sec, while the Battery Pack voltage rises to a steady 164V.

7 | Final Simulation Results

The final section of this thesis takes a closer look into running simulations of all 8 load cases. The objective is to understand how the power demand varies with time, and see if the Energy Management System appropriately takes SoC into account for balancing power output between the Generator and the Battery Pack. It should be observed how and when the Battery Pack is drawing power from the source, and how the SoC increases or decreases, based on how the Battery is behaving. While the simulations should ideally run for about 60 seconds each, all 8 simulations have been carried out for 10 seconds, due to computational restrictions of the author's system. To put things into perspective, running a 10-second simulation and mapping all plots takes about 30 - 40 minutes in the author's system. Conducting 8 such simulations for 60 seconds each would not be feasible, and therefore a 10-second limit has been set on the simulation time interval.

For the purpose of carrying out the full-system simulations of all the eight implement combinations, the following conditions have been imposed:

- The maximum Generator Speed has been set to 101.5 rad/sec.

- The Generator produces approximately 235V at maximum speed.

- The Battery Pack can supply voltages between 87V and 230V.

- All Harmonic Filters have been deployed and activated.

- Generator Speed and Battery Voltage Ramp is set to 2000.

- Ideal switches with a dead-time of 1μs have been used in the Battery.

- All signals have been sampled at 1MSPS.
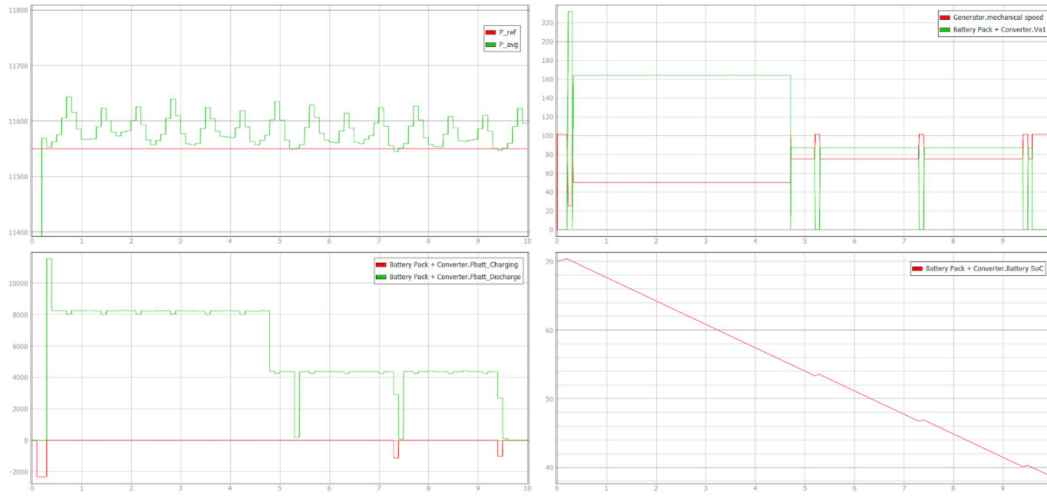
Figure 7.1: Powertrain Parameters with Battery Heater and Cultivator, at Starting SoC of 70.0%.

Battery Heater and Cultivator: The first case shown above is that of the Battery Heater and Cultivator, and the plots illustrate the variation of several different parameters when the simulation is running. The starting SoC for this simulation has been set to 70%. It can be observed that as the Average Power varies, the Battery Pack delivers power to the load whenever $P_{av} > P_{ref}$, which is the case for the most part of the simulation. During short intervals, when $P_{av} < P_{ref}$, the Battery draws power from the source, thereby increasing the SoC in short bursts. The SoC increases during the first few milliseconds of the simulation, and decreases as the Battery delivers powers, only to be momentarily charged when $P_{av} < P_{ref}$. It should be noted that when the SoC falls in different logic categories, the power delivered by the Battery pack varies. The same is illustrated by the change in the voltage values and Generator Speed, as the Energy Management System controls these values for different SoC levels.
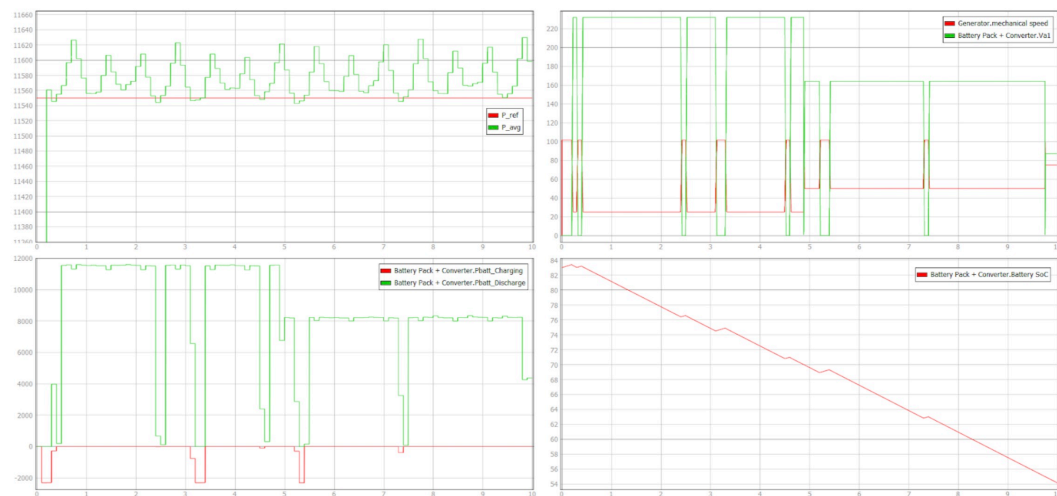
Figure 7.2: Powertrain Parameters with Battery Heater and Manure Spreader, at Starting SoC of 83.0%.

Battery Heater and Manure Spreader: The second case is the simulation of the Battery Heater and Manure Spreader, and the power variation in this case is slightly more complex. It can be seen that P_{av} crossed P_{ref} several times during the simulation, during which the Battery Pack rapidly charges and discharges. The SoC follows its trend accordingly, increasing in short bursts whenever $P_{av} < P_{ref}$, but decreasing overall, as the Battery Pack delivers more power in the simulation interval than it draws. The Generator Speed and Battery Voltage change continuously, and follow the logic prescribed by the Energy Management System, and the overall power output of the Battery Pack decreases, as the SoC gradually goes down from 83% to 54% during the simulation interval.
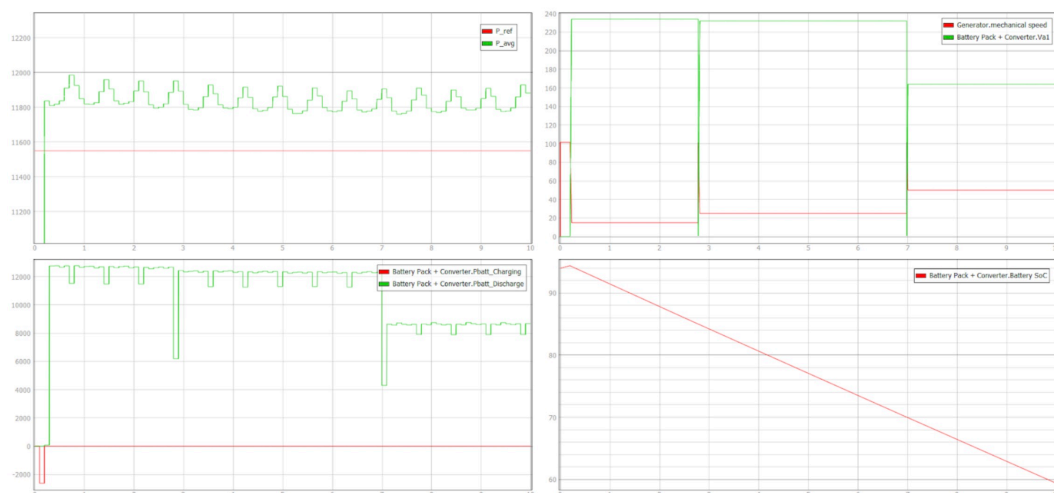
Figure 7.3: Powertrain Parameters with Battery Heater and Atomizer, at Starting SoC of 94.0%.

Battery Heater and Atomizer: The third case, shown above, is that of the Battery Heater and the Atomizer. The Average Power curve in this case is marked by sharp power demands, with values over the reference threshold for the entire simulation interval. The starting SoC for this simulation has been set to 94%, which can be observed in the graph. It must be noted that the Battery delivers power to the load by discharging in the entire time interval, and the SoC accordingly goes down after a short burst of initial charging during the first few milliseconds of the simulation.
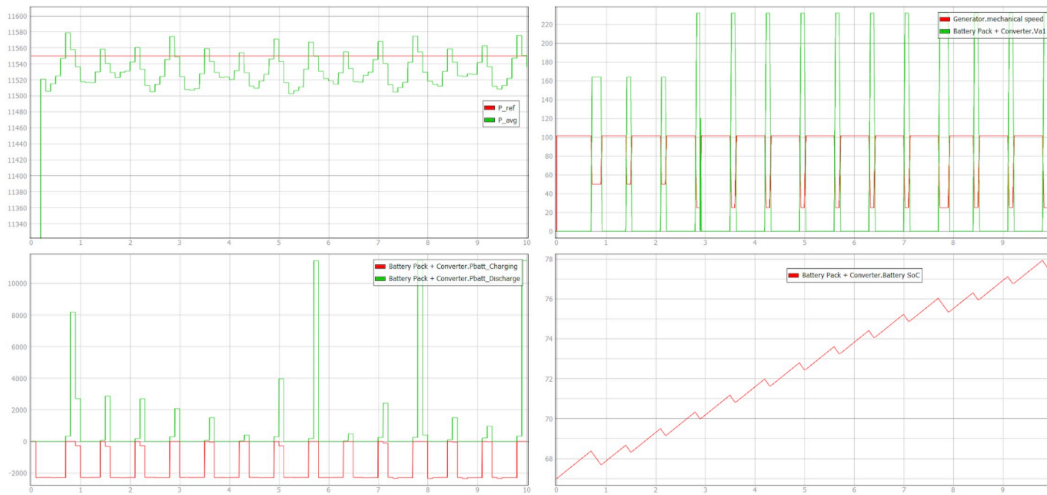
Figure 7.4: Powertrain Parameters with Battery Heater and Seed Spreader, at Starting SoC of 67.0%.

Battery Heater and Seed Spreader: The fourth simulation is that of the Battery Heater and the Seed Spreader. For this case, the starting SoC of the Battery Pack has been set to 67%. In this case, the Average Power alternates above and below the Reference Power threshold, due to which the Battery Pack only discharges energy and delivers power for brief intervals. It can be observed from the graphs that the Charging Power exceeds the Discharging Power, which explains why the SoC follows a zig-zag pattern, and gradually increases from 67% to 78% during the simulation interval. It should also be noted that as the SoC crosses the 70% mark at t = 2.6s, the power discharged by the Battery Pack increases. The short peaks of power appear in the simulation because the time duration of power delivery is less than the sampling time of 0.1s. The increase in involvement of the Battery Pack can also be seen in the top right graph, where the Battery voltage increases significantly, as the SoC crosses the 70% mark.
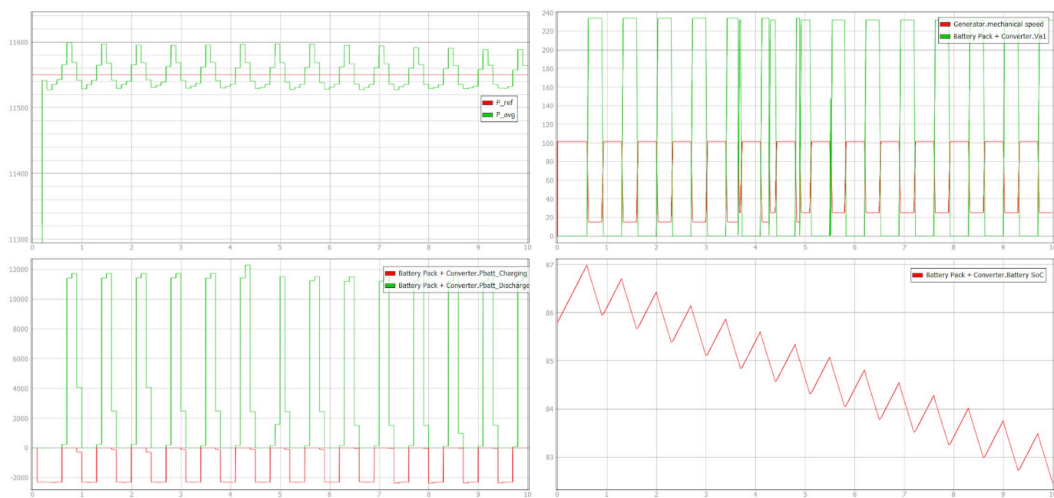
Figure 7.5: Powertrain Parameters with Snowblower and Cultivator, at Starting SoC of 85.8%.

Snowblower and Cultivator: The graph shown above is the fifth simulation case, where the selected implements are the Snowblower and the Cultivator. The Average Power curve in this case is characterized by sharp power variations, which alternate above the below the reference power value. The result is alternate charging and discharging of the Battery Pack, which can be observed in the graph. Due to this, the Battery SoC goes up and down in a zig-zag fashion, but has the overall trend going downward, as the electrical energy delivered by the battery pack exceeds the energy absorbed. The sharp variation of the Battery Pack SoC also perfectly aligns with the switching pattern dictated by the Energy Management System, as the Battery voltage alternated between zero and 230V.
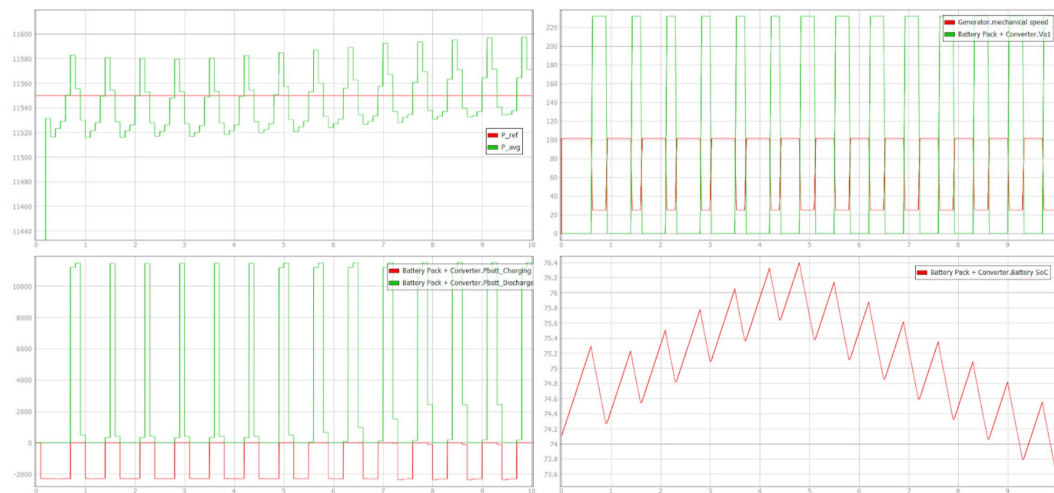
Figure 7.6: Powertrain Parameters with Snowblower and Manure Spreader, at Starting SoC of 74.1%.

Snowblower and Manure Spreader: Shown above is the sixth simulation case, where the Snowblower and the Manure Spreader have been selected. This is a particularly interesting case, where the trend of Average Power can be seen gradually going up and increasing with respect to the reference power. As a consequence, the Battery Pack delivers power in gradually increasing bands, almost in a PWM-like fashion. On the other hand, it can be observed that the power drawn by the Battery remains nearly identical throughout the simulation, which reflects an interesting pattern on the SoC. The SoC starts from around 74%, and has a tendency to increase when $P_{charging} > P_{discharge}$. The reverse happens when the net $P_{charging} < P_{discharge}$, as the width of the band increases after a point. It can be clearly observed that the Generator Speed and the Battery voltage undergo no change in "case" throughout the simulation, as the SoC remains in a fixed range, thanks to continuous charging.
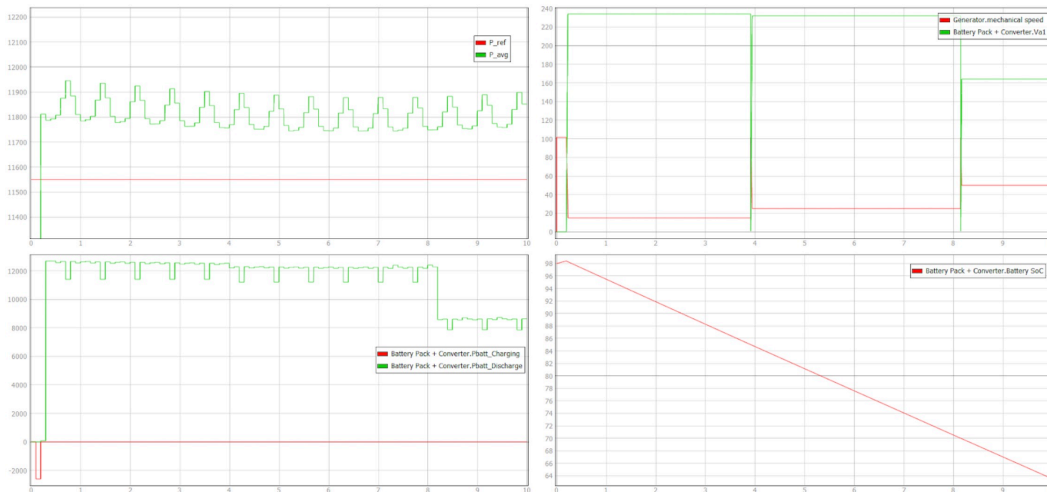
Figure 7.7: Powertrain Parameters with Snowblower and Atomizer, at Starting SoC of 98.0%.

Snowblower and Atomizer: The load case of the Snowblower and the Atomizer is the second-last simulation case, and a starting SoC of 98% has been selected to illustrate the Battery discharge process. It can be observed that the SoC goes down after a few initial milliseconds of charging, as the condition of $P_{av} > P_{ref}$ stays true for most of the simulation. As the SoC goes down, the Energy Management System governs the Generator Speed and Battery voltage accordingly. This change can be observed in the bottom left graph, where the Battery power delivered to the load sees a change at t = 4.2s and 8.3s.
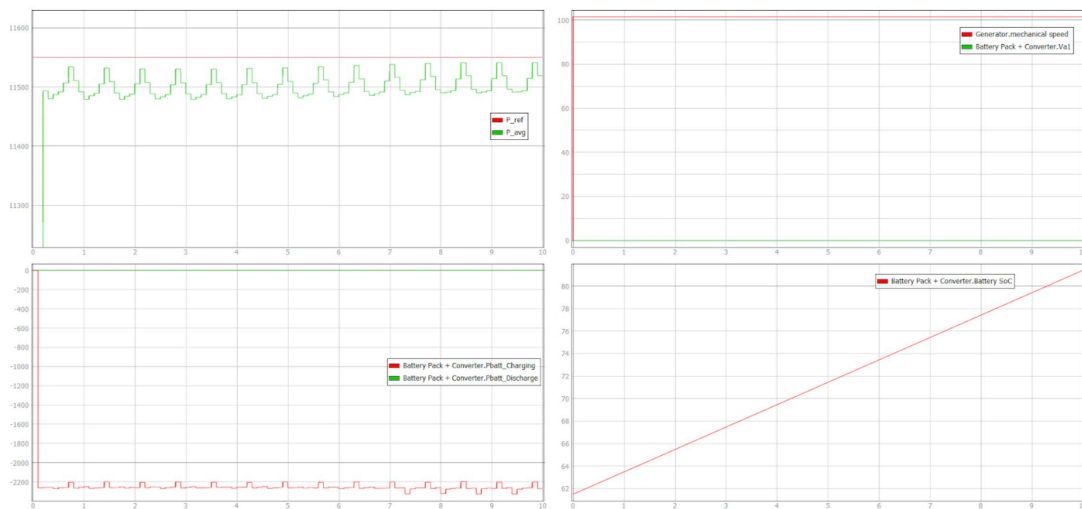
Figure 7.8: Powertrain Parameters with Snowblower and Seed Spreader, at Starting SoC of 61.5%.

Snowblower and Seed Spreader: The case of the Snowblower and Seed Spreader is the last simulation case, and for this simulation, a starting SoC of 61.5% has been chosen. From the top left graph, it can be observed that the Average Power stays below the reference value for the entire duration of the simulation. However, it must be noted that the Average Power curve eventually crosses the reference value at higher time intervals, as the trend is clearly upwards. As $P_{av} < P_{ref}$, the Battery Pack behaves as a load, and draws power from the source. During this time, the SoC gradually increases, and the Battery charges up to nearly 82%. It can also be seen that since the Battery Pack is not delivering any power to the load, the Energy Management System ensures that the Battery produces zero voltage output, and all of the power is supplied by the Generator, which runs at its maximum speed of 101.5 rad/sec.

8 | Conclusions

In this thesis, an attempt has been made to simulate a series-hybrid tractor powertrain, which deploys an efficient Energy Management System to distribute power delivery by the Internal Combustion Engine and the Battery Pack. For quantifying the results, all simulations were run using Typhoon-HIL SCADA, and observations were duly recorded. The simulation data present concrete results of the entire system functioning within the defined operating conditions, and all systems correctly manage to exchange power and data with each other. It has been observed that the Battery Pack successfully manages to bring down the power output of the Generator, which is the ultimate objective of the thesis. It has also been established that the Energy Management System successfully managed to charge the Battery Pack when the power demand is low, thereby increasing the longevity of the powertrain through continuous cycles of Battery charging and discharging.

Based on the simulations and obtained results of the thesis, it can be confidently concluded that the Energy Management System plays a vital role in optimizing system performance by balancing the energy flow from the Engine and the Battery Pack. The Energy Management Algorithm, combined with the Battery Pack, makes a significant impact on the overall requirement of the power produced by the Engine. Therefore, hybridization of automotive powertrains certainly serve an important purpose in reducing the need of a powerful Internal Combustion Engine, and in the process, help in significantly bringing down the carbon footprint of the vehicle during operation. In order to achieve this with higher levels of efficiency, a suitable Energy Management System can be employed to optimize powertrain performance.

Additionally, the design and deployment of more sophisticated Energy Management Strategies can serve to improve powertrain performance even to a further degree. By employing smarter control schemes, as well as using advanced tools such as Neural Networks and Reinforced Learning models, it is possible to predict the power demand of the loads, and make necessary corrections in the electrical network beforehand. This can not only lead to improved powertrain efficiencies, but can also help in bringing down system complexities, number of controllers and even power converter devices. The overall result could

potentially be a far more compact and energy-efficient hybrid powertrain.

Lastly, it is evident that the transition towards hybridized powertrains employing Energy Management Systems in tractor powertrains could be a positive indicator for the industry. Keeping technology, costs, and utility in mind, this shift in technology not only promotes a decline in carbon footprint, but gives way to effective agricultural process, improving farming yield, and potentially making a positive long-term impact on the economy.

Bibliography

[1] V. T. Articles. Construction and installation of lithium-ion battery packs. URL `https://www.vox.com/recode/23027110/solid-state-lithium-battery-tesla-gm-ford`.

[2] Q. A. Azze and X. Wang. Field-oriented control of permanent magnet synchronous motors based on dsp controller. *Southern Illinois University Edwardsville*, page 9, January 2014.

[3] R. P. Bajpai and U. Chandrasekhar. Innovative design and development practices in aerospace and automotive engineering. *Springer*, pages 211–229, February 2016.

[4] W. Bakkali, M. Tlich, P. Pagani, and T. Chonavel. A measurement-based model of energy consumption for plc modems. *18th IEEE International Symposium on Power Line Communications and Its Applications*, page 3, March 2014.

[5] C. Capital. Timeline of tractor powertain technology. URL `https://www.crestcapital.com/tax/timeline_of_tractors`.

[6] K. Chinnakani, A. Krishnamurthy, and J. Moyne. Comparison of energy consumption in hvac systems using simple on-off, intelligent onoff and optimal controllers. *IEEE Power and Energy General Meeting*, pages 3–5, October 2011.

[7] E. P. Converters. Battery state of charge calculation with epc converters. *Application Note - AN026*, pages 3–5, June 2020.

[8] i. Deere Company. John-deere sb11 series snowblower, . URL `https://www.deere.com/en/attachments-accessories-and-implements/utility-tractors-attachments-accessories/snow-removal-equipment/sb11-3-point-snowblowers/`.

[9] i. Deere Company. John-deere ms12 series manure spreader, . URL `https://www.deere.com/assets/publications/index.html?id=6c317b23#1`.

[10] i. Deere Company. John-deere2230fh floating hitch field cultivator, . URL `https://www.deere.com/en/tillage/2230-floating-hitch-field-cultivator/`.

[11] i. Deere Company. John-deere r4023 sprayer, . URL `https://www.deere.com/en/sprayers/r4023-sprayer/`.

[12] i. Deere Company. John-deere ss20b series broadcast spreaders, . URL `https://www.deere.com/en/attachments-accessories-and-implements/utility-tractors-attachments-accessories/seeding-equipment/ss20b-broadcast-spreader/`.

[13] i. Deere Company. John deere 60 hd snowblower 2-stage blades, . URL `https://cdn.datamanager.arinet.com/image/JDC/47681712-980c-4496-9b33-1a32558e5065/Small?ariz=5`.

[14] G. o. I. Department of Heavy Industries. National level ev-adoption policy. URL `https://e-amrit.niti.gov.in/national-level-policy`.

[15] i. Etrailer. Kat's kh222000 battery heater. URL `https://www.etrailer.com/Vehicle-Heaters/Kats-Heaters/KH22200.html`.

[16] M. Li, J. He, and N. Demerdash. A flux-weakening control approach for interior permanent magnet synchronous motors based on z-source inverters. *IEEE Transportation Electrification Conference*, page 1, June 2014.

[17] B. McFadzean and L. Butters. An investigation into the feasibility of hybrid and all-electric agricultural machines. *British Agronomy Journal*, pages 504–507, February 2019.

[18] F. Mocera and A. Soma. A review of hybrid electric architectures in construction, handling and agriculture machines. *Intechopen*, pages 3–5, August 2021.

[19] C. Quendo, E. Rius, C. Person, and M. Ney. Integration of optimized low-pass filters in a bandpass filter for out-of-band improvement. *IEEE*, pages 2–7, December 2001.

[20] E. Scolaro, M. Beligoj, and L. Alberti. Electrification of agricultural machinery: A review. *IEEE Vehicular Technology Society*, pages 1–4, December 2021.

[21] M.-K. Tran, M. Akinsanya, S. Panchal, R. Fraser, and M. Fowler. Design of a hybrid electric vehicle powertrain for performance optimization considering various powertrain components and configurations. *epartment of Mechanical and Mechatronics Engineering, University of Waterloo*, page 25, December 2020.

[22] P. J. Tritschler, S. Bacha, and G. H. E. Rullière. Energy management strategies for an embedded fuel cell system on agricultural vehicles. *The XIX International Conference on Electrical Machines - ICEM 2010*, page 4, June 2020.

[23] P. J. Tritschler, S. Bacha, and G. H. E. Rullière. Energy management strategies for an embedded fuel cell system on agricultural vehicles. *The XIX International Conference on Electrical Machines - ICEM 2010*, pages 1–2, September 2020.

[24] D. Troncon, L. Alberti, and M. Mattetti. A feasibility study for agriculture tractors electrification: Duty cycles simulation and consumption comparison. *2019 IEEE Transportation Electrification Conference and Expo (ITEC)*, page 3, June 2019.

[25] i. Typhoon-HIL. Hil 404 datasheet and comparison, . URL `https://www.megacal.com/sistemas-calibracion-potencia-energia-doc/productos/Potencia_y_Energia_HIL404_catalogo.pdf`.

[26] i. Typhoon-HIL. Hil 404 manufacturer overview, . URL `https://www.typhoon-hil.com/products/hil404-announcement-page/`.

[27] S. Vaez-Zadeh. *Control of Permananent Magnet Synchronous Motors*. Oxford University Press, 2018.

[28] K. Çag atay Bayindir, M. A. Gözüküçük, and A. Teke. A comprehensive overview of hybrid electric vehicle: Powertrain configurations, powertrain control techniques and electronic control units. *Science Direct*, pages 1306–1308, February 2011.

A | Appendix

Code for DC Load C-Function:

```
    if(SCADA == 1)
{
    load = heater;
}
else
    {
    load = sb;
    }
```

Code for 3∼ AC Load C-Function:

```
    if(scada == 1)
{
    out = cultivator;
}
else if (scada ==2)
    {
    out = manurespreader;
    }
    else if (scada==3)
    {
        out = atomizer;
    }
    else
    {
        out = seedspreader;
    }
```

Code for Decision C-Function:

```
    if (soc<40)
{
    out1=Pav;
    out2=0;
    out3=0;
    out4=0;
    out5=0;
    case_=1;
}
else if (soc<55 && soc>=40)
{
    out1=0;
    out2=Pav;
    out3=0;
    out4=0;
    out5=0;
    case_=2;
}
else if (soc<70 && soc>=55)
{
    out1=0;
    out2=0;
    out3=Pav;
    out4=0;
    out5=0;
    case_=3;
}
else if (soc<85 && soc>=70)
{
    out1=0;
    out2=0;
    out3=0;
    out4=Pav;
    out5=0;
    case_=4;
```

```
}
else
{
    out1=0;
    out2=0;
    out3=0;
    out4=0;
    out5=Pav;
    case_=5;
}
```

Code for User-Input C-Function:

```
    if (dc==1 && ac==1)
{
    load=1;
}
else if (dc ==1 && ac ==2)
{
    load =2;
}
else if (dc ==1 && ac ==3)
{
    load = 3;
}
else if (dc ==1 && ac ==4)
{
    load = 4;
}
else if (dc==2 && ac==1)
{
    load=5;
}
else if (dc ==2 && ac ==2)
{
    load =6;
```

```
}
else if (dc ==2 && ac ==3)
{
    load = 7;
}
else
{
    load = 8;
}
```

List of Figures

List of Tables

Acknowledgements

At the culmination of this incredible journey, I am overwhelmed with gratitude for the numerous individuals who have accompanied me along this path. It is with heartfelt appreciation that I express my deepest gratitude to those who have contributed to the completion of my Master's thesis.

First and foremost, I extend my utmost gratitude to my esteemed supervisor, Professor Giambattista Gruosso and co-supervisor, Professor Giancarlo Storti Gajani for their guidance, invaluable support, and immense knowledge. I am extremely grateful for the instrumental role played by my other co-supervisor, Marziyeh Hemmati, whose deep technical insights and impeccable software skills have brought this thesis to life.

I am also indebted to the faculty members of Politecnico di Milano, whose wisdom, expertise, and passion for their respective fields have enriched my academic experience. Their commitment to fostering an environment of learning and intellectual curiosity has been a constant source of inspiration throughout my journey.

My heartfelt appreciation also goes out to my family and friends who have supported me unconditionally throughout this journey. I reserve a special place of appreciation for my dear friend and colleague, Saloni Dhingra. Throughout this transformative journey, Saloni's support, camaraderie, and intellectual companionship have been truly remarkable.

Lastly, I would like to acknowledge the countless authors, researchers, and scholars whose works have formed the foundation of my research, and I am grateful for the wealth of knowledge they have contributed to the academic community.

I am humbled by the opportunity to have been part of this remarkable academic journey, and I am profoundly grateful to everyone who has played a role, big or small, in its realization. Their collective contributions have undoubtedly shaped the person I have become today, both academically and personally.

With deep appreciation and sincere gratitude,

Prateek Pati